学位論文

Effect of mass trasfer on the behavior of a catalyst.

小宮山　宏

指導教官
東京大学工学部
井上　博愛教授

昭和 47 年度

CONTENTS

Chapter 1 Introduction

1-1 Introduction

Recently in the chemical and petroleum industries, the catalytic process has become one of the most indispensable factors and in particular solid catalysts are frequently employed in the various kinds of reaction systems. These are usually of a porous structure in order that they can function effectively even with small volume. Their interior surface areas ordinarily range from 1 to 1000 m^2/gm. In such porous catalysts, reactant molecules must diffuse to get to the active interior surface and product molecules must be removed through the pores. If the mass transfer process is not faster than the reaction rate occuring in the pores, the whole interior surface area cannot be efficiently used. The behavior of an industrial solid catalyst, therefore, depends not only on its chemical characteristics but also on its physical properties, such as the size of the catalyst pellet and the diffusion coefficient of each component. The effect of the intraparticle mass transfer upon catalyst behavior will be studied in this dissertation.

A large number of studies have been undertaken since the effect of the mass transfer process on the behavior of the solid catalyst was pointed out independently by Damkoler,[D-1] Thiele,[T-3] and Zeldowitsch[Z-1] in the period of 1937 ~ 1939.

The activity of a catalyst under the influence of the mass transfer is the aspect which has been investigated most actively. A great deal of reseach from different points of view has been elucidating the effect of the various parameters on catalytic activity.

A desirable reaction catalyzed by a solid material is frequently accompanied undesirable side reactions so that the selectivity of the desirable product in

the complex reaction system becomes a subject of industrial importance. Selectivity is also influenced by the intraparticle mass transfer as pointed out in the pioneering work of Wheeler.[W-16] While a limited number of investigations has been carried out on this problem, they don't seem to have given us a powerful means to the interpretation of the true mechanism of the multiple reactions system and to the improvement of selectivity. This is possibly due to the fact that this research was carried out only on the theoretical level and was not supported by experiments. In this dissertation, the author tries to begin with the experimental approach on selectivity in a two step consecutive reaction system, which is the most interesting and important example of the complex reaction systems in relating to the intraparticle mass transfer effect.

Besides activity and selectivity, thereis another important characteristic in the industrial solid catalyst. Namely, time change of the catalytic behaviors. The present state of the investigation into time change is on about the same level as that of selectivity. Systematic investigation supported by experiment is required now. It is one of the main themes of this dissertation.

When the present level of study in this field is considered, it is noted that only the most fundamental assumption of the simple pore model, that is to say, one in which the catalytic activity is distributed uniformly within the whole catalyst volume and the mass transfer is characterized by only one diffusion coefficient, is used. This may oversimplify the actual system. More detailed examination of the pore structure is required in order to obtain a deeper insight into the role of the mass transfer in the catalytic behavior and to systematize the studies in this field, giving a clear boundary between the mass transfer effect and the intrinsic catalytic reaction. The author will present a more reasonable model for the actual porous catalyst, by which the various experimental results are analyzed systematically.

Furthermore, the studies on the solid catalyst have led to some idealized catalytic systems as a natural extension of the conception of the mechanism. One of them is the more effective operation for the solid catalyst by making use of the hydrodynamic flow through its pores caused by the longitudinal pressure gradient existing in a reactor. Another is an approach for a better holding system of liquid phase catalysts.

The historical review to be presented in this chapter will give a deeper understanding of this dissertation.

1-2 Effectiveness Factor

When a gas-solid catalytic reaction occurs in a porous catalyst, concentration, temperature and pressure may be different from the values at its exterior surface within the pore, owing to their transfer resistance. The effectiveness factor is defined as the ratio of this actual rate to the hypothetical rate which would occur if the whole interior surface was exposed to the same atomosphere as the exterior surface. In the simple system where a first order reaction without volume change takes place in a spherical pellet under isothermal condition, the actual rate may be reduced only due to the concentration decrease. The effectiveness factor for this system is solved as follows.[T-3)]

$$E_1 = \frac{3}{m_1} \left(\coth m_1 - \frac{1}{m_1} \right) \tag{1-1}$$

$$m_1 = R \sqrt{\frac{k_1}{D_e}} \tag{1-2}$$

m_1 is a dimensionless number named as 'Thiele modulus'.

The former studies concerning the effectiveness factor are classified roughly into the following three families.

1) Extending the above simple case to more complicated ones
2) Discussing the effectiveness factor by experiments[A-7,B-13,14,12,H-7,L-2, M-1,O-4,P-8,R-1,2,W-19)]

3) Determining the criterion free from transfer effects

1-2-1 Effect of Various Vactors upon the Effectiveness Factor

1) shape effects

Effectiveness factors have been solved for several geometries, such as flat plate,[T-3] cylinder with sealed end, cylinder,[A-7,K-2] hollow cylinder[S-5] other than sphere. Aris[A-7] showed that the differences in the relation between E_1 and m_1 for various pellet geometries become negligibly small when the ratio of the volume of its shape to its exterior surface area is taken as a dimension of pellet, that is, $m_1 = \frac{V_g}{S_g}\sqrt{\frac{k_1}{D_e}}$.

Recently Rester et al.[R-3,4] proved this fact using a lot of computed results for different geometries. Thus it is concluded that the shape effect doesn't need to be taken into account if the proper length is choosed.

2) reaction rate forms

Analytical solutions are presented for such reaction rate forms as, n'th order reaction,[T-3] reversible first order reaction,[C-2,S-13,W-1,17] Langmuir-Hinshelwood type of rate forms[C-5,H-6,R-5] and their reversible cases.[S-7] Numerical technique for estimating the effectiveness factor from kinetic data was also introduced.[K-10,11] Naturally, the effectiveness factor is dependent upon the reactant concentration at the exterior surface of the pellet except for first order systems.

3) effects of volume change

The volume change caused by a reaction brings about mass flow and affects the mass transfer rate. Thiele is the first who suggested the effect.[T-3] He employed a graphical technique for the first order reaction, $A \longrightarrow nB$. Recently, effectiveness factors were calculated numerically for 0, 1 and 2'nd order reactions, $A \longrightarrow nB$, where a new parameter relating to volume change $(n-1)x_{AS}$ was employed together with

m_1.[W-7] The larger these parameters the larger the effect. Even in the case of $m_1 > 10$ and $(n-1)x_{AS} = 2$, however, the effect reduces the effectiveness factor only by 30 %. As a result, it is concluded that the volume change effect may be usually neglected.

4) effects of the temperature gradient

The temperature difference between the exterior surface of the pellet and an interior point is related to the concentration difference between the same two points by the following equation.[D-3,P-6,W-16]

$$T - T_S = \frac{(-\Delta H)\, D_e}{\lambda}(C - C_S) \qquad (1\text{-}3)$$

On the basis of this equation, Prater[P-6] showed that there possibly exists a temperature difference of 53 °C in the case of the dehydrogenation of cyclohexane over a platinum-alumina catalyst. In such a condition, treating the system as an isothermal case may lead to noticeable error.

The effectiveness factor under the non-isothermal condition was numerically calcul~~ulated~~ for a first order reaction. To describe the system, two new dimensionless groups were introduced adding to Thiele modulus, which were related to the activation energy and the maximum temperature difference which could occur in the pellet. Several approximating methods for a first order reaction[B-4, C-1,G-2,P-2,T-4,5,W-15] and the numerical solutions for the rate forms other than a first order law[H-6] were also presented. Shilson et al.[S-10,11] proposed an approximation which is competent for the computational calculations and available regardless of the rate expression and the number of reactions. In the recent work[W-8] the volume change was taken into consideration together with the thermal effect. It was suggested by the latest work[I-1] that a larger temperature gradient may exist in a transient state than a steady state, possibly encountered in the start up of the reaction operations.

The condition that a system must satisfy to be considered to be isothermal was introduced by Andersen.[A-3] The significance of the thermal effect in practical catalyst systems is most important and interesting. Weisz et al.[W-15] discussed this problem using the numerical examination of the two dimensionless groups relating to the activation energy and the maximum temperature difference in the pellet. Their conclusion may be simply stated as; The thermal effect is appreciable when the reaction involves a large amount of heat and a large activation energy occuring in a catalyst of a very rough pore structure characterized by a large diffusivity and a small thermal conductivity. On the other hand, Akehata et al.[A-2], using a simplified analysis, showed that the thermal effect is not more than 10% of that of the concentration gradient in the five practical catalyst systems. According to the results of these investigators, it may be concluded that the thermal effect is not so large in ordinary catalyst systems.

Recently, several experimental studies[C-9,I-1,M-5,W-18] have been published in this field.

5) effects of the temperature, concentration or pressure gradients at the catalyst exterior surface

It is usually assumed that the atmosphere is uniform at the exterior surface of a single catalyst pellet. The catalyst in a reactor, however, may be exposed to the gradients of temperature, concentration and/or pressure in the reactor. Petersen[P-5] and Petersen et al.[P-4] investigated the reaction at the surface of a nonporous catalyst under the influence of a concentration gradient. They showed that using an average concentration on the surface doesn't make any difference to the estimated reaction rate, if the gradient is smaller than $C_I/2R$ which corresponds to a perfect conversion of a reactant by the length of a pellet. Similar conclusion was obtained for the effect of the temperature gradient at the surface of a porous catalyst.[B-8] If there exists a gradient of pressure, it may cause the hydrodynamic flow through

a catalyst pellet. Wheeler[W-16], however, showed that the mass flux brought about by the hydrodynamic flow is negligible compared to diffusional flux.

In summary, it is demonstrated that the usual assumption of the homogeneity at the surface of a single catalyst is valid under ordinary conditions.

The author,[K-9] however, pays attension to the possible effect of the hydrodynamic flow in a catalyst of a very rough pore structure in chapter 6, in order to develop a better method of operation for the solid catalyst.

1-2-2 Experimental Determination of the Effectiveness Factor

It is difficult in general to evaluate the intrinsic rate constant involved in Thiele modulus. Therefore, it is not so easy to determine the effectiveness factor for a given catalyst from kinetic measurements and the theoretical relation of the effectiveness factor and Thiele modulus. Three different methods have been proposed so far. The latter two of them require the knowledge of the reaction rate expression and the graph of E_1 versus m_1.

1) This is the most fundamental and reliable method. Reduce the size of the catalyst and one can attain to the true reaction rate uninfluenced by mass transfer processes. The effectiveness factor is obtained as the reaction rate each catalyst relative to that of the small particle.

2) This one is reffered to as 'triangle method', which was first introduced by Hougen et al.[H-5] The ratio of the catalyst pellets and the ratio of their reaction rates correspond respectively to the ratio of moduli and the ratio of effectiveness factors. Namely,

$$D_p^1 / D_p^2 = m_1^1 / m_1^2 , \qquad R^1 / R^2 = E_1^1 / E_1^2$$

If the rate form is known and the graph of E_1 versus m_1 is available, the effectiveness factors and the moduli which satisfy the above two relations simultaneously are determined theoretically. In practice, however, this

method possibly leads to appreciable errors. Furthermore, it is of no use in the region of large modulus as $m_1 > 10$ where $E_1 = 3/m_1$.

Another method similar to this one is also presented.)

3) The method employing the modified modulus, $\Phi_1 = m_1^2 E_1$, was proposed by Wagner.[W-1] For a first order reaction,

$$\overline{R}_1 = k_1 E_1 C_S \quad \text{and} \quad m_1 = R\sqrt{\frac{k_1}{D_e}} \tag{1-4}$$

Eliminating k_1 from these two equations yields the following relation.

$$\overline{R}_1 \frac{R^2}{C_S D_e} = m_1^2 E_1 = \Phi_1 \tag{1-5}$$

The left hand side of Eq.(1-5) contains only measurable parameters and one can obtain the effectiveness factor from the relation of E_1 and Φ_1. Similar modified modulus can be defined for the rate forms other than a first order law. Now, the charts are available for only an isothermal or non-isothermal first order reaction.[S-4]

1-2-3 Criteria Safe from the Influence of Mass Transfer Processes

This is one of the most useful aspects in the investigations on the mass t ısfer effect on the behavior of a catalyst. Because most of the industrial catalytic reactions are of complex rate forms, such as the synthesis of NH_3 and the oxidation of SO_2, it is a rather rare case that one can make use of the reported charts or the solutions for the effectiveness factor. Frequently, practical problems must be solved by means of a computer. On the other hand, the criteria shown in this section make it clear whether the mass transfer effect doesn't need to be taken into account at all or it should be examined in detail.

Weisz et al.[W-11] expressed the criteria as $\Phi_1 < 1$. Later, they introduced the following criteria by which the effectiveness factor is assured to be not less than 0.95.

$$\Phi_1 < 0.3 \quad (\text{ 2'nd order reaction })$$

$$\Phi_1 < 1 \quad (\text{ 1'st order reaction })$$

$$\Phi_1 < 6 \quad (\text{ 0 order reaction })$$

They argued that these criteria are available to almost all kinds of rate forms by approximating them by appropriate power law kinetics. These are well known as Weisz-Prator (or W-P) criterion. However, the generality of W-P criterion was disproved by the experiments pertaining to the reaction of carbon with carbon dioxide[A-9] and more general criterion was sought.[A-4,P-3]

In the latest publication, Bischoff[B-7] introduced the most general criterion as shown below.

A generalized modulus is defined as

$$m_{gen} = \frac{V_g \, R_1(C_S)}{\sqrt{2} \; S_g} \left[\int_{C_{equi}}^{C_S} D_e(C) \, R_1(C) \, dC \right]^{-\frac{1}{2}} \qquad (1\text{-}6)$$

This modulus makes the effectiveness factors asymptotically follow the same family of lines with the parameter relating to the thermal effect regardless of the rate expression of the reaction.[A-8,B-6] On the basis of this fact, Bischoff[B-7] presented the following general criterion.

$$\frac{\overline{R_1} \; (V_g / S_g)^2 \; g(C_S)}{2 \int_{C_{equi}}^{C_S} D_e(C) \; g(C) \; dC} < 1 \qquad (1\text{-}7)$$

Here, $g(C)$, $\overline{R_1}$ and C_{equi} represent respectively the rate form of the reaction nor involving the rate constant, the average reaction rate per unit catalyst volume and the equilibrium concentration of the reaction. The knowledge of the activation energy and the equilibrium constant and so on is required to use this

criterion.

The latest study[H-7] presented a more simple criterion.

$$\overline{R}_1 \frac{(V_g/S_g)^2}{C_S D_e} < \frac{1}{C_S} \frac{g(C_S)}{g'(C_S)} \qquad (1\text{-}8)$$

Here g' represents the first derivative of g with repect to the concentration. This criterion is obtained employing an approximation of the rate form and a simple assumption of the concentration profile. The simplicity of this criterion should be greatly appreciated, while inferior to Bischoff's criterion in strictness.

1-2-4 Observed Activation Energies and Reaction Orders

Weisz et al.[W-11] derived the relationship between the observed activation energy and the effectiveness factor as follows.

The true activation energy is represented as

$$E_a = -R \frac{d \ln k_1}{d\,(1/T_S)} \qquad (1\text{-}9)$$

The activation energy measured under the influence of mass transfer is

$$E_{obs} = -R \frac{d \ln (k_1 E_1)}{d\,(1/T_S)} \qquad (1\text{-}10)$$

Combining Eqs.(1-9) and (1-10) yields

$$E_{obs}/E_a = 1 + \frac{1}{2} \frac{d \ln E_1}{d \ln m_1} = 1 + \frac{1}{2} \Psi \qquad (1\text{-}11)$$

When a process is subject to a strong diffusion effect, Ψ approaches the limiting value -1. A catalyst operated under such condition, therefore, shows a half of the true activation energy. Recently, Gupta et al.[G-3] presented a more general relationship considering the temperature dependency of a

diffusion coefficient.

The observed activation energy for 0, 1'st order reaction and Langmuir-Hinshelwood type of reaction was treated under non-isothermal condition. It may be larger than the true value and lower than one half of it under some special conditions.

Observable reaction order in power law kinetics, n_{obs}, is also related to the effectiveness factor. According to Weisz et al.,[W-11]

$$n_{obs} = n + \Psi \frac{d \ln m_1}{d \ln C_S}, \qquad m_1 = R\sqrt{\frac{k_1 C_S^{n-1}}{D_e}} \tag{1-12}$$

When the mass transfer mechanism is characterized by Knudsen diffusion, D_e is independent of C_s so that $d\ln m_1 / d\ln C_S = (n-1)/2$. Consequently, at large values of modulus,

$$n_{obs} = (n + 1)/2 \tag{1-13}$$

On the other hand, the diffusion coefficient is inversely proportional to total pressure in the ordinary diffusion range. In this case, $d\ln m_1/d\ln C_S = n/2$ and therefore,

$$n_{obs} = n/2 \tag{1-14}$$

It should be noticed, however, that if the kinetic measurements are carried out at a constant total pressure, $n = (n + 1)/2$ holds true for the range of ordinary diffusion.

It should be also noticed that the equilibrium constants in a reaction which follows Langmuir -Hinshelwood model change with the effectiveness factor, though it has not been pointed out. This is easily interpreted by a typical example of the limiting 1/2 order behavior of an intrinsic zero order reaction under the influence of mass transfer. It means that the infinitely large equilibrium constants of a reactant is reduced apparently due to the mass transfer effect.

1-3 Selectivity

The occurence of multiple reactions in a solid catalyst is more usual than a single reaction. The selectivity of some desired product is, therefore, one of the major subjects of the investigation. The mass transfer effect on selectivity was first treated by Wheeler[W-16] for the following three types of reaction systems.

Type I $A \xrightarrow{k_1} B + C$

$X \xrightarrow{k_2} Y + Z$

Type II $A \xrightarrow{k_1} B$, $A \xrightarrow{k_2} C$

Type III $A \xrightarrow{k_1} B \xrightarrow{k_2} C$

First order reactions and a single pore model which is mathematically equivalent to a flat plat were assumed . Type I selectivity, as termed by Wheeler, is easily solved as

$$s_{obs} = \frac{k_{1obs}}{k_{2obs}} = \sqrt{\frac{k_1 D_X}{k_2 D_A}} \frac{\tanh m_1}{\tanh m_2} \qquad (1\text{-}15)$$

It is obvious that this type of selectivity is affected by the mass transfer.

Type II selectivity is independent of the mass transfer process because $R_1/R_2 = k_1/k_2$ holds true at anywhere inside the catalyst. That is to say,

$$s_{obs} = \frac{k_{1obs}}{k_{2obs}} = \frac{k_1}{k_2} = s \qquad (1\text{-}16)$$

Type III selectivity is most important and interesting and it is strongly influenced by mass transfer, since the concentration of a reactant decreases with depth of penetration but that of an intermediate product increases. This type of selectivity was defined as the rate of an intermediate relative to that of a reactant and derived as follows.

$$S = \frac{s}{s-1} - \left(\frac{P_{BS}}{P_{AS}} + \frac{s}{s-1} \right) \frac{\tanh (m_1/\sqrt{s})}{\sqrt{s} \tanh m_1} \qquad (1\text{-}17)$$

Furthermore, the relations of the yield of an intermediate product to the conversion of a reactant in a plug flow reactor were obtained under two limiting conditions, one of which is safe from mass transfer and another is strongly affected by it. This type of selectivity was solved for the other geometries such as a sphere[W-11)*] and a cylinder.[W-3)] The results seem to show that the selectivity for different shapes of catalyst follow the same relation to modulus, provided that the length of a catalyst is taken as V_g/S_g. Selectivity under the combined effects of mass and heat transfer was studied numerically by Butt[B-14)] and Carberry[C-1)], employing six dimensionless groups as the system parameters.

While a large number of the experimental studies have been carried out on the effectiveness factor and these have made significant contributions to advance, there have been few experimental investigations concerning selectivity with only two exceptions.

Weisz et al.[W-12)] carried out the catalytic dehydrogenetion of cyclohexane and measured the selectivity of the intermediate product, cyclohexene, for three different sizes of catalyst. Selectivity increased with decreasing the catalyst size. This is the first report showing the dependence of selectivity to mass transfer. Johnson et al.[J-1)] found that the selectivity of gasoline in the cracking of gas oil increased with decreasing the catalyst size or increasing the pore diameter of the catalyst, indicating a diffusion effect in this system.

It is desired to do more experimental investigations to the advance in this field. In this point of view, the investigation on the hydrogenation of acetylene will be carried out in chapter 2.[K-4)]

* The solution of the paper is mistaken possibly by miss prints.

1-4 Time Change in Catalytic Behavior

Usually, the activity of a solid catalyst gradually decreases in the course of a reaction by various causes. The pattern of a time change in activity depends on the catalyst systems and they are classified into several types.[M-3] While a large number of investigations have been published in this field, here are listed those pertaining to the mass transfer effect.

Wheeler[W-16] suggested two different types of deactivation process, as termed as homogeneous poisoning and selective poisoning. By homogeneous poisoning, it is assumed that the whole interior surface is poisoned homogeneously so that the relative activity of a poisoned catalyst to its initial activity is represented as $(k_1 E_1)_{poisoned} / (k_{10} E_{10})$. Here, $E_{1poisoned}$ E_{10} because $k_{1poisoned}$ k_{10}. This fact indicates that the decrease in the rate constant is partially compensated by the increase in the effectiveness factor in this type of deactivation. Alternately, when deactivation occurs preferentially near the pore mouth, as termed as selective poisoning, the deactivated shell formed at the pore mouth strongly hinders the diffusion of reactant molecules. It results in rapid deactivation. These two types of deactivation process were numerically compared to each other, together with that of a nonporous catalyst. Recently, Carberry[C-4] investigated the deactivation which follows the shell progressive mechanism (selective poisoning according to Wheeler) under the effect of film resistance. Olson et. al.[O-1] extemded the treatment of Carberry[C-4] to the behavior of a reactor.

Assuming the deposition of some poisoning species to be the cause of deactivation, Takeuchi et al.[T-2] and Masamune et al.[M-2] calculated the time change of catalytic activity for the following two types of coke formation mechanism.

$$\begin{tikzcd} A \arrow[r, "k_1"] \arrow[dr, "k_2"'] & B \\ & \text{coke} \end{tikzcd} \quad ; \quad A \xrightarrow{k_1} B \xrightarrow{k_2} \text{Coke}$$

The deactivation due to the deposition of coke produced from a reactant A is approximated by a shell-progressive mechanism and that from a product B is approximated by a core-progressive mechanism. There is a recent publication concerning the deactivation under a non-isothermal condition in a catalyst.

Recent experimental studies in this field are gradually elucidating the mechanism of the deactivation due to the deposition of some poisoning species.

Murakami et al.[M-10] undertook the dehydrogenation of butanol and found that the coke formation proceeds from the exterior surface of a catalyst at a hi temperature level and on the contrary from the pellet center at a low temperature level. This fact was interpreted comprehensively by the concentration profile of the intermediate product.

Suga et al.[O-4, S-10] investigated the hydrogenation of n-butane considering the mass transfer effect, but unfortunately the modulus under the operation condition was 2 at most so that the effect was not obvious. Balder et al.[B-1] measured the rate of the hydrogenolysis of cyclopropane and the concentration at the pellet center simultaneously, employing a special type of reactor. The proceeding of deactivation was between homogeneous deactivation and shell-progressive one.

There has been few reported studies on the change in selectivity with deactivation with one exception of the latest study based on shell-progressive model.

1-5 Microscopic Structure of Catalysts

All the materials in the preceding sections have been based on the simple pore model for the pore structure of a catalyst. It is well known, however, that the porous material such as pellets prepared by compacting fine microporous powders are of a bi-modal pore structure, which contains micropore together with macropore. Some of the solid catalysts may be of such pore structure.

Based on the consideration, Mingle et al.[M-6] Carberry[C-2] and Wakao et al.[W-4] analyzed the effectiveness factor and the selectivity in a consecutive reaction system.

According to Carberry[C-4], who employed the model of a straight macropore with many branches of micropore on its inner wall, the observable rate constant is expressed by the product of the intrinsic rate constant and the effectiveness factors both of the macropore and the micropore. Point selectivity defined as $-\frac{dP_{BS}}{dP_{AS}}$ and the yield of an intermediate product in a plug flow reactor were also derived for the model.

$$\text{point selectivity} = -d\pi\left(\frac{P_{BS}}{P_{AS}} + \frac{s}{sd-1}\right) + d\,\frac{s}{s-1} \qquad (1\text{-}18)$$

$$\text{yield} = \left(\frac{\pi-d}{\pi-1}\right)\frac{s}{sd-1}\left(X^{\pi} - X\right) + \frac{P_{BI}}{P_{AI}}X^{\pi} \qquad (1\text{-}19)$$

Here, π represents the dimensionless group relating to the moduli of the macropore and the micropore. While these approaches were not based on the detailed examination of the actual solid catalyst structure, it should be greatly appreciated that the micropore process was first taken into account.

In practical analyses of catalyst behaviors, no attension has been given to the micropore process. To be sure, its effect is often indstinguishable from an intrinsic reaction. For example, the reaction rate measured for sufficiently small catalysts may be still influenced by the diffusion in micropore. Even in the case of a complex reactions system, the consecutive reactions under the influence of mass transfer is hardly distinguished from a parallel and consecutive reaction system, as will be shown in chapter 4.[K-5] This is the reason why this field of research is difficult.

Considering the progress in the investigation on the mass transfer effect

on the catalyst behavior as stated above, the effect of the microscopic structure is the field which is the most tardy in research and is yet unsolved.

1-6 Summary

Except for the effect of the microscopic structure, the effectiveness factor has been investigated in detail from various approaches, containing the investigations which were published after this study was begun. In the present stage, one can state as follows.

1) It is possible to conclude by only the measurable parameters whether a catalytic system is safe from the mass transfer process or not.

2) If the system may be influenced by mass transfer, the effectiveness factor is able to be estimated by a lot of charts or analytical solutions presented in literatures. When the proper chart is not available, the prediction of the effectiveness factor can be performed by numerical method, the techniques of which have been established pretty well.

On the contrary, selectivity has not been so cleared as the effectiveness factor. More systematical investigation supported by experiments are required in this field. The present state of the investigation into time change of atalytic behaviors is on about the same level as that of selectivity. Particularly, there has been few study concerning with the change of selectivity in complex reactions.

The mass transfer process in the microscopic structure has been practically ignored, possibly owing to the fact that it is hardly distinguishable from an intrinsic catalytic reaction. The intrinsic catalytic process undoubtedly plays an important role in industrial solid catalysts. It should be discussed, however, eliminating the mass transfer effect. The role of the microscopic structure is one of the important problems to be solved by chemical engineers.

Based on the above consideration, the author begins with the investigation into the consecutive hydrogenation of acetylene, concentrating his attension on selectivity, time change of catalytic behavior and the microscopic structure of a catalyst.

Chapter 2 Selectivity in the Hydrogenation of Acetylene

2-1 Introduction

The distribution of the products is of greatest importance in industrial reactions on solid catalysts, because a desirable reaction is frequently accompanied with undesirable reactions in parallel and/or in series with it. The selectivity in a reaction system of parallel undesirable reaction is not affected by the mass transfer inside a catalyst. On the contrary, the degree of undesirable reaction in series may be strongly influenced by mass transfer, owing to the different concentration profiles of the components inside a catalyst. The selectivity of a desirable product in a consecutive reaction system, therefore, may depend not only on the intrinsic characteristic of catalyst surface but also on the physical properties such as the size of the catalyst and the diffusion coefficients. Some features of this type of selectivity have been analyzed theoretically by a few investigators[C-4,W-3,11,16] but few experimental proof has been given to the theoretical results. This field is in the stage in which experimentation is urgently required.

In this chapter, the hydrogenation of acetylene, which is considered to be two step consecutive reactions as

$$C_2H_2 \xrightarrow{H_2} C_2H_4 \xrightarrow{H_2} C_2H_6$$

, is investigated by experimental and theoretical analyses. Though the reaction schemes of various industrial reactions may be much more complicated, the analysis of the two step consecutive reactions will be give a deeper insight into the mechanism of the general complex reactions in relation to the mass transfer inside a catalyst.

2-2 Basic Theory*

* Detailed derivations are presented in Appendix 1.

Here, two step consecutive reactions $A \xrightarrow{k_1} B \xrightarrow{k_2} C$, which occur in a porous catalyst are analyzed on the following assumptions.

1) The reaction rates follow a first order law.
2) Heat effects are not considered. The temperature is uniform throughout each catalyst pellet and a reactor.
3) The reactions take place on the interior surface of the catalyst.
4) Mass transfer inside the catalyst is characterized by diffusion. The rate of diffusion is expressed by Fick's law with one effective diffusion coefficient. All components are of same effective diffusion coefficient, which may be often a good approximation for a consecutive reaction system.
5) Film resistance is not considered.

The conservation equations in a catalyst pellet, in which consecutive reactions take place under the condition as stated above, are written as

$$D_e \left(\frac{d^2P_A}{dr^2} + \frac{2}{r}\frac{dP_A}{dr} \right) = R_1 \qquad (2\text{-}1)$$

$$D_e \left(\frac{d^2P_B}{dr^2} + \frac{2}{r}\frac{dP_B}{dr} \right) = -R_1 + R_2 \qquad (2\text{-}2)$$

with boundary conditions,

$$\text{at } r = R, \quad P_A = P_{AS} \quad \text{and} \quad P_B = P_{BS} \qquad (2\text{-}3)$$

$$\text{at } r = 0, \quad \frac{dP_A}{dr} = 0 \quad \text{and} \quad \frac{dP_B}{dr} = 0 \qquad (2\text{-}4)$$

R_1 and R_2 represent the first and second step catalytic reaction rates on the interior surface per a unit volume of the catalyst. By the assumption of first order reactions, $R_1 = k_1 P_A$ and $R_2 = k_2 P_B$.

These equations are analytically solved with the boundary conditions.

The selectivity, defined as the ratio of the rate of formation of B to the rate of depletion of A, is given by

$$S = \frac{s - 1/E}{s - 1} - \frac{1}{Es}\frac{P_{BS}}{P_{AS}} \qquad (2\text{-}5)$$

$$E = E_1/E_2 , \qquad E_i = \frac{3}{m_i}\left(\coth m_i - \frac{1}{m_i} \right) \qquad (2\text{-}6)$$

$$s = k_1/k_2 ; \qquad m_i = R\sqrt{\frac{k_i}{D_e}}$$

Selectivity for a single catalyst pellet is represented in terms of the ratio of the two rate constants s, the ratio of the two effectiveness factors E and the partial pressures of A and B at the exterior surface of the catalyst.

The actually observable selectivity in a reactor depends not only on the single catalyst process derived above, but also on the conversion of a reactnat and the mixing characteristic in a reactor. Here, two types of ideal reactor are considered and selectivity is derived from the individual conservation equations in each reactor.

For a packed bed reactor (plug flow type)

$$S_p = \frac{(1 - X)^{1/Es} - (1 - X)}{X\,(1 - 1/Es)} \; \frac{s - 1/E}{s - 1} \qquad (2\text{-}7)$$

$$S_m = \frac{1}{1 + \dfrac{X}{(1 - X)\,Es}} \; \frac{s - 1/E}{s - 1} \qquad (2\text{-}8)$$

This type of selectivity is proved to depend on the conversion X and the mixing characteristics in the reactor besides s and E.

At the limiting condion where X approaches zero, S_p and S_m converge to the same value S^o, which is determined by s and E.

$$S^o = \frac{s - 1/E}{s - 1} \qquad (2\text{-}9)$$

The relations of S_p and S_m to X for two limiting values of E are illustrated in Figs.2-1, 2-2 and 2-3, where the values of s are respectively 7 , 1 and 0.09. The relations between S^o and m_1 are shown in Fig.2-4, for several values of s.

From the analysis, it is demonstrated as follows.

1) Selectivity decreases with increasing the conversion of a reactant and the pattern of the conversion dependence of selectivity is determined promarily by the value of s.

2) Selectivity decreases with decreasing the effectiveness factor and this effect is represented more obviously by considering the limiting selectivity at low conversion S^o. S^o is considered to be an intrinsic selectivity for a definite size of catalyst, by the fact that it is not affected by the mixing characteristic in a reactor. It is unity when Thiele modulus is smaller than unity and converges to the minimum value at a large value of it.

3) Back-mixing in a reactor decreases selectivity.

Experimental measurements of the selectivity at different conversions and different sizes of catalyst, the extrapolation of selectivity to X = 0 and so on make it possible to discuss a catalyst system on the basis of the above analysis.

Though this analysis is analogous in some parts to those presented by Wheeler[W-16] or Weisz et al.[W-11], it covers the wider range with the characteristics of the catalyst and of the reactor. Adding to it, it gives more obvious interpretation by introducing E and S^o in the expression of the results.

2-3 Experiments

2-3-1 Equipments and Methods

The flow system employed in the experiments is presented schematically in Fig.2-5. Acetylene, hydrogen and nitrogen gases were supplied to the reactor at constant flow rates after purified individually. The reactor of brass tube (I.D. 0.95 cm) was heated by an electric heater and controled within 2°C. Nitrogen gas was used to moderate the reaction by decreasing the partial pressures of hydrogen and acetylene and to reduce the temperature gradient in the catalyst bed. Feed line of ethylene was employed in the kinetic study of the second step reaction of the hydrogenation of acetylene. The measurement of the reaction temperature was made by three thermo-couples, equipped at the bottom, the top and the wall surface of the catalyst bed.

2-3-2 Catalysts

A nickel catalyst, "N111" supplied by the Nikki Chemical Co., was employed. The catalysts are of the following sizes.

No.1	No.2	No.3	No.4	No.5	No.6
0.097,	0.42	0.73	1.0	1.4	3.5×3.5 (mm)

The last one is the original cylindrical catalyst as supplied, and the others were made by crushing the catalyst with a coffee mill and were classified according to size. Since these catalysts are too active for the hydrogenation of acetylene, they were poisoned by dipping for 24 hrs. in $Na_2S_2O_3$ solution (5 gm / 100 gm H_2O).

2-3-3 Measurement of Selectivity

For each experimental run, 3 gm of catalysts was set in the reactor and preactivated at 280°C for 40 min. under hydrogen stream. At the beginning of the reaction operation, the catalyst was so active that methane was produced. After 30 min. from the start of the operation, however, the activity became moderate and nearly constant though it decreased gradually. In this stage, the product gas mixture was analyzed by means of gas chromatography.

Hydrocarbons containing more than two carbon atoms were not detected in the effluent gas, while their formation was reported in several literatures[S-12, 13].

2-3-4 Experimental Results

The conversion of acetylene and the selectivity of the intermediate product, ethylene, were obtained by the composion of the effluent gas in each experimental run. In most of the experiments, the feed gas mixture was of the same composition (Feed rates: acetylene 0.2 l/min., hydrogen 0.4 l/min. and nitrogen 2.0 l/min.). In this condition, the obtained selectivity for a catalyst of definite size depends only the conversion of acetylene. The reaction temperature doesn't exert any appreciable effect on selectivity as shown in Fig.2-8. This may be considered strange but it is probably due to the small activation energy of both the first and second step of the reaction, as shown later. Fig.2-6 shows the observed selectivity and conversion, for different sizes of catalyst. Fig.2-7 shows the selectivities of No.2 catalyst in the wide range of the conversion, which was measured for various values of contact time in the reactor.

Comparing the experimental results with the theoretical analysis described in 2-2, the agreements and the discrepancies between them are as follows.

1) The experimental tendency of selectivity on the conversion is quite similar to the theoretical results in Fig.2-1, where s = 7.

2) Experimental selectivity is improved by reducing the size of catalyst, indicating the increase in the effectiveness factor.

3) For the catalysts smaller than 0.73 mm. , selectivity becomes independent of the size of catalyst. This fact seems to show that the effectiveness factor is unity below the size. Even under such limiting condition, however, selectivity doesn't reach the theoretical value, unity, but remains at 0.82.

4) The dependency of selectivity on catalyst size is quantitatively different from the theory. Based on the theoretical consideration, the selectivity for a catalyst of large modulus approaches to the curve S_p ($E = 1/s$) in Fig.2-1. Experimental selectivity for the largest catalyst is much smaller than the estimated curve.

Though the qualititative agreements demonstrate that the treatment described before may simulate the reaction system pretty well, the quantitative discrepancies indicate that the assumption made for the analysis, that is first order rate forms and a simple pore model for the catalyst structure, oversimplify the real system. The rate forms and the pore structure should be examined in detail experimentally.

2-3-5 Kinetic Studies of the Hydrogenation of Acetylene

The hydrogenation of acetylene is considered to be two step consecutive reactions.

$$R_1 \quad C_2H_2 + H_2 \longrightarrow C_2H_4 \qquad (2\text{-}10)$$

$$R_2 \quad C_2H_4 + H_2 \longrightarrow C_2H_6 \qquad (2\text{-}11)$$

No.3 catalyst was employed for the kinetic studies, if not stated otherwise. The effectiveness factor of this catalyst was proved to be unity by the measurements of selectivity. Owing to the low conversion, the reactor can be considered a differential type.

R_1 is proportional to the partial pressure of hydrogen as shown in Fig.2-9. The dependency of R_1 on the partial pressure of acetylene is well expressed by a rate expression which follows Langmuir-Hinshelwood model. The adsorption equilibrium constant of acetylene is consedered larger than 100 atm^{-1}, though the exact value cannot be obtained from the results. These results are

well in accord with the experimental results of many investigators.[B-10,11,12, S-7,8)]

As a result, R_1 is expressed as

$$R_1 = \frac{k_1 P_A P_{H_2}}{1 + K_A P_A} \qquad (2\text{-}12)$$

The temperature dependency of the rate was measured for No.5 catalyst and resultant activation energy was 3 kcal/mol. Taking the decrease in the observable activation energy under the influence of mass transfer, the true activation energy may be about 6 kcal/mol.

2-3-6 Kinetic Studies of the Hydrogenation of Ethylene

The experimental results are shown in Figs. 2-11, 12 and 13. R_2 is proportional to the partial pressure of ethylene and to the squre root of that of hydrogen. The effect of acetylene on the rate is remarkable and interpreted by its adsorption effect. The adsorption equilibrium constant of acetylene was found to be about 230 atm^{-1}. The obtained rate form is summarized as follows.

$$R_2 = \frac{k_2 P_{H_2}^{\frac{1}{2}} P_B}{1 + K_A P_A} \qquad (2\text{-}13)$$

The dependency of the rate on the partial pressure of hydrogen is , however, unfamiliar and there have been no such data in the usual temperature range. This is probably due to the structual effect on the reaction rate. As shown in the next section, the catalyst is of a micro-macropore structure so that there remains the possibility that the micropore effectiveness factor doesn't reach unity in these rate measurements. Especially, in the absence of acetylene, which was actually the condition for the measurements, this diffusional effect might play an important role. Assumption of the rapid diffusion of hydrogen and the intrinsic first order dependences of the rate on the partial pressures of ethylene and hydrogen leads to the observed kinetics.

That is to say, in the range where the effectiveness factor is approximated by $3/m_1$,

$$\eta_2 = 3/\mu_2 = \frac{3}{L}\sqrt{\frac{D_K}{k_2 P_{H_2}}}$$

$$R_{2obs} = k_2 P_{H_2} \frac{3}{L}\sqrt{\frac{D_K}{k_2 P_{H_2}}} P_B \propto P_{H_2}^{\frac{1}{2}} P_B \qquad (2\text{-}14)$$

Then, the estimated rate form in the micropore may be expressed by Eq.(2-15).

$$R_2 = \frac{k_2 P_{H_2} P_B}{1 + K_A P_A} \qquad (2\text{-}15)$$

The activation energy observed for No.2 catalyst is about 4.4 kcal/mol. below 160°C and 0 kcal/mol. above the temperature level. Such change in activation energy has been reported by other investigators[C-9,F-1,L-1] and interpreted in terms of the dependency of the amount of ethylene adsorbed on the catalytic surface upon temperature.

Owing to catalyst deactivation, it is impossible to determine the ratio of the rate constants for R_1 and R_2 from the individual rate measurements. The most reliable method is to supply both acetylene and ethylene at the same time to the reactor. Then, R_1 is obtained by the conversion of acetylene and R_2 is by the increase in ethane production compared to the case of the absence of ethylene. The average value of s was 7 ($\pm$ 0.5). This agrees well with the experimental relations between S and X as shown in Figs.2-6 and 2-7.

As a result, the rate forms of the reaction system may be expressed as

$$R_1 = \frac{k_1 P_{H_2} P_A}{1 + K_A P_A}, \qquad R_2 = \frac{k_2 P_{H_2} P_B}{1 + K_A P_A}$$

$$K_A = 230 \text{ atm.}^{-1} \qquad s = 7$$

2-3-7 Analysis of the Catalyst Structure by means of an Electron Microscope

Photo.1 and 2 are the examples of many photographs of the catalyst used in the experiments. Photo.1 shows the total figure of the catalyst, though it was taken by a replica method. The black part of the photograph was proved to be nickel aggregated microparticles, by two facts that only this part is dissolved in a solution of nitric acid and that their electron diffraction pattern coincides with that of pure Ni_2O_3 crystals. The other part corresponds to the carrier structure so that the catalyst was proved to be composed of the dispersed fine nickel aggregates inside the carrier block. The space outside the nickel aggregates may be regarded as macropore structure.

Photo.2 is the enlarged nickel aggregate. From this photograph the aggregate is considered to be composed of fine nikel crystals (10 ~ 40 Å). The void space between the fine crystals is probably very small and is regarded to be micropore. Other examples of such photographs of solid catalysts are found in some books S-12)

2-4 Analyses and Discussions

First, the effect of rate forms is analyzed. A simple pore model is ployed for simplicity and the fundamental equations (2-1) and (2-2) are solved with the experimental rate forms.

$$R_1 = \frac{k_1^{o} P_A}{1 + K_A P_A}, \qquad R_2 = \frac{k_2^{o} P_B}{1 + K_A P_A}$$

Here, the diffusion rate of hydrogen is so rapid that its concentration was assumed to be constant within the catalyst. The equations are unable to solve analytically so that the numerical method by means of a digital computer was employed. According to the experimental results, the condition for the computation was determined as follows:

$$s = k_1^o / k_2^o = 7, \qquad K_A P_A = 10 \text{ and } 30 \text{ (18 in the experiments)}$$

$$m_L = R \sqrt{\frac{k_1^o}{(1 + K_A P_{AS})\, D_e}} = 1 \sim 50, \qquad P_{BS} = 0$$

The assumption of $P_{BS} = 0$ corresponds to the limiting selectivity as the conversion approaches zero.

Curve II and Curve III in Fig.2-14 show respectively the computational results for $K_A P_{AS} = 10$ and 30. Curve I shows the selectivity for the linear kinetics (Eq.(2-9)). S^o for the reactions which follow Langmuir-Hinshelwood model becomes much smaller than the first order reaction system and the effect of adsorption becomes remakable with the increase in $K_A P_{AS}$. S^o's extrapolated from the experimental results are also plotted in Fig.2-14. They are similar to the computational results in its shape.

When the value of $K_A P_{AS}$ is sufficiently larger than unity, the mass balance equations at a large value of modulus are reduced to the following approximated forms .

$$D_e \left(\frac{d^2 P_A}{dr^2} + \frac{2}{r} \frac{dP_A}{dr} \right) = D_e \frac{d^2 P_A}{dl^2} = \frac{k_1^o}{K_A} \qquad (2\text{-}16)$$

$$D_e \left(\frac{d^2 P_B}{dr^2} + \frac{2}{r} \frac{dP_B}{dr} \right) = D_e \frac{d^2 P_B}{dl^2} = - \frac{k_1^o}{K_A} + \frac{k_2^o P_B}{K_A P_A} \qquad (2\text{-}17)$$

with boundary conditions

$$\text{at } l = 0, \qquad P_A = P_{AS}, \qquad P_B = 0$$

$$\text{at } P_A = 0, \qquad \frac{dP_A}{dr} = 0, \qquad \frac{dP_B}{dr} = P_B = 0$$

These system is analytically solved* and the selectivity S^o is expressed by

* Detailed derivation is presented in Appendix 3.

Eq.(2-18).

$$S^{o} = \frac{s}{s-1} \; \frac{3 - \sqrt{1 + 8/s}}{4} \qquad (2\text{-}18)$$

Curve IV in Fig.2-14 shows the selectivity for the same value of s as the other curves. From these analysis, it may be clear that the rapid decrease in selectivity as catalyst size becomes large is due to Langmuir-Hinshelwood type of rate expressions.

Next, the following model, named a micro-macropore model according to the author, is introduced for the analysis of the effect of the micropore and macropore structure. This model implys;

1) The catalyst is consisted of the aggregates of catalytic micro nickel crystals, as termed "microparticle" in this study, and inactive porous carrier material.

2) Reactant molecules diffuse through the macroporous structure of the carrier material and arrive at the microparticles dispersed uniformly in the catalyst.

3) The void within the microparticles is regarded as a micropore, in which reactions take place. A simple pore model is applicable to the micropore process.

The conservation equations in a single catalyst are expressed as follows with boundary conditions.

$$D_M \left(\frac{d^2P_A}{dr^2} + \frac{2}{r}\frac{dP_A}{dr} \right) = \varepsilon k_1' \eta_1 P_A \qquad (2\text{-}19)$$

$$D_M \left(\frac{d^2P_B}{dr^2} + \frac{2}{r}\frac{dP_B}{dr} \right) = -\varepsilon k_1' \eta_1 \frac{s - 1/\eta}{s-1} P_A + \varepsilon k_2' \eta_2 P_B \qquad (2\text{-}20)$$

at $r = R$, $\quad P_A = P_{AS}$ and $P_B = P_{BS}$

at $r = 0$, $\quad \frac{dP_A}{dr} = \frac{dP_B}{dr} = 0$

Here, ε is the fraction of a catalyst volume occupied by microparticles and η_i's are the effectiveness factors for the microparticle.

$$\eta_i = \frac{3}{\mu_i}\left(\coth\mu_i - \frac{1}{\mu_i}\right), \qquad {}_i = L\sqrt{\frac{k_i'}{D_K}}, \qquad \eta = \eta_1 / \eta_2 \tag{2-21}$$

The selectivity S^o derived from these equations is represented as*

$$S^o = \frac{s - 1/\eta E'}{s - 1} \tag{2-22}$$

where

$$E' = E_1'/E_2', \qquad E_i' = \frac{3}{m_i'}\left(\coth m_i' - \frac{1}{m_i'}\right), \quad m_i' = R\sqrt{\frac{\varepsilon k_i' \eta_i}{D_M}} \tag{2-23}$$

The resultant selectivity S^o doesn't converge to unity even when the macropore effectiveness factor is unity. It depends on the micropore effectiveness factor. Curve V in Fig.2-14 is the example of the relation between S^o and m_1' by the micro-macropore model, where the micropore effectiveness factor was assumed to be very small. Under the condition,

$$s_{obs} = s'\eta = s'^{\frac{1}{2}} \quad \left(\text{For, } \eta_i = 3/\mu_i \text{ and } \eta = 1/s'^{\frac{1}{2}}\right) \tag{2-24}$$

Curve V, s' was taken as 49, corresponding to the experimental condition ($s = 7 = s'^{\frac{1}{2}}$). This curve is a little larger than the experimental data, but the difference may be reasonable owing to Langmuir-Hinshelwood type of rate expressions. The detailed comparison of the experiments with the computational results based on the micro-macropore model and the experimental kinetics was carried out, because of a long computational time.

In the extreme case where $K_A P_{AS}$, m_i' and μ_i are very large, the analysis based on the similar approximation as Eqs.(2-16) and (2-17) is possible for this micro-macropore model. The limiting selectivity S^o is given by*

$$S^o = \frac{1}{8}\left(7 - \sqrt{13 + 12\sqrt{1 + 8/s'}}\right)\frac{s'}{s' - 1} \tag{2-25}$$

* Detailed derivation is presented in Appendix 3.

Curve VI in Fig.2-14 shows the selectivity for $s' = 49$. This is minimum selectivity for Langmuir-Hinshelwood type of rate forms and micro-macropore model and coincides with the minimum selectivity observed experimentally. This coincidence, however, may be not necessarily resonable since $K_A P_{AS}$ is not so large as the above assumption is valid. This unbiguity will be discussed in the next chapter.

2-5 Summary

This chapter is the first systematic investigation into the effect of the mass transfer process upon selectivity in a consecutive reaction system based on, 1) the analysis of a basic catalytic system, 2) the measurements of the selectivity in the wide range of operation conditions, 3) the analysis of the reaction kinetics and 4) the microscopic analysis of the catalyst structure.

In summary, the following facts are demonstrated.

1) The kinetics of the hydrogenation of acetylene is expressed by the consecutive reaction system which follows Langmuir-Hinshelwood model.

2) The selectivity of ethylene, the intermediate product, is affected strongly by catalyst size, that is , the catalytic effectiveness factor. The dependency of selectivity on catalyst size is not so simple as the case of linear kinetics and a simple pore model. The experimental results are interpreted comprehensively based on the micropore and macropore structure of the catalyst and the reactions which follow Langmuir-Hinshelwood model.

The comparison of the analysis described here with the other analyses by different reaction models and the effect of catalyst deactivation were not discussed at all, avoiding complexity. These will be discussed in the succeeding chapters. The mass transfer mechanisms were also not discussed. Within the macropore, ordinary diffusion and/or Knudsen diffusion will occur depending on the pore diameter. What type of mass transfer characterizes the micropore process is

,however, a difficult problem because the pore may be so small that even Knudsen diffusion may not occur. Surface diffusion or some unknown transfer mechanism may characterize the process. This is a problem to be taken up in future studies.

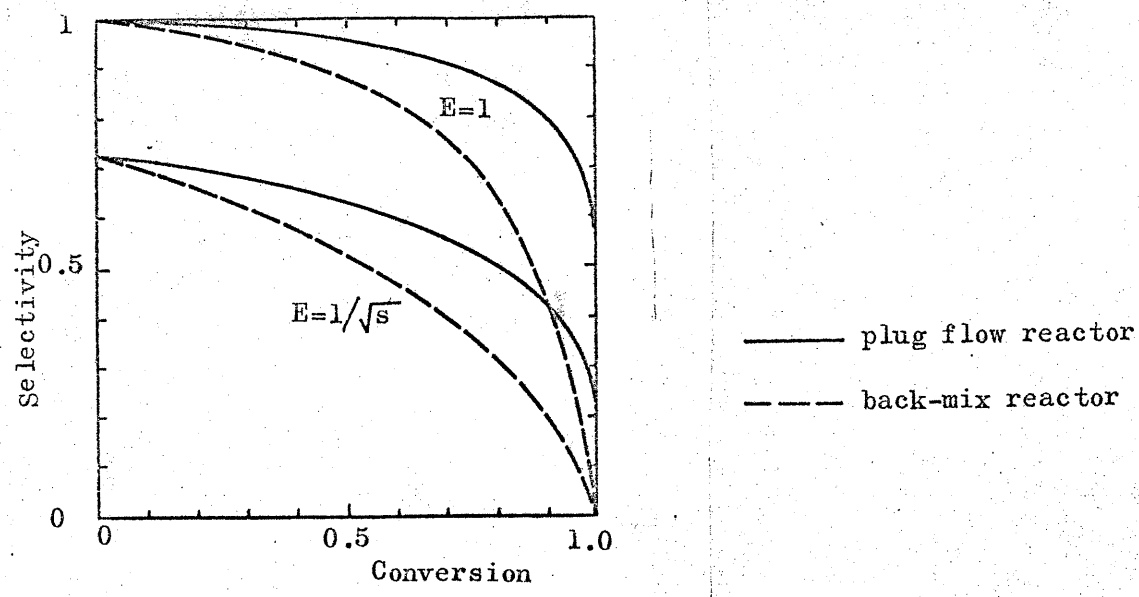

Fig.2-1 Selectivity vs. Conversion

(s = 7)

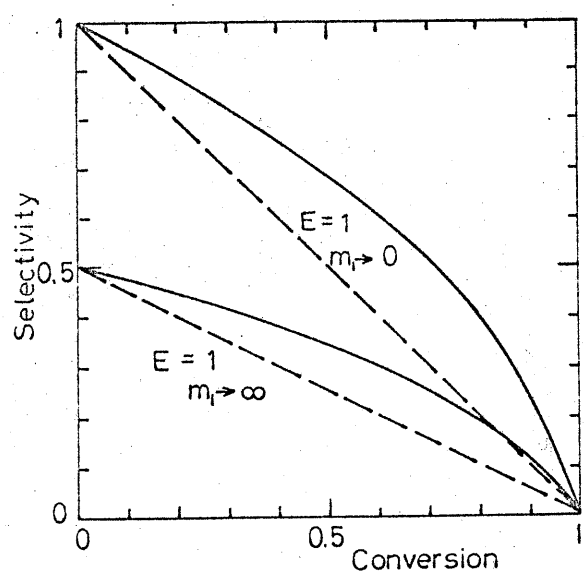

Fig.2-2 Selectivity vs. Conversion

(s = 1)

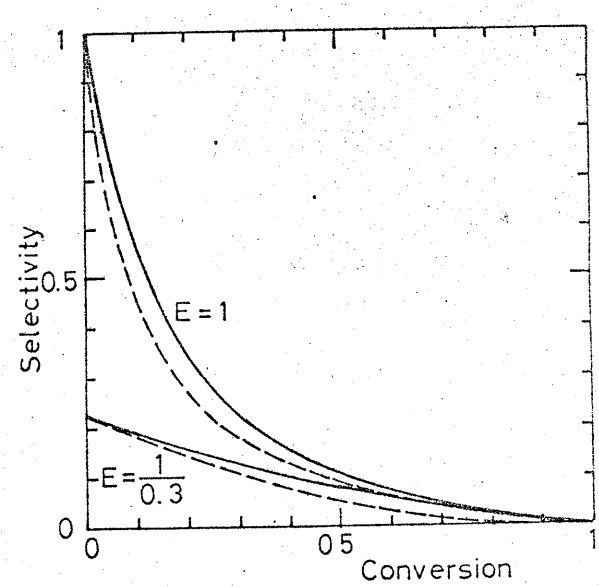

Fig.2-3 Selectivity vs. Conversion

(s = 0.09)

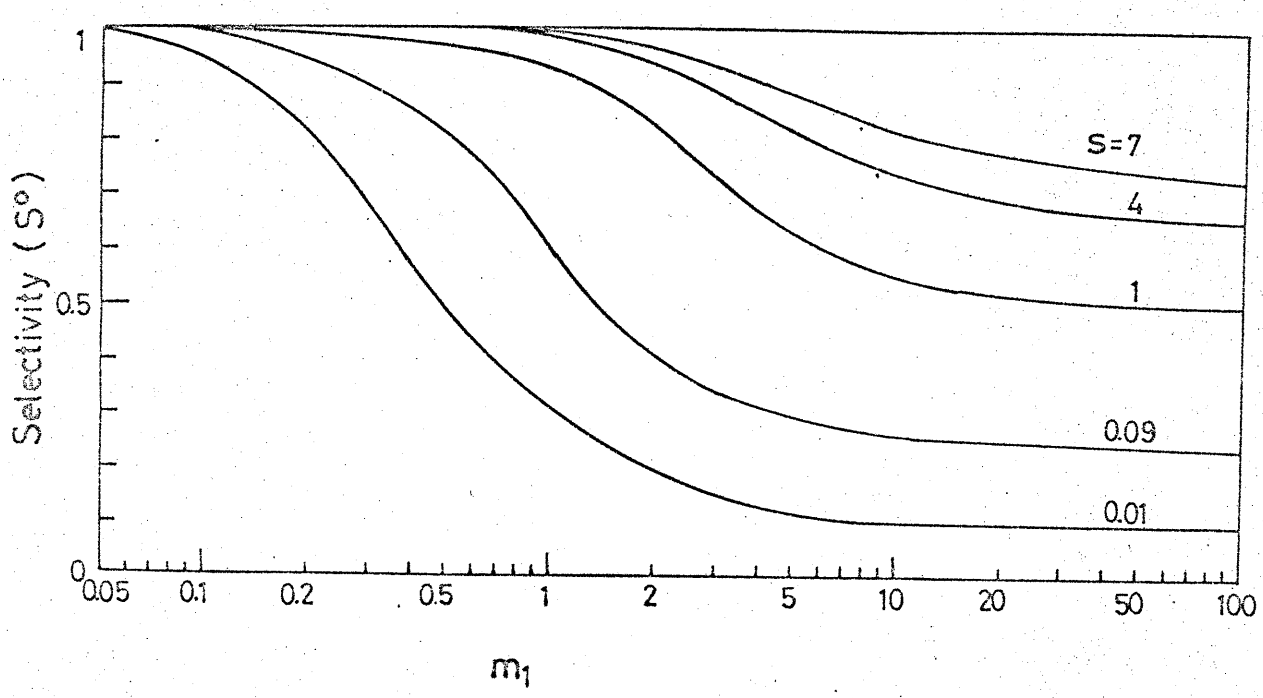

Fig.2-4 S^o vs. Modulus (m_1)

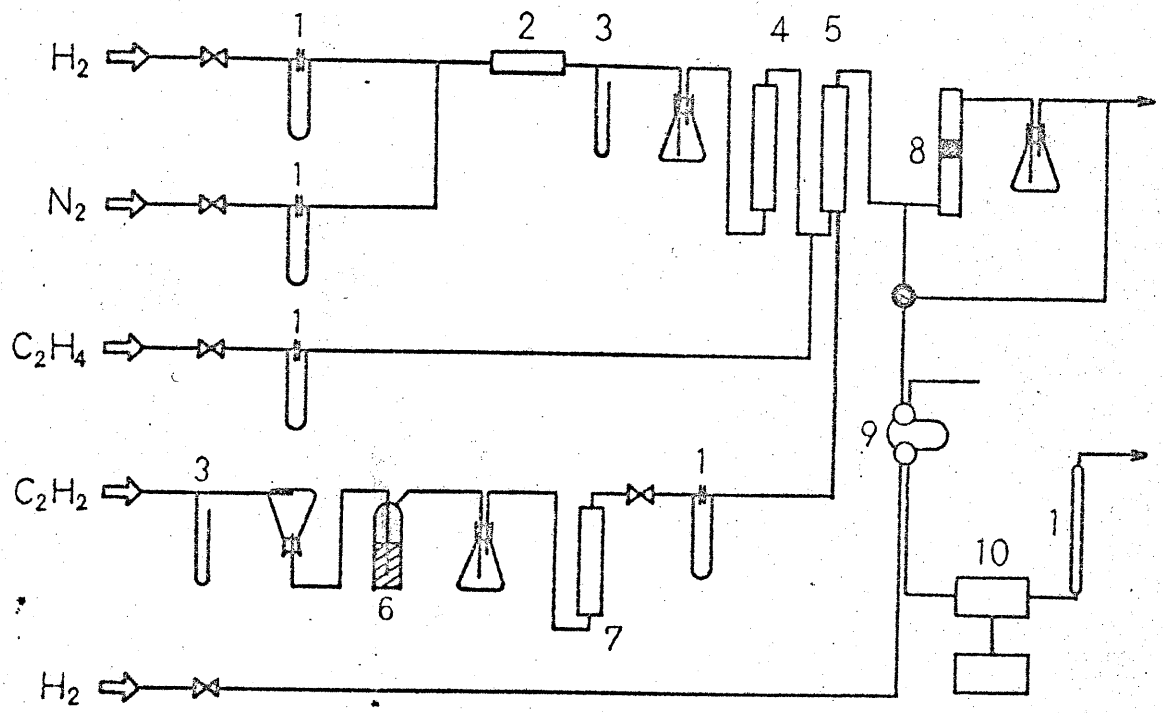

1	flow meter	6	conc. H_2SO_4
2	oxygen removal furnace	7	Soda lime & $CaCl_2$
3	manometer	8	Reactor
4	Al_2O_3	9	Sampler
5	gas mixer	10	gas fracto-meter

Fig.2-5 Schematic Diagram of Apparatus

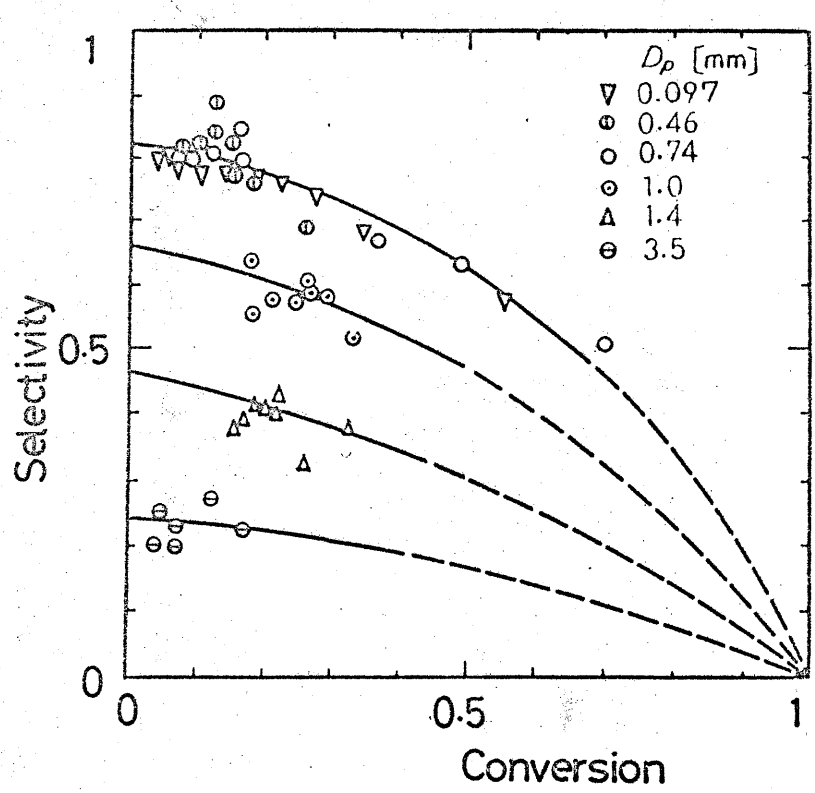

Fig.2-6 Selectivity vs. Caonversion

(Different Sized Catalysts)

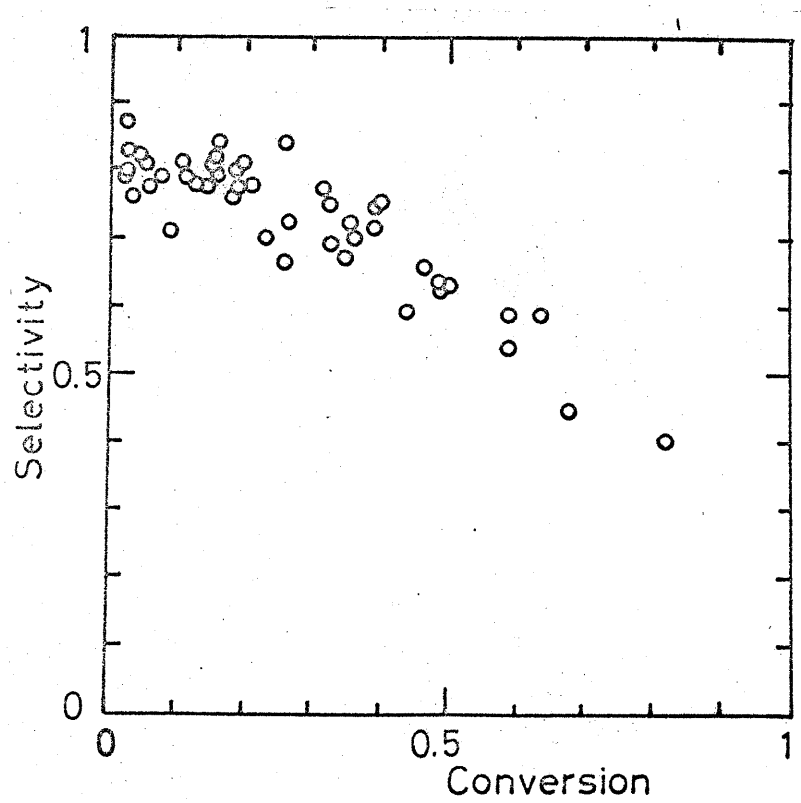

Fig.2-7 Selectivity vs. Conversion

(Different Values of Contact Time, D_p = 0.46 mm.)

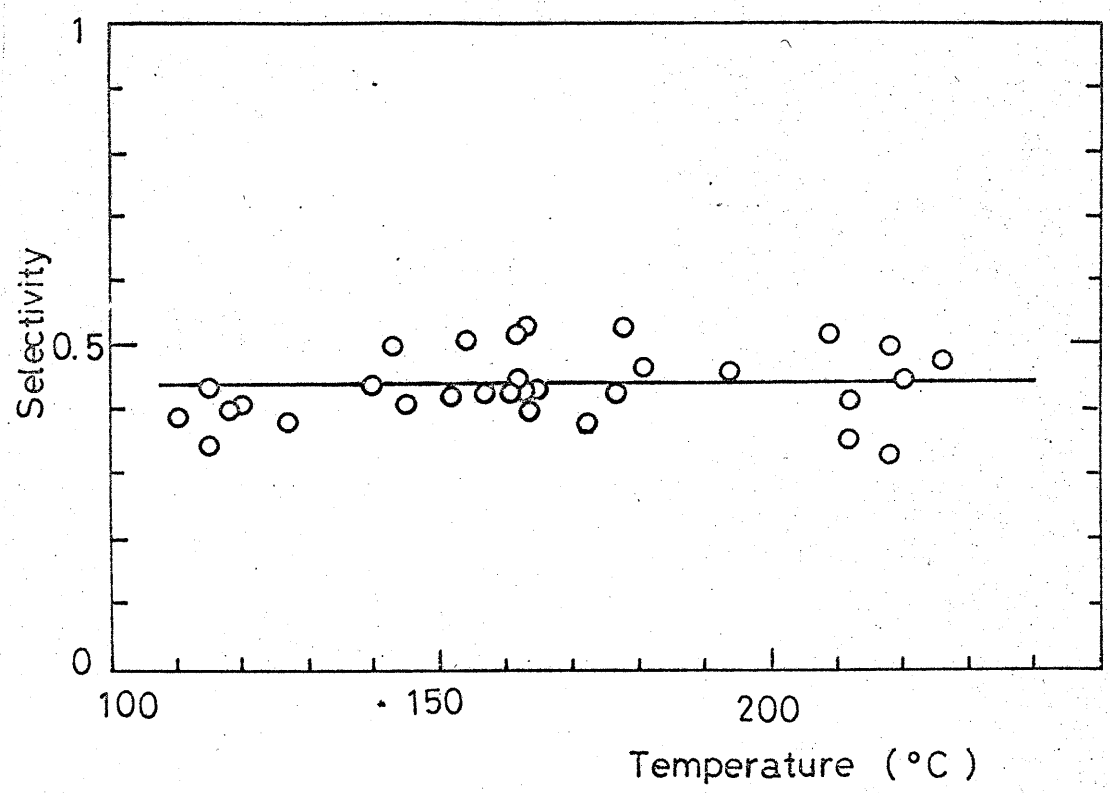

Fig.2-8 Dependency of Selectivity on Reaction Temperature

(D_p = 1.4 mm)

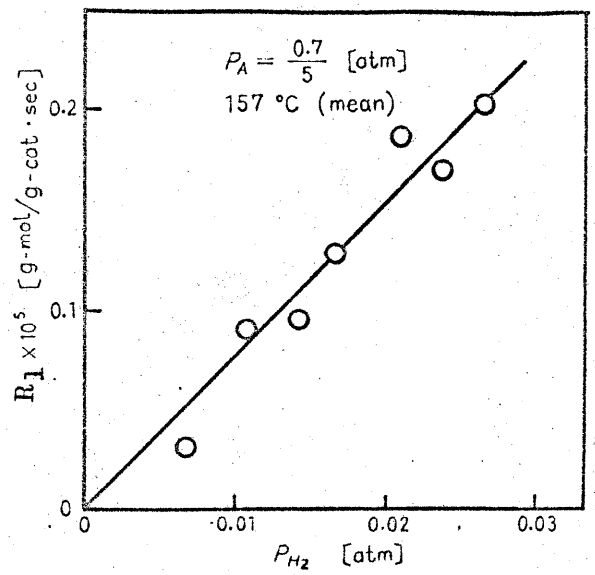

Fig.2-9 R_1 vs. P_{H_2}

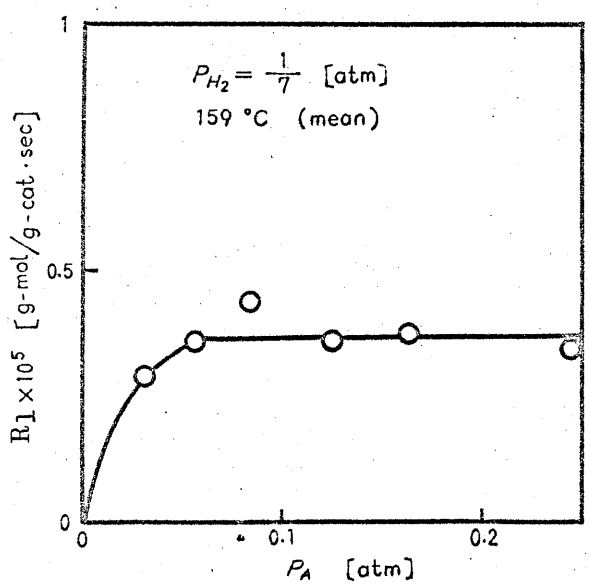

Fig.2-10 R_1 vs. P_A

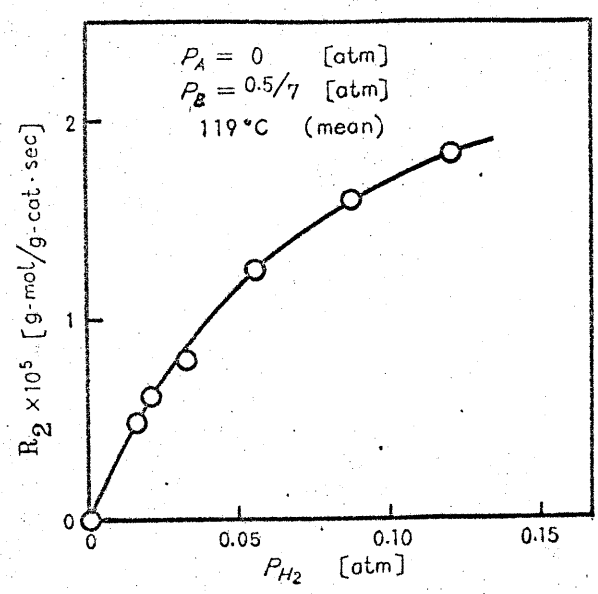

Fig.2-11 R_2 vs. P_{H_2}

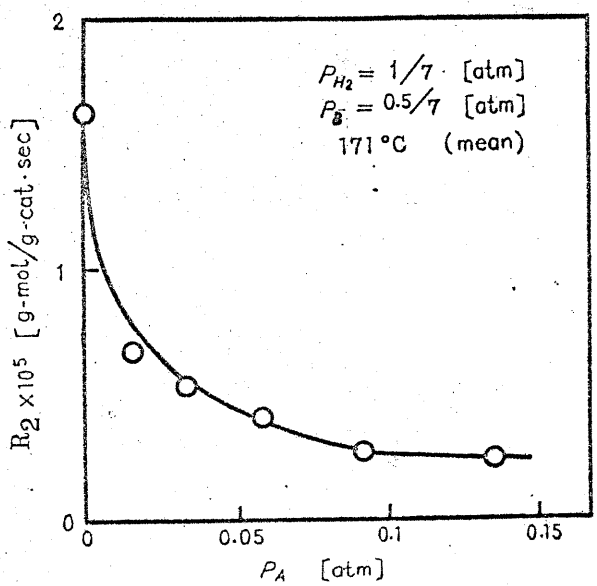

Fig.2-12 R_2 vs. P_A

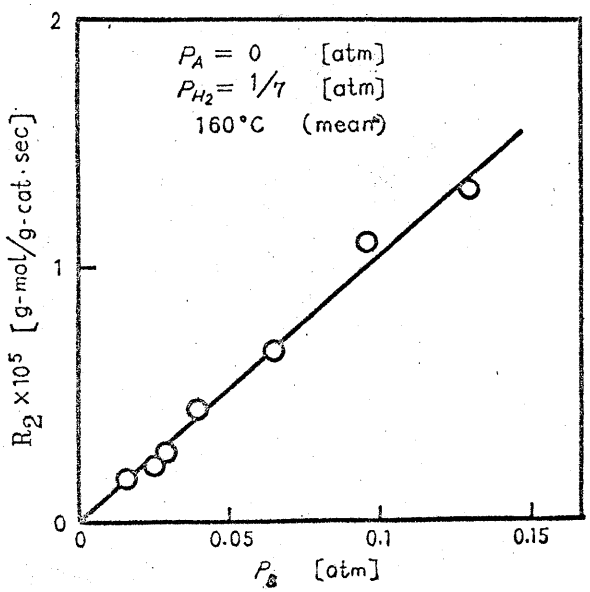

Fig.2-13 R_2 vs. P_B

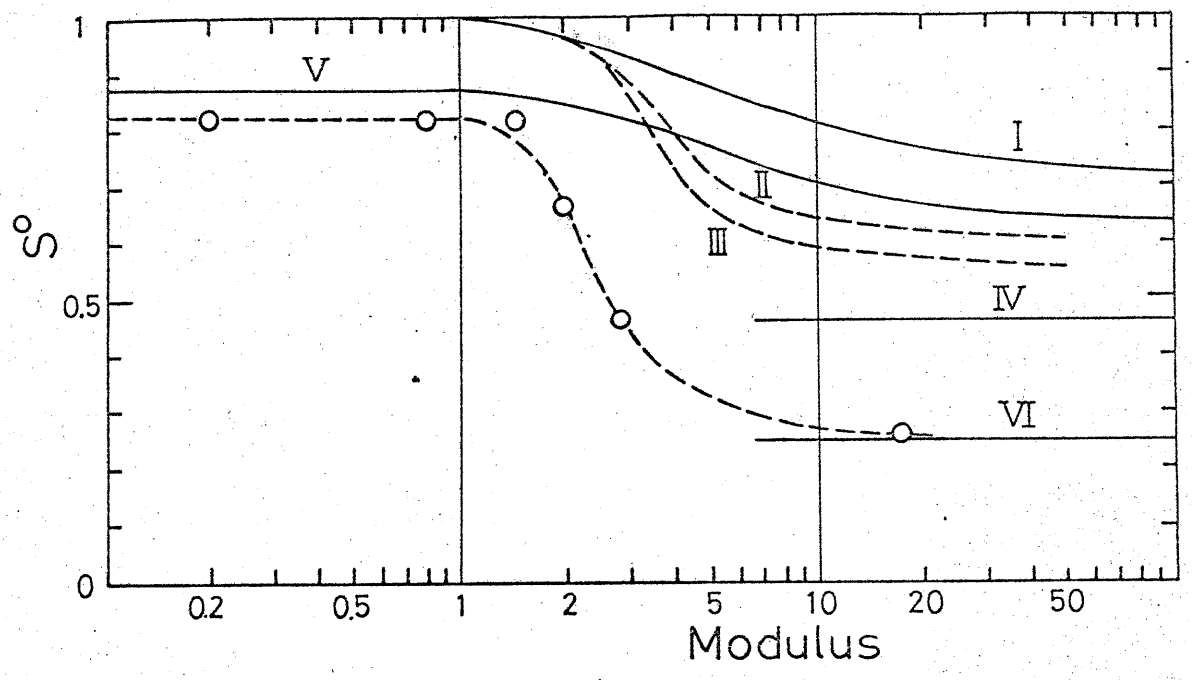

Fig.2-14 S^o vs. Modulus

Moduli for actual catalysts are assumed to be 4R (mm.) and 8R for original cylindrical one.

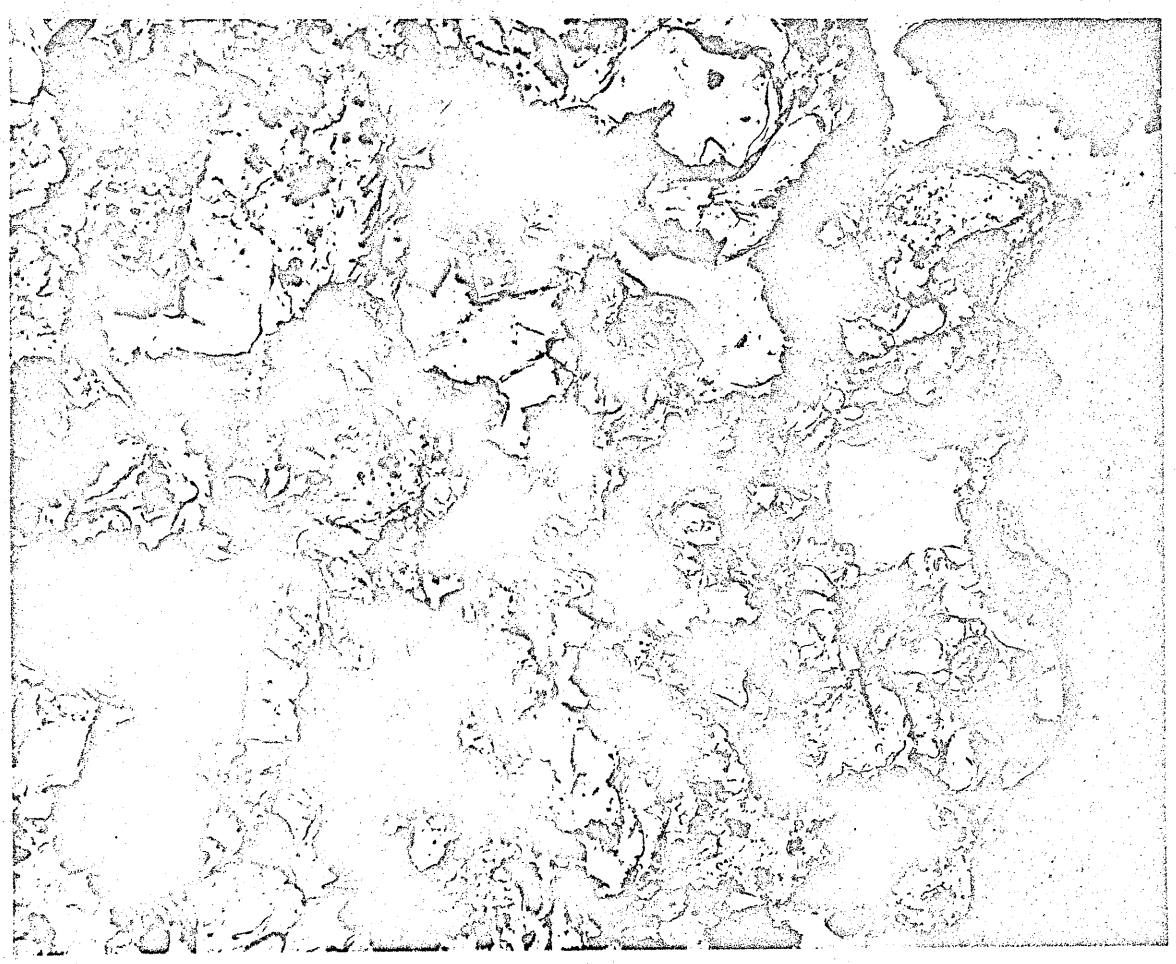

× 4500

1 μ

Photo.1 Photograph of Cross Section of the Catalyst by an Electron Microscope

× 300000

10^3 Å

Photo.2 Photograph of Microparticles by an Electron Microscope

Chapter 3 Selectivity Change with Deactivation of Catalysts

3-1 Introduction

Usual solid catalysts gradually lose their activity in the course of the reaction. Recently, it is being elucidated that the deposition of poisoning species on active sites sometimes casuses deactivation. Poisoning species may be due to the side reactions in parallel or series with a main reaction and it may be the result of the adsorption of impurities involved in a reactant stream. If the deposites are produced by a side reaction in parallel with the main reaction, they will accumulate on the outer shell of the catalyst to a greater extent than the core part of it. Alternately, the formation of poisoning species from some products of the main reaction will lead to preferential deactivation of the core part of the catalyst. In the case that the poisoning species are deposited through an impurity in the feed to the reactor, the number of the active sites may decrease uniformly throughout the catalyst, if the diffusion rate is fast enough compared to the poisoning reaction.

While such different mechanisms of deactivation in a catalyst have been a theme of recent research, the attension have been focused on the change in activity in the course of the reaction. It should be noted, however, that selectivity in a complex reaction system may also change with deactivation. Particularly, the selectivity in consecutive reactions is so sensitive to the activity distribution within a catalyst, as will be shown in chapter 5, that the tendency of the selectivity change may be strongly dependent on the deactivation mechanism. The analysis of the selectivity change will greatly contribute to the clarification of the deactivation mechanism and adding to it the structure of a catalyst.

From this point of view, the selectivity change in the hydrogenation of acetylene is investigated in this chapter. The main purposes are

1) to analyze the selectivity change with deactivation experimentally and theoretically and

2) to examine the validity of the micro-macropore model suggested in the preceding chapter, mainly by the behavior of the small catalyst particles of which effectiveness factor is unity.

3-2 Basic Theory

In order to get the outline of the selectivity change with different deactivation mechanisms, the following three models are considered for a two step consecutive reaction system $A \xrightarrow{k_1} B \xrightarrow{k_2} C$.

1) homogeneous poisoning

The rate constants of the reactions decrease uniformly inside a catalyst.

2) shell poisoning

2-a) The shell which has no catalytic activity progresses towards the pellet center.

2-b) The rate constants of the deactivated shell are assumed to be δk_{i0} instead of zero ($0 < \delta < 1$)

3) core poisoning

The core of no catalytic activity grows to the pellet exterior.

Some of these models were applied to a simple reaction by other investigators.[M-2,T-2] It has been found that the shell progressive mechanism approximates deactivation due to the poisoning reaction in parallel with the main reaction and that the core progressive one approximates the case where the poisoning species are formed from a product of the main reaction.

In this analysis, the ratio of the two rate constants are assumed to be unaltered during the deactivation process. This assumption is not a fiction, for example, when the two step reactions take place on the same active sites. The fact that the two steps of the hydrogenation of acetylene were expressed by a single adsorption term may indicate the validity of the assumption for the system.

For a consecutive reaction system governed by a first order law, the mass balance equations in a catalyst characterized by each deactivation model were solved. From the resultant rates of A and B, the process in a back-mix reactor was derived analytically.* The results are shown in Table 3-1. The conversion and the selectivity were expressed by the inner parameters of the catalyst without a description of their time dependency. The change of selectivity in the reactor is determined by the deactivation mechanism, the ratio of the two rate constants and the condition at which the reaction is started (initial modulus m_{10} and initial conversion X_0).

Some examples where

$s = 7$, $X = 0.4, 0.7$ and $m_{10} = 3$

$s = 7$, $X = 0.4, 0.7$ and $m_{10} = 10$

are shown in Figs.3-1 and 2. The thick lines represent the dependences of selectivity versus conversions as deactivation proceeds and the small circles show the starting point of the operation. The thin lines represent the selectivities at different conversions for a non-deactivated catalyst of modulus m_{10}. The difference in the mode of the selectivity change for the different deactivation mechanisms is surprisingly remarkable, in particular for catalysts of a poor effectiveness factor.

The approximation of deactivation due to a poisoning reaction involving the same reactant of the main reaction by shell poisoning model 2-a was examined. For the former case, the two steps of the reactions may be of the following rate expressions.

$$R_1 = \phi\, k_{10}\, P_A \qquad R_2 = \phi\, k_{20}\, P_B \tag{3-1}$$

The activity factor, ϕ, is defined as $\phi = 1 - \alpha C_D$, where C_D is the concentration of the deposits on the interior surface of the catalyst. The rate of the accumulation of the deposits (dC_D/dt) is assumed to be proportional to the partial pressure of the reactant and the activity factor. Namely,

* Detailed derivation is presented in Appendix 4.

$\frac{d}{dt} = -\alpha\left(\frac{dC_D}{dt}\right) \propto \phi P_A$. As a result, the decreasing rate of ϕ is expressed as

$$\frac{d\phi}{dt} = -\phi k_D P_A \qquad (3\text{-}2)$$

The conservation equations in a catalyst, including these rate equations and diffusion, were solved by means of a digital computer. The results are shown in Fig.3-3 together with the selectivity change derived from the shell poisoning model. It is demonstrated that the shell progressive mechanism is a good approximation of deactivation by a reactant of the main reaction.

3-3 Experiments

3-3-1 Equipments

A schematic diagram of the flow system is shown in Fig.3-4, which is similar to that employed in chapter 2 except for some modifications for steady, long and safe operations. The reactor of a stainless steel tube of 10mm. I. D. is heated by a fluidized sand bath and controled within $1^{o}C$.

3-3-2 Catalysts

Two groups of catalyst were employed. One of them was the same as used in chapter 2 and the other was prepared by the same operations for the catalyst of the same brand. The former is named 'old catalyst' and the latter is 'new catalyst'. Their sizes are listed below.

	No.0	No.1	No.2	No.3	No.4	No.5	No.6	
new catalyst	0.2	0.35	0.63	1.26	1.83	2.4	6 × 6	(mm)
old catalyst			0.42		1.0	1.4	3.5 × 3.5	

3-3-3 Measurements of Selectivity and Degree of Deactivation

1.5 gm. of the catalysts was set in the reactor for each experimental run. After preactivating the catalyst under the hydrogen stream in the same way as in chapter 2, reacting gas mixture (C_2H_2 0.03 l/min. H_2 0.06 l/min. N_2 0.6 l/min.) was introduced stepwise to the reactor employing a bypass arrange-

ment, in order to analyze the behavior at the beginning of the operation as precisely as possible. The composition of the effluent gas was determined by means of gas chromatography.

For some interval after the operation started, no hydrocarbon was detected in the effluent gas. Their concentrations increased gradually and the mass balance between the inlet and the outlet gases improved. After such period, which was usually about 15 or 20 min., the material balance was pretty well satisfied. All experimental data were obtained in this stage.

3-4 Experimental results

The results are shown in Figs.3-5 and 6, in terms of the relation between selectivity and the conversion. The thin lines in the figures show the dependency of selectivity on the conversion for the catalyst of constant activity. They were calculated numerically on the basis of the kinetic measurements in chapter 2 and the assumption of a complete mixing in a reactor and of a constant reactant content in the feed gas to the reactor.

The hysteresis of the catalytic behavior may be divided into two types.

Type I (No.4 and 6 of old catalyst as shown in Fig. 3-6)

From the beginning of the operation, selectivity continues to increase with a small decrease in the conversion.

Type II (All the new catalysts in Fig.3-5 and No. 2 and 6 of old catalyst in Fig.3-6)

At the beginning of the operation, the conversion decreases pretty rapidly with a slight decrease in selectivity. When the reaction continues for a long time, the decreasing rate of the conversion becomes slow and selectivity gradually increases.

The tendency of Type I is easily interpreted by considering the natural breaking of the catalyst pellets, which actually happened when this type of deactivation was observed. The increase in the effectiveness factor by reduced

pellet size gives a reasonable explanation to the tendency of Type I.

The breaking of the catalyst pellets usually happened when the reaction temperature was higher than 200°C.

The time history of Type II resembles the curves derived for the shell poisoning mechanism in Figs.3-1 and 2. Some experimental runs to examine the effect of acetylene on deactivation were undertaken. After the catalyst was preactivated, the gas mixture of nitrogen (0.6 l/min.) and acetylene (0.03 l/min.) was supplied to the reactor and then the hydrogenation reaction was started. If the gas mixture was fed for longer than one hour, the catalyst didn't show any appreciable change in their performance with time. This fact possibly indicates that the deactivation process was completed. In these cases, the conversion was very low as expected but the selectivity was higher than those under the ordinary reaction operations. These selectivity and conversion are shown in Figs. 3-5 and 6. At these steady states, the new catalyst No.2 shows the same selectivity as the new catalyst No.1, indicating that the effectiveness factor of the macropore is unity by the decrease in activity.

According to the observation of the preadsorption of acetylene and of the rapid deactivation due to the pretreatment by acetylene, it is concluded that acetylene is the main poisoning species in the system. This conclusion agrees with the shell-progressive mechanism of the deactivation process. Furthermore, it is proved experimentally that the steady state observed in the experiments after the pretreatment with acetylene is the same as the ultimate state of the catalyst deactivated under the ordinary operations.

Thus, the experimental tendency is considered to be explained based on the deactivation of model 2-a. The following discrepancies, however, are noticed, comparing Figs. 3-5 and 6 to Figs.3-1 and 2.

1) In the ultimate state of deactivation, the conversion is not zero and the selectivity is not unity in contrast with model 2-a.

2) In Fig.3-5 (new catalyst) , the value of the conversion at which selectivity begins to increase is larger than that predicted by model 2-a.

3) The selectivity observed experimentally is lower than those predicted by the model based on a simple pore model and linear kinetics.

3-5 Analyses and Discussions

3-5-1 Analyses by Micro-macropore Model

The discrepancies shown above may be attributed to the following reasons, considering the results of chapter 2 and the experiments in this chapter.

1) The hydrogenation reaction follows Langmuir-Hinshelwood type of rate forms.
2) The catalyst is of the micro-macropore structure.
3) The rate constants at the ultimately deactivated state are not zero in contrast with the assumption made for model 2-a.

It is very difficult to discuss these three factors simultaneously because of the nonlinearlity of the rate forms. First, the effects of 2) and 3) are discussed.

Owing to the third discrepancy, model 2-b should be applied to this system. For a catalyst of small size (new catalyst No.0 and 1, old catalyst No.2), the macropore effectiveness factor is unity. Therefore, the results of the basic analysis is reasonably applied to the process in their microparticles. Curve I in Fig.3-7 and Curve III in Fig.3-8 show respectively the examples in which the parameters are

$$(\mu_{10} = 10, \ X_0 = 0.4, \ \delta = 1/9) \text{ and } (\mu_{10} = 3, \ X_0 = 0.4, \ \delta = 1/9).$$

These curves closely resemble the experimental results of new catalyst No.1 and old catalyst No.2, though the abolute values of experimental selectivity are a little lower because of the difference in the rate forms.

For the catalysts of larger size, the macropore process must be considered together with the micropore. The exact conservation equations for the micro-macropore model, however, are so difficult to solve that an approximated treatment is carried out. That is, deactivation in macropore of the catalyst of very large modulus was assumed to proceed as a shell-progressive type. Based on the approximation, the catalyst is consisted of the two parts, one of which is the poisoned shell containing the ultimately deactivated microparticles and the other is the core part containing non-deactivated microparticles.

The mass balance equations for this simplified micro-macropore model can be solved analytically. The resultant relation between the selectivity and the conversion for a back-mix reactor is represented as*

$$X = \frac{\tau \varepsilon k_{10} \eta_1 E_{f1}}{1 + \tau \varepsilon k_{10} \eta_1 E_{f1}}$$

$$S = \frac{1}{1 + \frac{X}{1 - X} \frac{1}{s E_f}} \quad \frac{s - 1/E_f}{s - 1}$$

Examples of the results are expressed by Curve II in Fig.3-7 and Curve IV in Fig.3-8, in which the parameters are respectively

$$(\mu_{10} = 10, \ m_{10} = 10, \ \delta = 1/9) \text{ and } (\mu_{10} = 3, \ m_{10} = 10, \ \delta = 1/9).$$

The initial conversion X_0 was determined by the same contact time in the reactor as Curve I or Curve III. The intermediate region of macropore modulus, $1 < m_1 < 10$, is difficult to be discussed precisely. However, it is supposed that the time change of the catalysts in such region may fall on the hatched region in Figs.3-7 and 8.

* Detailed derivations are presented in Appendix 5.

Beacause the curves in each figure were obtained for a definite value of the modulus of microparticles, it is clearly shown that the diffusion process in macropore exerts a significant influence on the deactivation process. Furthermore, the effect of macropore is dependent on the value of the miropore modulus. When the micropore modulus is large, the difference in the time change with or without the macropore effect becomes small and vice versa. For example, the time change for diffrent size catalysts of the small value of the micropore modulus ($\mu_{10} = 3$) will be observed in the hatched region between Curves III and IV in Fig.3-8. On the other hand, the time change for the large value of the micropore modulus ($\mu_{10} = 10$) will be observed in the narrow region between Curves I and II in Fig.3-7.

As shown in Figs.3-5 and 6, the behaviors of the new catalyst group and the old catalyst one are quite different from each other. It may be stated that the new catalyst group corresponds to Fig.3-7 and the old catalyst group to Fig.3-8.

Old catalyst No.4 didn't show the decrease in selectivity at the beginning of the operation in contrast with Curve IV. The process may be too rapid to be detected experimentally.

Though the above analysis is qualititative, the coincidence in the tendency of deactivation, Fig.3-5 and Fig. 3-7 or Fig.3-6 and Fig.3-8, shows that the deactivation process of this catalytic system is approximately expressed by the modified shell poisoning model on micro-macropore diffusion.

3-5-2 Computational Analyses of Microparticle Process

To discuss the mechanism more precisely, numerical analyses by means of a digital computer was carried out. The analysis on the micro-macropore diffusion process requires too long computational time. The time change of new catalyst No.1 and old catalyst No.2, in which the effect of macropore diffusion is negligible, was simulated computationally.

Since the deactivation of this catalytic system was proved to be due to the adsorption of acetylene, the poisoning mechanism by a reactant is applied. The rate expressions taking the poisoning on the interior surface of the catalyst into consideration was assumed to be expressed as follows.

$$R_1 = \frac{\phi\, k_{10}\, P_A}{1 + K_A P_A}, \qquad R_2 = \frac{\phi\, k_{20}\, P_B}{1 + K_A P_A} \tag{3-3}$$

$$\frac{d\phi}{dt} = -\frac{\phi\, k_D P_A}{1 + K_A P_A} \tag{3-4}$$

$$\begin{aligned} &\text{at } t = 0 \quad \phi = 1 \\ &\quad t > 0 \quad \phi \geq \delta \end{aligned} \tag{3-5}$$

Eq.(3-5) is obtained in the same manner as Eq.(3-2), on the assumption that the poisoning species is produced from adsorved acetylene.

The conservation equations in a back-mix reactor packed with the catalyst governed by the above rate equations are written as follows. The assumption of a back-mix reactor may approximate well the experimental condition where the bed of these small catalysts was very thin and fluidized.

$$D_K \left(\frac{d^2 P_A}{dr^2} + \frac{2}{r}\frac{dP_A}{dr} \right) = R_1 \tag{3-6}$$

$$D_K \left(\frac{d^2 P_B}{dr^2} + \frac{2}{r}\frac{dP_B}{dr} \right) = -R_1 + R_2 \tag{3-7}$$

$$\begin{aligned} &\text{at } r = 0, \quad \frac{dP_A}{dr} = \frac{dP_B}{dr} = 0 \\ &\text{at } r = L \quad P_A = P_{AS} \quad \text{and} \quad P_B = P_{BS} \end{aligned} \tag{3-8}$$

$$F\,(P_{AI} - P_{AS}) = \varepsilon W \frac{3}{L} D_K \left.\frac{dP_A}{dr}\right]_{r=L} \tag{3-9}$$

$$F\, P_{BS} = -\varepsilon W \frac{3}{L} D_K \left.\frac{dP_B}{dr}\right]_{r=L} \tag{3-10}$$

These equations are reduced to dimensionless forms as

$$\frac{d^2 a'}{d x^2} + \frac{2}{x}\frac{da'}{dx} = \mu_{10}^2 \frac{1 + K_A P_{AI}}{1 + K_A P_{AI}\, a'} \phi a' \tag{3-11}$$

$$\frac{d^2 b'}{d x^2} + \frac{2}{x}\frac{db'}{dx} = -\mu_{10}^2 \frac{1 + K_A P_{AI}}{1 + K_A P_{AI}\, a'} \phi a' + s'\mu_{10}^2 \frac{1 + K_A P_{AI}}{1 + K_A P_{AI}\, a'} \phi b' \tag{3-12}$$

$$X = \tau_c \left.\frac{da'}{dx}\right]_{x=1} \tag{3-13}$$

$$SX = -\tau_c \left.\frac{db'}{dx}\right]_{x=1} \tag{3-14}$$

$$\text{at } x = 0 \quad \frac{da'}{dx} = \frac{db'}{dx} = 0$$

$$\text{at } x = 1 \quad a' = 1 - X \quad \text{and} \quad b' = SX \tag{3-15}$$

where $a' = P_A / P_{AI}$, $b' = P_B / P_{AI}$, $x = r/L$, $\mu_{10} = L\sqrt{\dfrac{k_{10}}{D_K(1+K_A P_{AI})}}$ and $\tau_c = \dfrac{3\varepsilon W D_K}{F L^2}$

(3-16)

The parameters determining the deactivation process are initial mosulus of microparticle μ_{10}, ratio of the two rate constants s', the relative activity at the final state of deactivation to the initial activity δ, the parameter representing the effect of the adsorption $K_A P_{AI}$ and τ_c relating time in the reactor. The use of the initial conversion X_0 instead of τ_c is more convenient for the comparison of the computations with the experiments. The rate constant of the poisoning reaction k_D doesn't exert any effect on the relation of selectivity to the degree of deactivation.

X_0, s and $K_A P_{AI}$ were determined from the experimental results and conditions. At the initial state, catalytic activity is uniform within the microparticles so that it is possible to determine the modulus at the state from the thin lines in Figs.3-5 and 6. δ was so determined that the initial and final conversions

satisfy the relation of the effectiveness factor to the modulus.

The parameters used for the computations are as follows.

	10	X_0	
a. new catalyst No.1 (150°C)	15	0.35	1/9
b. new catalyst No.1 (200°C)	20	0.42	1/20
c. old catalyst No.2 (150°C)	2.5	0.35	1/5

The obtained results are I, II and III as shown in Fig.3-9. Though the coincidence between the experiments and the calculated results is not so complete, it is enough to prove the rationality of the model employed here. Furthermore, the obtained moduli 15 and 20 for the cases of a and b show the reasonable tendency that the modulus of the same microparticle is greater at the elevated temperature due to the increase in the rate constant.

In the above computations, there yet remains uncertainty with the initial and the final state. It is very difficult to get experimentally the true initial state because of the transient phenomenon at the beginning of the operation. Furthermore, the true final state may be different from the observed one because it possibly takes a very long time to reach the state as shown by the computations. New computations assuming appropriate initial states were carried out. The corrected parameters are listed below.

a. new catalyst No.1 (150°C)	9	0.42	1/12
b. new catalyst No.1 (200°C)	10	0.48	1/25
c. old catalyst No.2 (150°C)	3	0.4	0.15

The calculated results on these parameters almost perfectly with the experimental results.

Thus, the modulus of the microparticles was obtained numerically and the moduli of the same kinds of catalyst were proved to be different with the two different baiches. The most interesting to note is that the difference in the initial selectivity and the tendency of the selectivity change with deactivation between these two batches is explained simultaneously and quantitatively by taking into account the mass transfer process inside the microparticles. This fact possibly proves the rationality of the micro-macropore model.

3-6 Summary

On the basis of the experiments and the analyses described in this chapter/, the following facts were clarified.

1) The deactivation mechanism inside a catalyst pellet has a strong effect on the selectivity change with time. Particularly, the effect is remarkable for a catalyst of a poor effectiveness factor.

2) In the hydrogenation of acetylene on the nickel catalyst, the observed selectivity change with deactivation resembles that predicted from the shell poisoning model. Some discrepancies, however, were noticed. They are explained comprehensively by considering the micro-macropore model and Langmuir-Hinshelwood types of rate expression, instead of the simple pore model and first order rate expressions.

3) Two different batches of the same nickel catalyst show the different tendencies of selectivity with deactivation. This difference is the result of the different moduli of their microparticles.

Supplement

In chapter 2, the effect of deactivation was not taken into cinsideration. The analysis of this chapter showed that the catalyst used in chapter 2 (old catalyst group) has a small mosulus of microparticles. Therefore, the change in selectivity with deactivation may not influence significantly on the relation of selectivity to the conversion. It doesn't exert any appreciable effect for the small catalyst particles. On the other hand, catalysts of a large modulus of macropore will behave as Curve IV in Fig.3-8 so that the selectivity observed in the experiments may correspond to the bottom of the curve. For, the initial decrease in selectivity is rather rapid compared to the succeeding increasing process. These consideration may make it clear the discrepancy stated in chapter 2 that the selectivity of No.5 or 6 is too small in comparison with the theoretical minimum value under the condition that K_A , μ_1 and m_1 are very large.

When the small modulus of the old catalyst group is considered, it may not lead to appreciable errors to use the value of s or K_A measured in chapter 2 as an intrinsic one. The analyses in chapter 3 was based on this consideration. Furthermore, this is supported by the close agreement of the experimental results in Fig.2-7 with the predicted curve shown in Fig.2-7'. The curve was calculated numerically on these values of s and K_A and the operation condition in chapter 2. In this calculation, the simple pore model was properly applied to this small catalyst.

Table 3-1 Change in Selectivity and Conversion in a Back-Mix Reactor

Deactivation model	Conversion and selectivity	Parameters
1. homogeneous poisoning 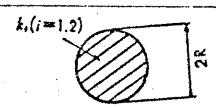	$X=\frac{\tau k_1 E_{H1}}{1+\tau k_1 E_{H1}}$ $S=\frac{1}{1+\frac{X}{1-X}\cdot\frac{1}{sE_H}}\cdot\frac{s-1/E_H}{s-1}$	$E_{Hi}=\frac{3}{m_i}\left(\coth m_i-\frac{1}{m_i}\right)$ $E_H=\frac{E_{H1}}{E_{H2}}$ $m_i=R\sqrt{\frac{k_i}{D}}$
2. shell poisoning 2-*a* 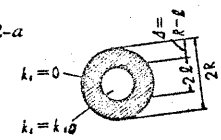	$X=\frac{\tau k_{10} E_{Sa1}}{1+\tau k_{10} E_{Sa1}}$ $S=\frac{1}{1+\frac{X}{1-X}\cdot\frac{1}{sE_{Sa}}}\cdot\frac{s-1/E_{Sa}}{s-1}$	$E_{Sai}=\frac{\left(\frac{l}{R}\right)^3 E_{il}}{\frac{m_{il}^2}{3}E_{il}\left(1-\frac{l}{R}\right)+1}$ $E_{il}=\frac{3}{m_{il}}\left(\coth m_{il}-\frac{1}{m_{il}}\right)$ $m_{il}=l\sqrt{\frac{k_{i0}}{D}}$ $E_{Sa}=\frac{E_{Sa1}}{E_{Sa2}}$
2-*b* 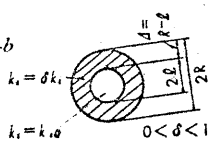	$X=\frac{\tau k_{10} E_{Sb1}}{1+\tau k_{10} E_{Sb1}}$ $S=\frac{1}{1+\frac{X}{1-X}\cdot\frac{1}{sE_{Sb}}}\cdot\frac{s-1/E_{Sb}}{s-1}$	$E_{Sbi}=\frac{3m_i'}{m_{i0}^2}\left\{\frac{\left(\frac{m_{il}^2}{3}E_{il}+1\right)\cosh(m_{iJ}')+m_{il}'\sinh(m_{iJ}')}{\left(\frac{m_{il}^2}{3}E_{il}+1\right)\sinh(m_{iJ}')+m_{il}'\cosh(m_{iJ}')}-\frac{1}{m_i'}\right\}$ $m_{i0}=R\sqrt{\frac{k_{i0}}{D}}$ $m_i'=R\sqrt{\frac{\delta k_{i0}}{D}}$ $m_{iJ}'=(R-l)\sqrt{\frac{\delta k_i}{D}}$ $m_{il}'=l\sqrt{\frac{\delta k_{i0}}{D}}$ $E_{Sb}=\frac{E_{Sb1}}{E_{Sb2}}$
3. core poisoning 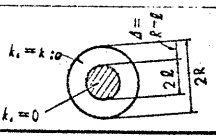	$X=\frac{\tau k_{10} E_{C1}}{1+\tau k_{10} E_{C1}}$ $S=\frac{1}{1+\frac{X}{1-X}\cdot\frac{1}{sE_C}}\cdot\frac{s-1/E_C}{s-1}$	$E_{Ci}=\frac{3}{m_{i0}}\left\{\frac{\cosh(m_{iJ})+m_{il}\sinh(m_{iJ})}{\sinh(m_{iJ})+m_{il}\cosh(m_{iJ})}-\frac{1}{m_{i0}}\right\}$ $m_{iJ}=(R-l)\sqrt{\frac{k_{i0}}{D}}$ $E_C=\frac{E_{C1}}{E_{C2}}$

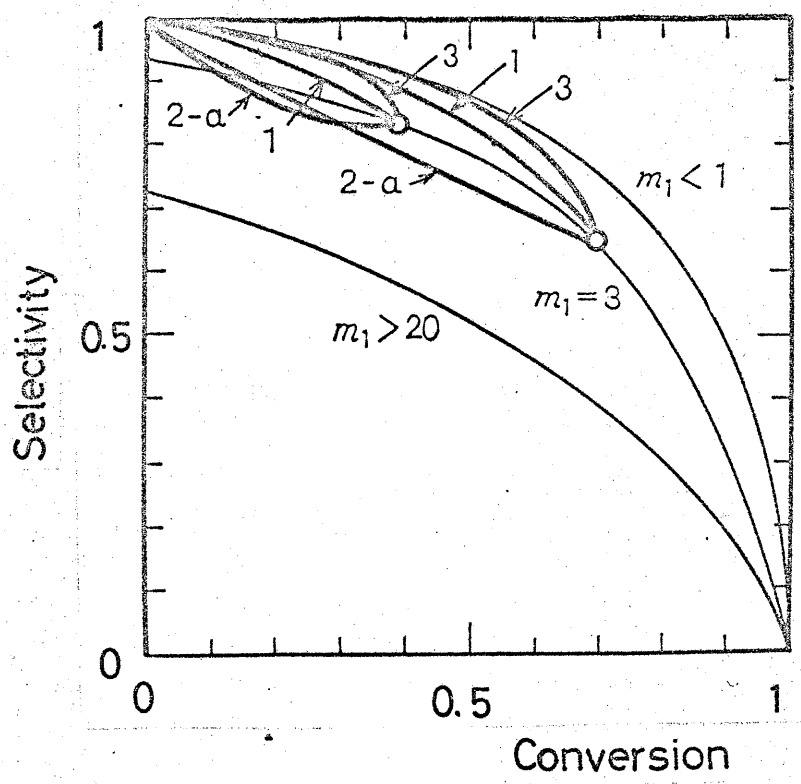

Fig.3-1 Change in Selectivity and Conversion with Deactivation

(m_{10}= 3, X_0= 0.4 and 0.7, s= 7)

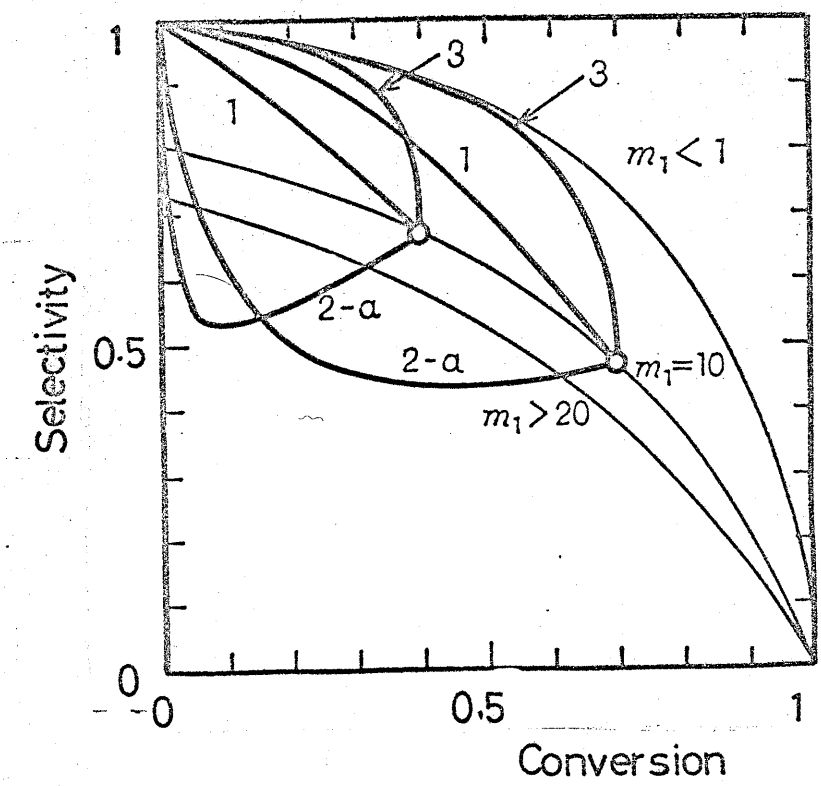

Fig.3-2 Change in Selectivity and Conversion with Deactivation

(m_{10}= 10, X_0= 0.4 and 0.7, s= 7)

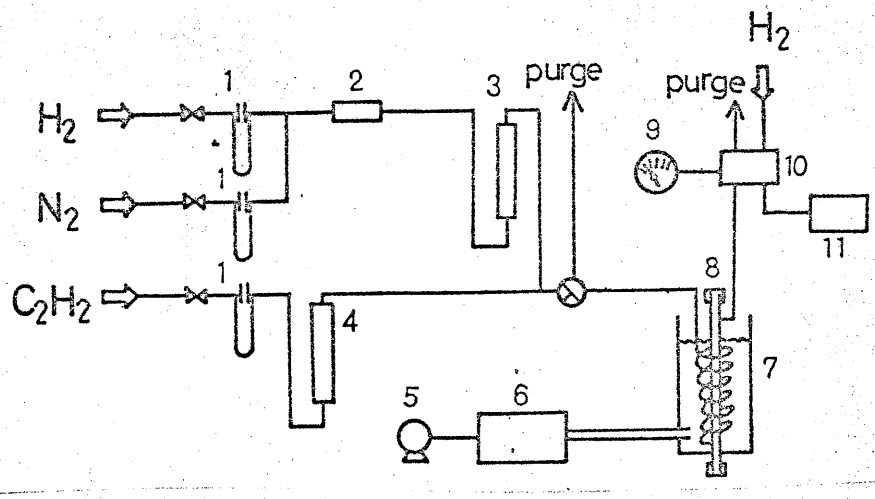

Fig.3-4 Schematic Diagram of Flow System

1	flow meter	7	fluidized sand bath
2	oxygen removal furnace	8	reactor
3	Al_2O_3	9	timer
4	soda lime and $CaCl_2$	10	auto gas sampler
5	blower	11	gas fracto-meter
6	pre-heater		

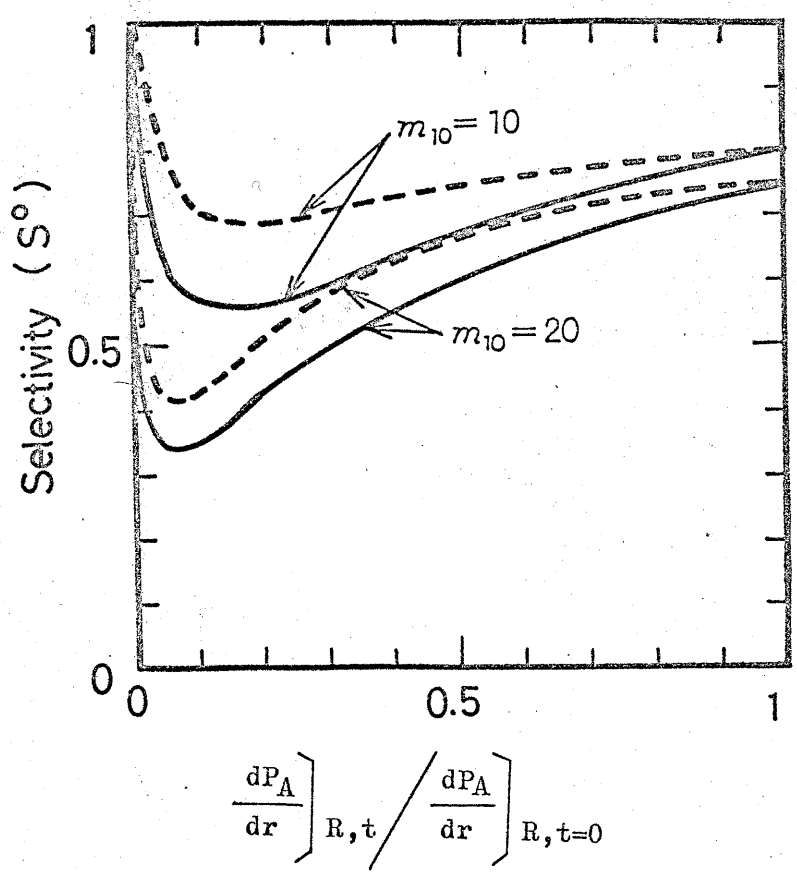

Fig.3-3 Comparison between Shell Poisoning Model (2-a) and Reactant Poisoning Model

--- reactant poisoning

—— shell poisoning

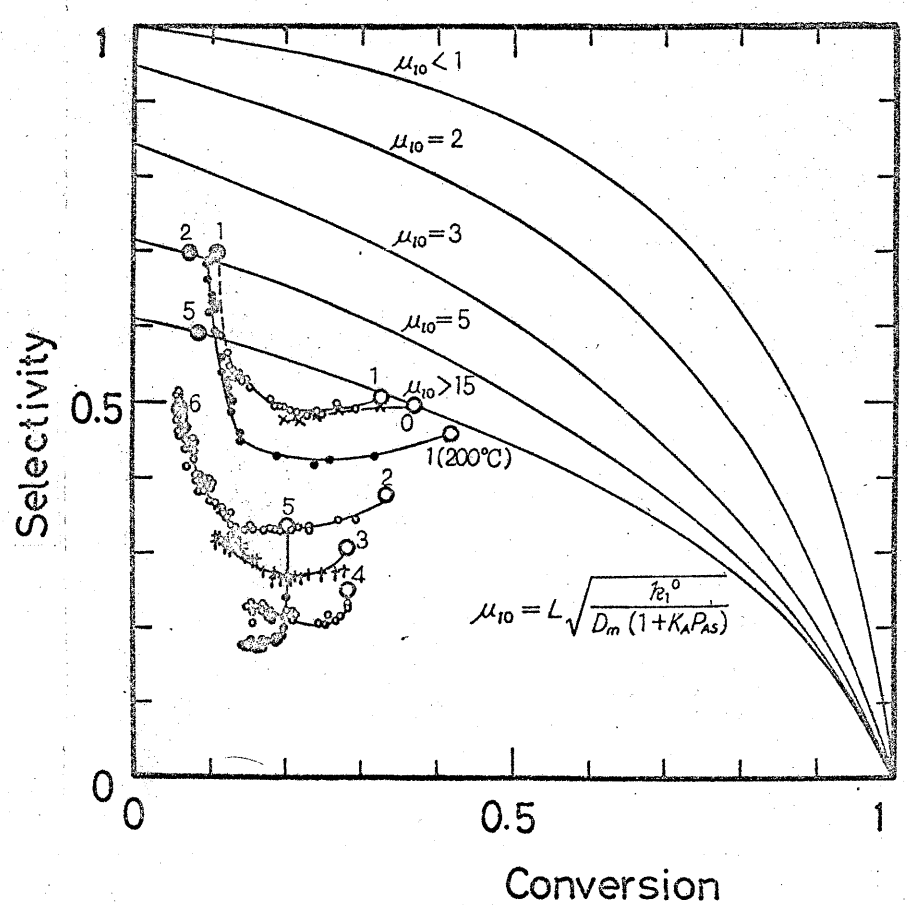

Fig.3-5 Change in Selectivity and Conversion with Deactivation

(new catalyst group, reaction temperature = 150°C)

$\overset{i}{\bigcirc}$ initial state of operation

$\overset{i}{\bigcirc}$ ultimate state of deactivation, measured by the pre-treatment with acetylene

superscript i reffers to No.i catalyst

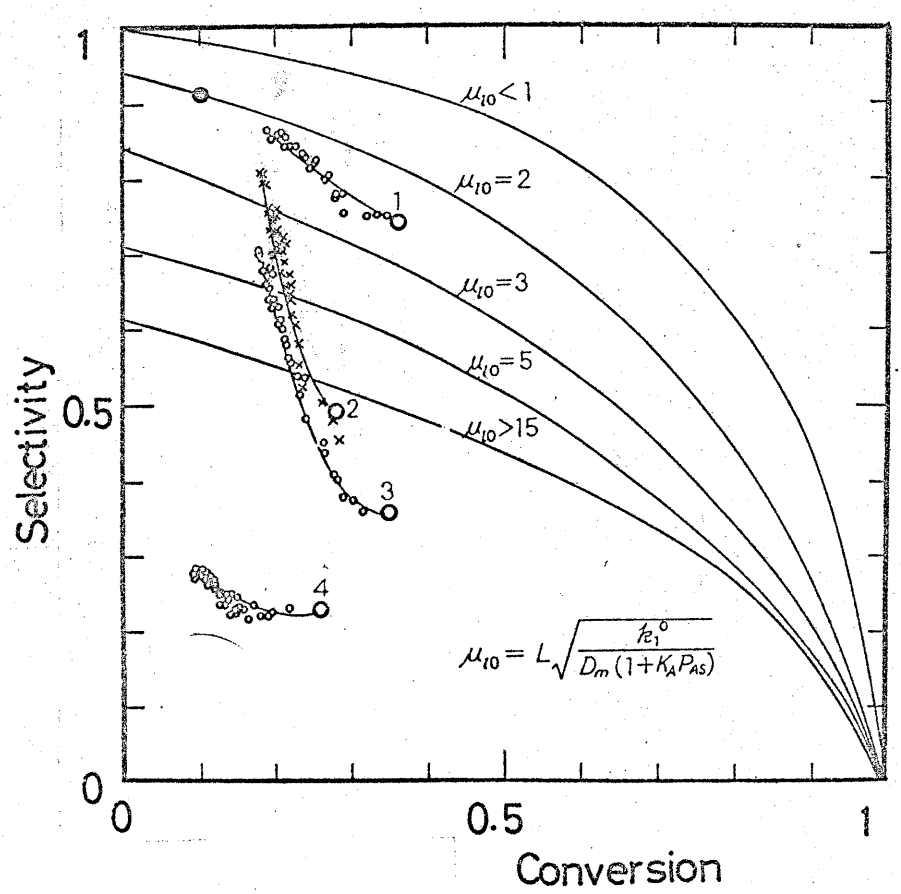

Fig.3-6 Change in Selectivity and Conversion with Deactivation

(old catalyst group, reaction temperature ≒ 150°C)

○ ^{i} initial state of operation

● ^{i} ultimate state of deactivation, measured by the pre-treatment with acetylene

superscript i reffers to No.i catalyst

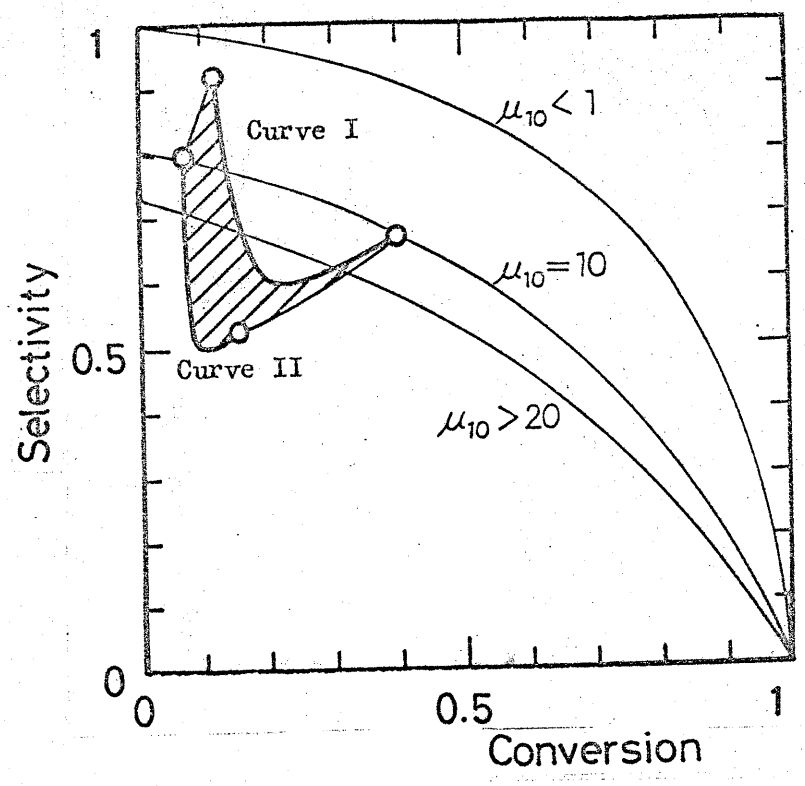

Fig.3-7 Change in Selectivity and Conversion for Different Sized Catalysts of the Same Modulus of Microparticles ($\mu_{10} = 10$)

Curve I ($m_{10} \leq 1$, $\delta = 1/9$), Curve II ($m_{10} = 10$, $\delta = 1/9$)

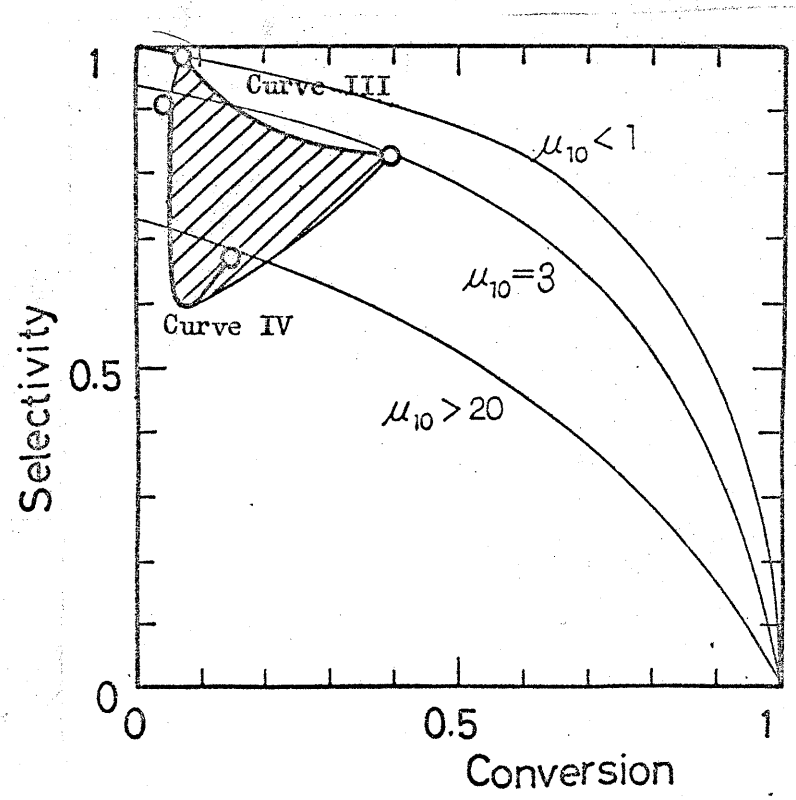

Fig.3-8 Change in Selectivity and Conversion for Different Sized Catalysts of the Same Modulus of Microparticles ($\mu_{10} = 3$)

Curve III ($m_{10} \leq 1$, $\delta = 1/9$), Curve IV ($m_{10} = 10$, $\delta = 1/9$)

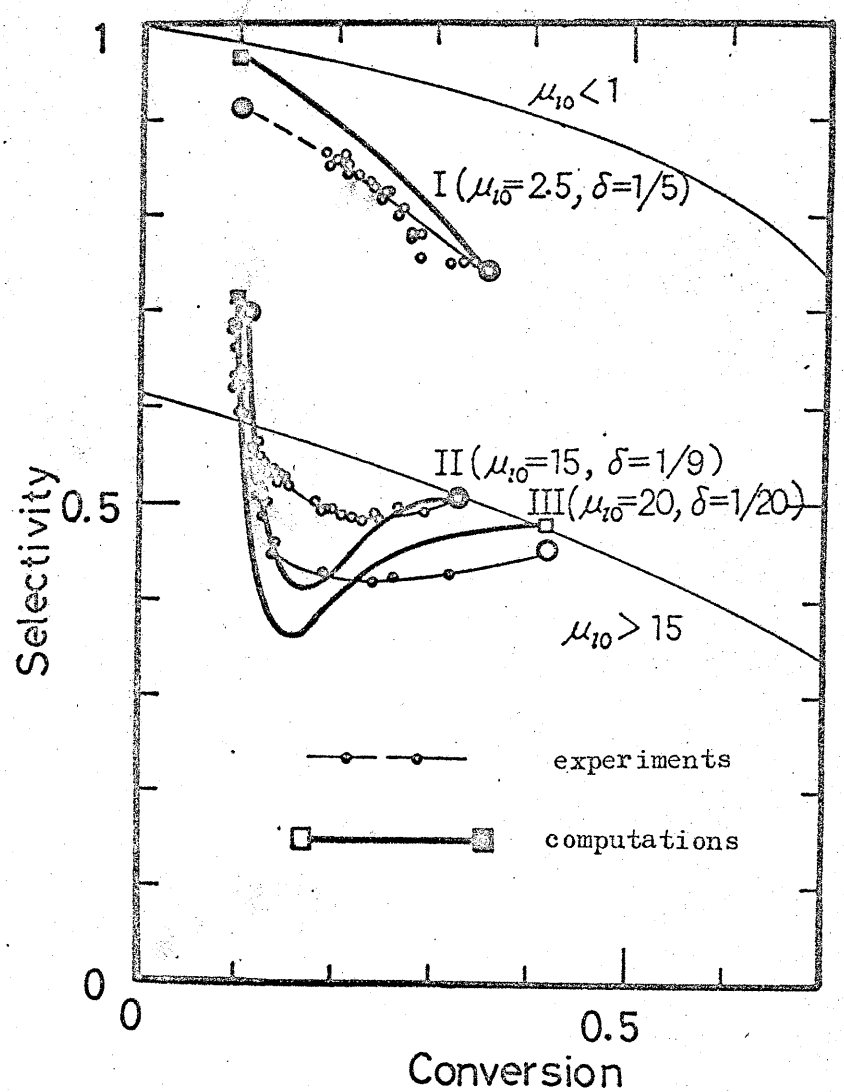

Fig.3-9 Comparison between Computational Results and Experimental Ones for Small Sized Catalysts

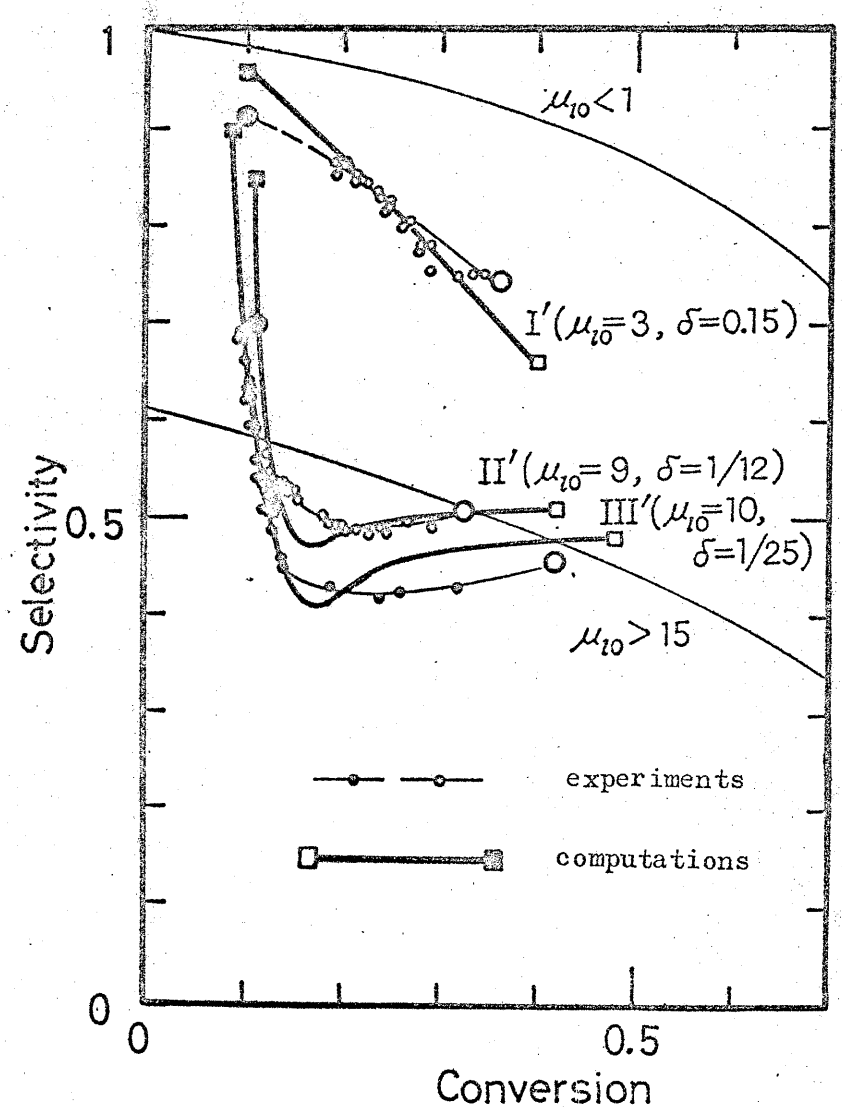

Fig.3-10 Comparison between Computational Results and Experimental Ones for Small Sized Catalysts

Chapter 4 Comparison of the Micro-macropore Model to the Other Catalytic Reaction Model

Analysis of the Synthesis of Ethylene Oxide

4-1 Introduction

For many years, much effort has been expended on the analysis of solid catalyzed complex reactions. Such analyses are based on certain assumptions for the scheme of the reaction system and the structure of the catalyst. It is usual that various kinds of combinations of parallel and consecutive reactions are assumed, not taking the mass transfer effect into account. On the other hand, the complicated behavior of the selectivity in the hydrogenation of acetylene has been analyzed systematically on the basis of the micro-macropore model and a consecutive reaction system, as has been shown in chapters 2 and 3. Some parts of the experimental results may be explained by the other model for the reaction scheme, that is, a parallel and consecutive reaction system, instead of the mass transfer effects on a two-step consecutive reaction system. Such phenomenological analysis, however, cannot lead to the interpretation of the true mechanism and the improvement of selectivity. While it was pointed out by a few investigators that an intraparticle mass transfer affects selectivity in consecutive reactions, one of the most important aspects of it has been overlooked so far. That is, its effect upon the apparent reaction scheme. A deeper insight into complex catalytic reactions will be gained when the relation between the model used for the analysis of the measured kinetics and the significance of the derived system parameters are taken into consideration.

In this chapter, the following three catalytic reaction models, all of which are characterized by the apparent scheme of parallel and consecutive reactions, are analyzed and compared to one another.

1) a micro-macropore model and a consecutive reaction system
2) a simple pore model and a consecutive and parallel reaction system

3) a consecutive and parallel reaction system, not taking the mass transfer effects into account.

In the first place, it is demonstrated that the relation of selectivity to conversion derived from the models are quite equivalent in their forms so that the coincidence of the experimental results with the estimated ones doesn't prove the rationality of the model. A detailed evaluation of the mass transfer process is necessary to reach a conclusion.

Next, the criteria by which the applicability of the micro-macropore model is examined are proposed. The criteria are applied to the synthesis of ethylene oxide by a silver catalyst, which has been considered to be a typical consecutive and parallel reaction system by many investigators.

4-2 Basic Theory

The relation between selectivity of an intermediate product and the conversion of a reactant, the extrapolated selectivity at $X = 0$ and the apparent reaction rate constant are derived for each model. The assumption made common to the models are as follows:

1) First order irreversible reactions with no volume change take place under an isothermal condition.
2) The reactor in which the reaction proceeds is of plug flow type.
3) The catalyst pellet is spherical, though this assumption has nothing to do with the third model.

Model 1

A consecutive reaction system and a micro-macropore model

The details of the micro-macropore model has been given in chapters 2 and 3 for the supported nickel catalyst. The catalyst pellet is a porous carrier material in which small aggregates of fine nickel crystals are dispersed.

The porous structure of the carrier material is correspondent to the macropore and the void space between the fine nickel crystals is the micropore. The application of the model may not be restricted to such supported catalyst. It may be applicable to the pelletized catalyst of fine active particles, a carrier material coated by active precipitates and so on.

The results are represented below without detailed derivations.*

Reaction scheme A $\quad A \xrightarrow{k_1'} B \xrightarrow{k_2'} C$

$$S = \frac{(1-X)^{1/\eta E' s'} - (1-X)}{X\,(1 - 1/\eta E' s')} \; \frac{s' - 1/\eta E'}{s' - 1} \tag{4-1}$$

$$S^o = \frac{s' - 1/\eta E'}{s' - 1} \tag{4-2}$$

$$k_{1obs} = \varepsilon\, k_1'\, \eta_1\, E_1' \tag{4-3}$$

Here, $s' = k_1'/k_2'$, $\quad \eta_i = \frac{3}{\mu_i}\left(\coth \mu_i - \frac{1}{\mu_i}\right)$, $\quad \mu_i = L\sqrt{\frac{k_i'}{D_K}}$

$\eta = \eta_1/\eta_2$, $\quad E_i' = \frac{3}{m_i'}\left(\coth m_i' - \frac{1}{m_i'}\right)$,

$$m_i' = R\sqrt{\frac{\varepsilon\, k_i'\, \eta_i}{D_M}} \quad \text{and} \quad E' = E_1'/E_2' \tag{4-4}$$

The system parameters determining the selectivity are the ratio of the two rate constants s', the product of the ratios of the effectiveness factors for the catalyst pellet and the microparticle $\eta E'$ and the conversion of the reactant X. Fig.4-1 shows the relation of the selectivity to the conversion at a constant value of s' (= 16), for different values of $\eta E'$. Curve I is obtained for $\eta E' = 1$ where the catalytic process is safe from the mass transfer effect, so that it gives the maximum selectivity for the model. Curve II, where $\eta E' = 1/4$ $(= 1/s'^{\frac{1}{2}})$, will be observed, for example, when η or E' is $1/s'^{\frac{1}{2}}$ as a result of a significant mass transfer effect and the other is unity. Curve III represents the minimum selectivity for the model, where both micropore

* Detailed derivation is presented in Appemdix 2.

and macropore processes are subject to a significant effect of mass transfer.

S^o depends only upon s' and $\gamma E'$ so that it is regarded as an intrinsic selectivity for a catalyst of definite size. It is shown in Fig.4-2 as a function of m_1', the macropore modulus, for the two limiting cases of the micropore process.

Model 2

a consecutive and parallel reaction system and a simple pore model

The simple pore model assumes that a catalyst is homogeneous in reactivity and diffusibility throughout the whole region. The selectivities and the apparent rate constants are derived in a similar way as shown in Appendix 1.

Reaction scheme B

$$\begin{tikzcd} A \arrow[r, "k_1"] \arrow[rr, bend right, "(1-\gamma)\,k_1"'] & B \arrow[r, "k_2"] & C \end{tikzcd}$$

$$S = \frac{(1 - X)^{1/sE} - (1 - X)}{X\,(1 - 1/sE)} \; \frac{s - 1/E}{s - 1}\,\gamma \tag{4-5}$$

$$S^o = \frac{s - 1/E}{s - 1}\,\gamma \tag{4-6}$$

$$k_{1obs} = k_1 E_1 \tag{4-7}$$

Here, $E_i = \dfrac{3}{m_i}\left(\coth m_i - \dfrac{1}{m_i}\right)$, $\quad m_i = R\sqrt{\dfrac{k_i}{D_e}}$, $\quad s = k_1/k_2$

$$E = E_1/E_2 \tag{4-8}$$

Model 3

A consecutive and parallel reaction system, not taking the intraparticle mass transfer effect into consideration

The apparent reaction rate is taken as an intrinsic rate on the interior surface of a catalyst. The selectivities and the apparent rate constant are

derived from the conservation equations in a reactor.

Reaction scheme B

$$\begin{tikzcd} A \arrow[r, "k_1"] \arrow[rr, bend right, "(1 - \ ) k_1"'] & B \arrow[r, "k_2"] & C \end{tikzcd}$$

$$S = \frac{(1 - X)^{1/s} - (1 - X)}{X\,(1 - 1/s)}\,\gamma \qquad (4\text{-}8)$$

$$S^{o} = \gamma \qquad (4\text{-}9)$$

$$k_{1obs} = k_1 \qquad (4\text{-}10)$$

These three relations between the selectivity and the conversion for the different models, Eqs.(4-1), (4-5) and (4-8) are quite equivalent in their forms to one another. This is also true for the other mixing characteristics in a reactor, though a plug flow reactor was assumed in the above analysis. Therefore, one cannot decide a true reaction mechanism from only the apparent kinetic studies without evaluation of the effect of mass transfer.

To clarify the descroption, an example is shown.

The experimentally measured selectivity as Curve III in Fig.4-1 may be interpreted as the case where $s = 2$ and $\gamma = 0.533$ according to Model 3 or the case where $s = 4$, $E = 1/2$ and $\gamma = 0.8$ according to Model 2. Either interpretaion does never lead to any contradiction. The catalytic system, however , may be the case of $s = 16$ and $\gamma E' = 1/8$ according to Model 1.

Nowadays, various reactions, such as the partial oxidation of ethylene or butadiene, the hydrogenation of acetylene or benzene and so on, are considered to be a consecutive and parallel reaction system according to Model 3. While the diverse values of γ and s have been obtained for the same catalytic system by many investigators, it may be the result of the neglected effect of mass transfer. If it is the case, it will be possible not only to interpret the various

catalytic reactions systematically but also to give a detailed suggestion for the improvement of selectivity. This is the reason why the research in this field is of scientifical and practical importance.

4-3 Criteria by Which the Applicability of Model 1 is Examined

If the selectivities are measured for different sized catalysts or microparticles, the applicability of Model 1 will be examined. But it is sometimes difficult to change the catalyst size and more difficult to control the size of the microparticles. In such cases, the following criteria will give a reasonable proof to the model.

Criterion 1

The selectivities of catalysts of the same kind are in a definite region of the figure of S and X.

According to the model the selectivity with a definite value of s' changes only with the effectiveness factors of macropore and micropore so that it must be in a definite region as shown in Figs 4-1 and 2.

Criterion 2

There exists an obvious quantitative relation between the boundaries of the region or the upper and lower liniting S^0's, and the ratio of the two rate constants experimentally observed.

Fig.4-3 shows the relation of η to μ_1 which is the Thiele modulus for a microparticle. The value of η converges rapidly to a definite value with the increase of μ_1. When the value of μ_1 is larger than 20, the value of η is nearly constant as $1/s'^{\frac{1}{2}}$ independent of the size of the microparticle. In the condition, the ratio of the effectiveness factors in macropore changes from unity to $1/s'\eta^{\frac{1}{2}}$ with the increase of m_1' as shown in Fig.4-3, and the

upper and lower limiting S^o's are given by the following equations.

upper limiting value

(where $E' = E'_{maximum} = 1$)

$$S^o = \frac{s' - s'^{\frac{1}{2}}}{s' - 1} \qquad (4\text{-}11)$$

lower limiting value

(where $E' = E'_{minimum} = 1/s^{\frac{1}{4}}$

$$S^o = \frac{s' - s'^{3/4}}{s' - 1} \qquad (4\text{-}12)$$

The observed rate oconstant ratio s_{obs}, which is derived from k_{iobs} $(= \Sigma k_i' \eta_i E_i')$ given in Appendix 2, is related to the true rate constant ratio s' at the limiting conditions.

$$s_{obs} = \frac{k_{1obs}}{k_{2obs}} = \frac{k_1' \eta_1 E_1'}{k_2' \eta_2 E_2'} = s' \eta E$$

$$= \begin{cases} s'^{\frac{1}{2}} & (\text{ at } E' = 1) \qquad (4\text{-}13) \\ s' & (\text{ at } E' = 1/s') \qquad (4\text{-}14) \end{cases}$$

As a result,

upper limiting value $$S^o = \frac{s_{obs}^2 - s_{obs}}{s_{obs}^2 - 1} \qquad (4\text{-}15)$$

lower limiting value $$S^o = \frac{s_{obs}^4 - s_{obs}^3}{s_{obs}^4 - 1} \qquad (4\text{-}16)$$

Criterion 3

The apparent activation energy of the first step reaction decreases with the decrease in selectivity.

This is easy to understand. Because the decrease in selectivity for the model is caused by the decrease in the effectiveness factor, the apparent activation energy which is also affected by the effectiveness factor is related to selectivity.

In the region stated in criterion 2, $\eta_1 = 3/\mu_1$. Therefore, in the upper limiting case of $E_1' = 1$,

$$k_{1obs} = \varepsilon k_1' \eta_1 E_1' = \frac{3\varepsilon}{L} D_K^{\frac{1}{2}} k_1'^{\frac{1}{2}} \tag{4-17}$$

Consequently,

$$E_{obs} = E_a/2 \tag{4-18}$$

Similarly, in the lower limiting case of $E_1' = 3/m_1'$.

$$k_{1obs} = \frac{3}{R} \frac{\sqrt{3\varepsilon D_M \sqrt{D_K}}}{L} k_1'^{1/4} \tag{4-19}$$

consequently,

$$E_{obs} = E_a/4 \tag{4-20}$$

While the quantitative expressions for criteria 2 and 3 were given for the case of a significant effect of mass transfer for the micropore process, other expressions are possible for different micropore characteristics.

4-4 Analysis of the Synthsis of Ethylene Oxide by the Criteria

Many papers have been published on the direct oxidation of ethylene by air on a silver catalyst . This is because of the vast potentialities of ethylene oxide as an organic intermediate in the chemical industry. In most of the papers the experimental results were analyzed by the simple treatment (Model 3), and the following mechanism, which equivalent to Reaction scheme B, has been proposed.

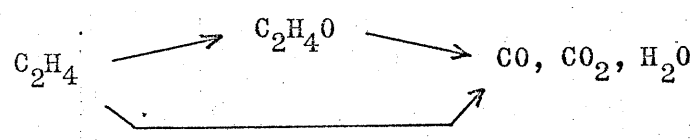

On the basis of the various experimental data, the author wishes to investigate the applicability of Model 1 to this catalytic system. As expected, the direct examination of the applicability is impossible because of the lack of the detailed information concerning the characteristics of the pore structure.

The criteria shown above are of use.

Before the model is applied, it must be proved whether the assumption of first order kinetics is valid for the reaction. According to the results in chapter 5, the dependency of selectivity on the rate forms of reactions is remarkable. The reported rate expressions for the reaction are varied and the slight effect of adsorption of the products were reported by some investigators. The author plotted the data of Kano et al[K-1] and Wan[W-6] and found that a sufficiently good linear relation between the rate of depletion of ethylene and the product of the partial pressures of ethylene and oxygen exists, as shown in Figs.4-4 and 5. When an excess amount of oxygen exists, therefore, the reaction can be regarded as a first order one in respect to the partial pressure of ethylene.

For the oxidation of ethylene oxide, few experimental results have been reported with the exceptions of Andrianova et al.[A-6] and Orzechowski[O-5].

According to Andrianova et al., the rate expression is ,

$$R_2 = -\frac{d\,P_{C_2H_4O}}{d\,\tau} = k_1 P_{C_2H_4O}\,P_{O_2} \qquad (4\text{-}21)$$

According to Orzechowski, it is,

$$R_2 = \frac{A}{1 + a/P_{C_2H_4O} + b/P_{O_2}} \qquad (4\text{-}22)$$

The latter is not a linear function of $P_{C_2H_4O}$ but it may be considered to follow approximately a first order law in the region where the partial pressure of ethylene oxide is small.

The experiments in all the litertures reffered to here were carried out under the existence of an excess amount of oxygen so that the linear kinetics in respect to ethylene and ethylene oxide are good approsimations. Thus, the criteria can be examined without modifications.

The selectivity of the reaction, which is defined as the ratio of ethylene oxide produced to ethylene consumed, is shown in Figs.4-6 and 7. Fig.4-6 involves almost all data except for a high pressure region, which have been put forward by Hirasa.[H-3] In his work, the experiments were carried out throughout a very wide range in respect to the method of making the catalyst, the carrier material, the pretreatment of the catalyst, the operating condition and so on. Fig.4-7 comprised the data of the other investigators.[A-6,K-1,O-1,Y-1,W-6] Almost all data are in a definite region . The upper and lower boundaries of the region may be given by the two lines in the figures, which are equivalent to Curve II and Curve III in Fig.4-1.

Obviously criterion 1 is satisfied.

Next, in order to check the criterion 2, the apparent rate constant ratio must be known. The data of Orzechowski are near the upper boundary and for the condition he obtained the following forms of the rate expression for the first and second reaction steps.

rate expression of the reaction from ethylene to ethylene oxide

$$R_1 = \frac{R_1'}{0.75} = \frac{1}{0.75} \cdot \frac{0.20}{1 + 86/P_{C_2H_4} + 225/P_{O_2}}$$

rate expression of the reaction from ethylene oxide to carbon dioxide

$$R_2 = \frac{0.032}{1 + 90/P_{C_2H_4O} + 270/P_{O_2}}$$

In his experiments, R_1', the formation rate of ethylene oxide at differential conditions, was measured. R_1, the rate of depletion of ethylene, is calculated by dividing R_1' by 0.75 which is the extrapolated selectivity at $X = 0$. As R_1 and R_2 are non-linear functions in respect to the partial pressure of ethylene or ethylene oxide, the apparent rate constants may be changeable with the

degree of the reaction. However, these rates can be regarded as pseudo first order reactions under the existence of a excess amount of oxygen. In the experimental conditions where the feed compositions are

$P_{C_2H_4} = 0.047$ atm (36 mmHg), $P_{C_2H_4O} = 0$ and $P_{O_2} = 0.198$ atm (151 mmHg)

, the ratio of the apparent rate constants is calculated as follows:

$$s_{obs} = \frac{k_{1obs}}{k_{2obs}} = \frac{\frac{1}{0.75} \quad \frac{0.20}{36 + 86 + 225\ (36)/151}}{0.032/\ 90} = 4 \qquad (4\text{-}23)$$

In this condition, where the macropore effectiveness factor E_1' may be regarded as about unity, the ratio is connected with the true rate constant ratio as Eq.(4-13). Therefore,

$$s' = s_{obs}^{\ 2} = 16 \qquad (4\text{-}24)$$

On the other hand, Andrianova et al.[A-6] measured the selectivity corresponding to the lower boundary, Curve III. In his paper, the apparent rate constants are not given but the overall conversion were plotted in the figures. The correlation of the partial pressure and the contact time in a first order reaction is given by

$$P_A/\ P_{AI} = \exp\ (-\ k_1 \tau\ ) \qquad (4\text{-}25)$$

s_{obs} is therefore determined by the following relations.

$$s_{obs} = \frac{k_{1obs}}{k_{2obs}} = \frac{-\ \ln\ (\ P_{C_2H_4}\ /\ P_{C_2H_4,I})/\tau}{-\ \ln\ (\ P_{C_2H_4O}\ /\ P_{\ C_2H_4O})/\tau} \qquad (4\text{-}26)$$

$$s_{obs} = 2.2 \qquad (4\text{-}27)$$

By Eq.(4-14), the true rate constant ratio is,

$$s' = s_{obs}^{\ 4} = 16 \qquad (4\text{-}28)$$

Thus, the calculated true rate constant ratio in the two limiting cases

coindide with each other and they agree with the observed selectivities for the cases, because Curve II and Curve III are correspond to s' = 16. It is concuded that criterion 2 is satisfied.

Criterion 3 is proved to be satisfied by Table 4-1, Where the apparent activation energy was determined by the experimental data in each paper.

The experiments reffered to here are not exactly under the same operating conditions in respect to temperature, the composition of the feed to the reactor and so on, because they are gathered by many investigators. The comparison of the model to the experiments, therefore, is not so accurate. For example though the rate constant ratio was assumed to be a definite malue in the discussion, it may be changeable with temperature because of the difference between the activation energies of the two step reactions. Furthermore, the effect of deactivation and of the mixing characteristics in the reactor are not taken into consideration at all. These may be a reason that some observed data lie out of the region derived from the very simplified assumption made for the model. Anyway, this catalytic system is interpreted comprehensively by a consecutive reaction system under the influence of the mass transfer process in macropore and micropore/.

Table 4-2 shows the predicted values of E' and η for each family of data according to Model 1 and the parameters in the cases of the other two models. It will clarify the difference of Model 1 to the other models.

In Model 1, the difference in selectivity for different conditions is attributed to the effectiveness factor of the macropore, and the maximum selectivity exists owing to a significant effect of mass transfer for the micropore process in this catalytic system. In order to improve the selectivity, the mass transfer resistance in the macropore should be reduced. In model 2, the selectivity also changes with the effectiveness factor of the macropore.

The existence of the maximum selectivity is, however, caused by γ which may be determined by the properties of the catalytic surface itself. In Model 3, the diverse values of the two parameters, and S^o are attributed to the difference in the nature of the catalytic surface.

It is clear that Model 1 explains the selectivity in this catalytic system most systematically. It should be noticed, however, that the analysis given here is not enough to prove the model definitely. To be sure, an intrinsic parallel and consecutive reaction system may exist as a result of the heterogeneity of a catalytic surface or the competition of the desorption and the catalytic reaction of an intermediate product. On the other hand, the rationality of Model 1 has been proved by various experiments on the hydrogenation of acetylene in chapters 2 and 3. Similar approaches are desired for the systhesis of ethylene oxide and various other catalytic systems.

4-5 Summary

1) The relations of selectivity to conversion derived from the three models are quite equivalent in their forms and the apparent consecutive and parallel reaction system doesn't always reflect the true kinetics of a reaction system. A detailed evaluation of mass transfer is required to reach a conclusion.

2) Three criteria are presented, by which the micro-macropore model for a consecutive reaction system is examined. These criteria are useful when the detailed information concerning macropore and micropore are not available.

3) The synthesis of ethylene oxide on a silver catalyst, which was considered to be a parallel and consecutive reaction system by many investigators, was examined. It is demonstrated that the reaction satisfies the all criteria so thatthe apparent consecutive and parallel reaction system may be the result of the mass transfer effect upon a consecutive reaction system.

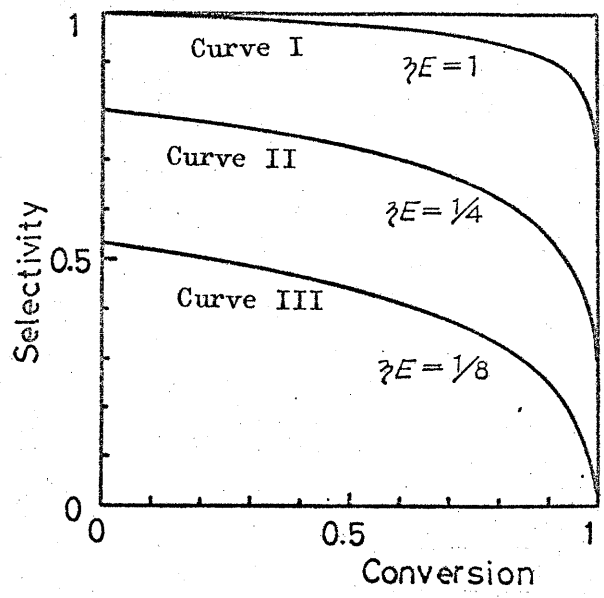

Fig.4-1 Relation between Selectivity and Conversion for a Definite Value of s' (= 16)

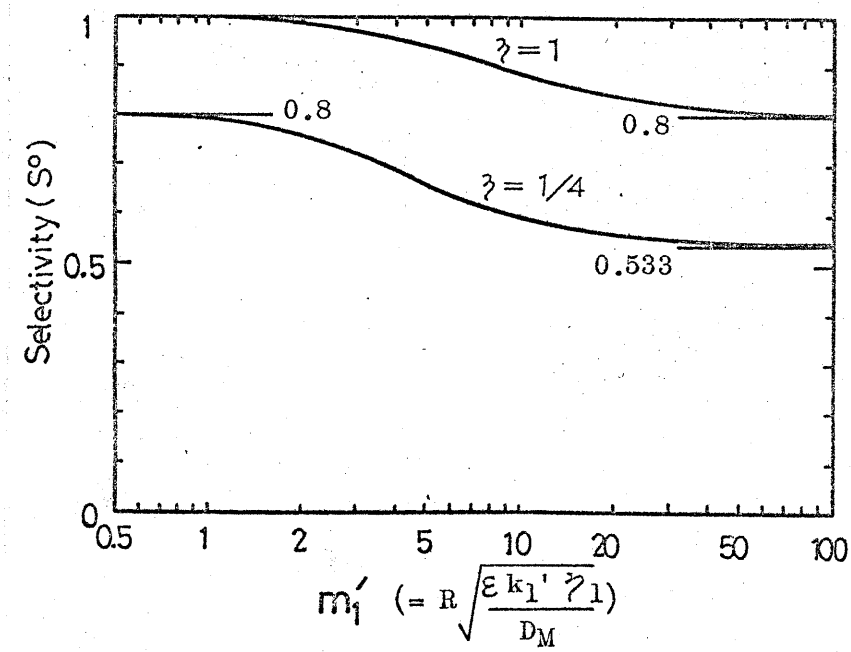

Fig.4-2 Relation between Selectivity S^o and Modulus of Macropore for Definite Values of s' (= 16) and η

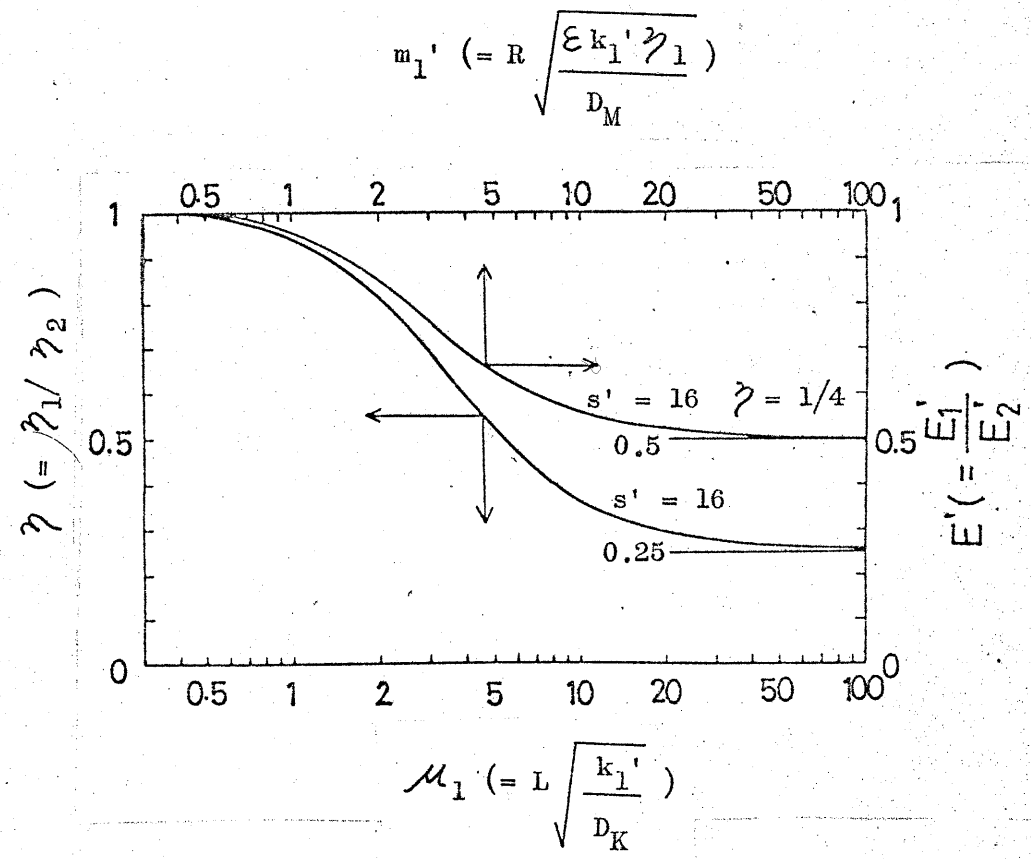

Fig.4-3 Relation between η (or E') and μ_1 (or m_1') for a Definite Value of s' (or s'η)

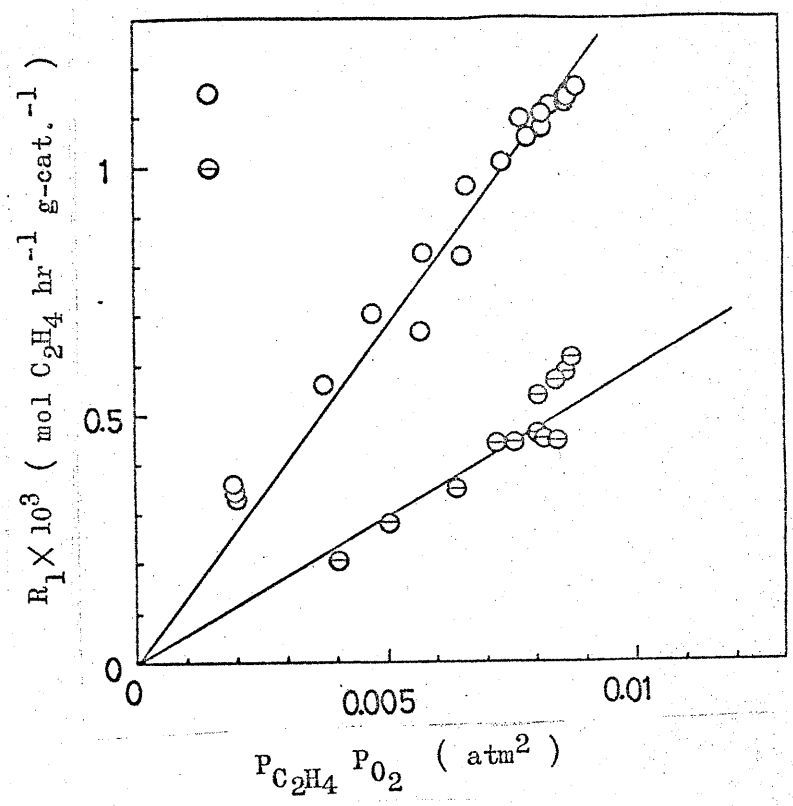

Fig.4-4 Reaction Rate of Ethylene (K-1)

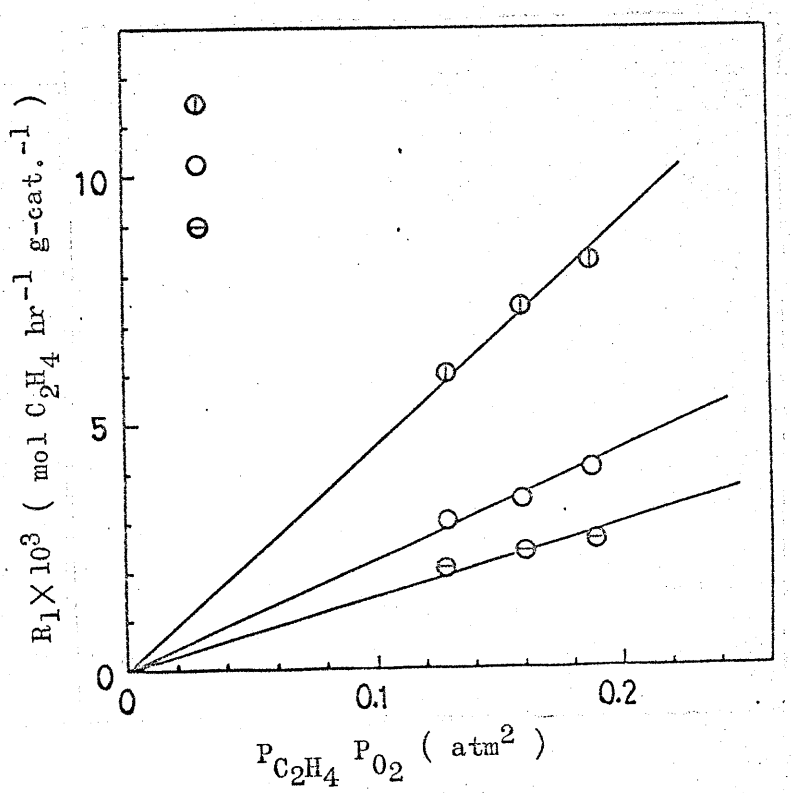

Fig. 4-5 Reaction Rate of Ethylene (W-6)

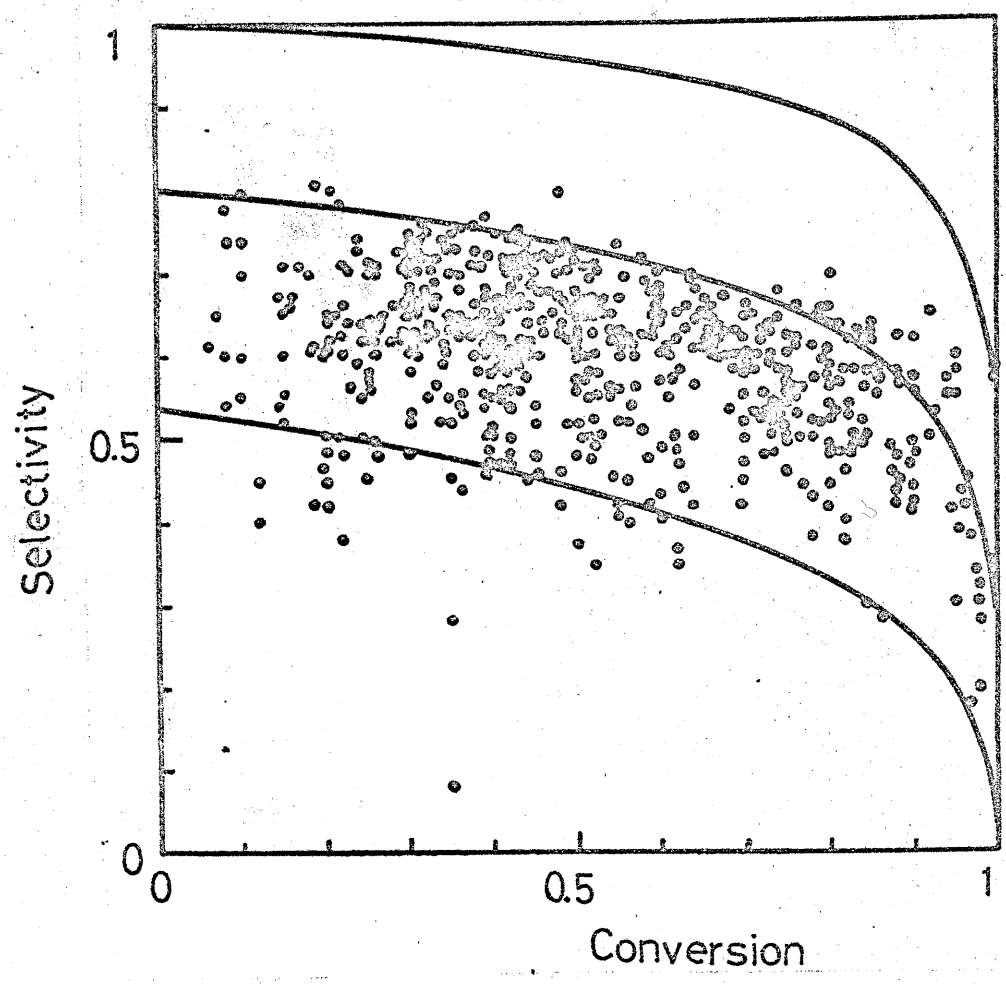

Fig.4-6 Selectivity vs. Conversion

Each point shows the experimental data put forward by Hirasa[H-3)]

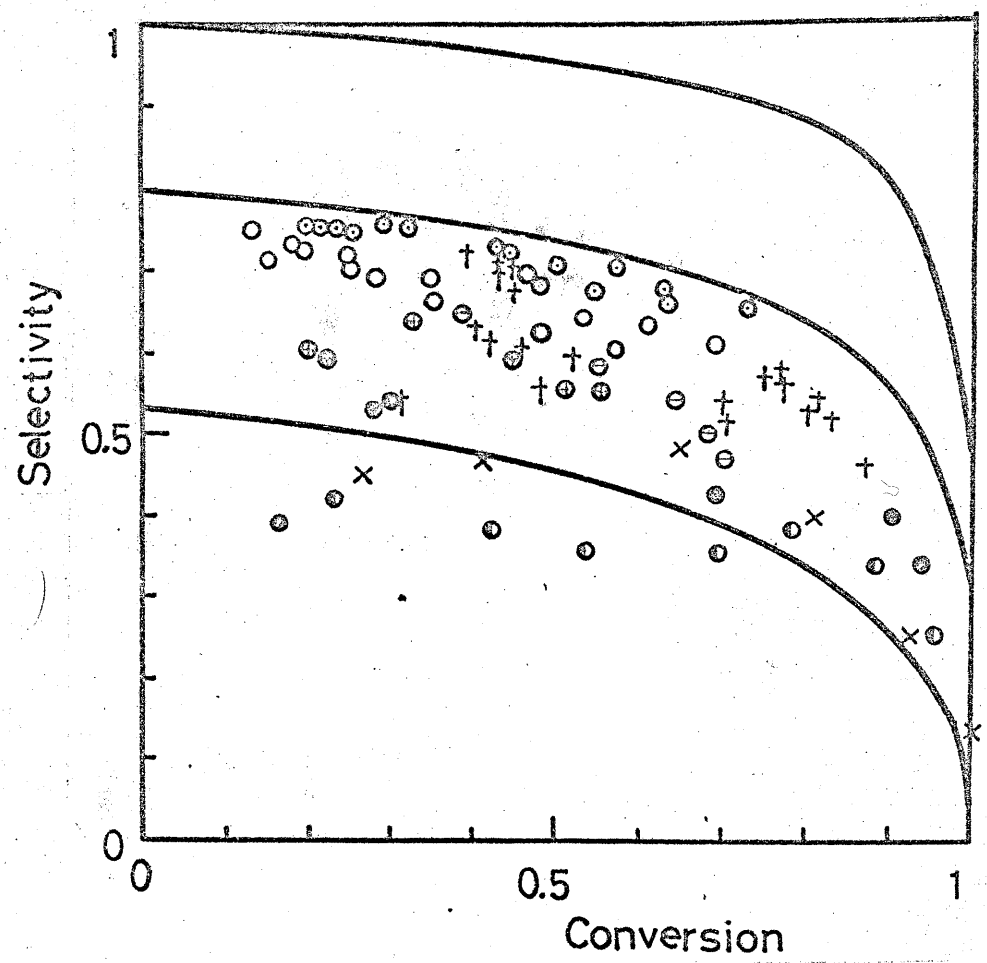

keys	Literature	Reaction temparature [°C]	Feed composition [%]
⊙	Wan W-6	230 270	C_2H_4 20 O_2 80 N_2 0
○		215 260	30 70 0
+	Orzechowski O-5	234 and 274	4.7 19.8 75.5
⊖	Kano K-1	257	C_2H_4 4.5 air 95.5
⊕		231	
◉	Tabata T-1	200 208	2~3 98~97
◐		221 232	
×	Todec A-6	255	2 98

Fig.4-7 Selectivity vs. Conversion

Table 4-2 Comparison of Micro-Macropore Model with the Other Models

	The micro-macropore model			The simple treatment		The simple pore model		
The reaction scheme	(A) $C_2H_4 \longrightarrow C_2H_4O \longrightarrow CO_2, CO$			(B) $C_2H_4 \longrightarrow C_2H_4O \longrightarrow CO_2, CO$				
The relation between S and X								
key \ the parameters	s'	η	E'	s	γ $(=S^0)$	s	γ	E'
⊙ Wan W-6)	16	1/4 ($\eta_{minimum}$)	0.9	3.6	0.77	4	0.8	0.9
○ Wan			0.84	3.4	0.75			0.84
+ Orzechowski 0-5			0.84	3.4	0.75			0.84
⊖ Kano K-1)			0.67	2.7	0.67			0.67
⊕ Kano			0.64	2.6	0.65			0.64
◉ Tabata T-1)			0.55	2.2	0.58			0.55
◉ Tabata			0.50	2.0	0.53			0.50
× Todec A-6)			0.50 ($E_{minimum}$)	2.0	0.53			0.50 ($E_{minimum}$)

Chapter 5 Effect of Reaction Rate Forms on Selectivity and Conversion

5-1 Introduction

As shown in chapter 1, there have been few studies concerning selectivity dependency on the intraparticle mass transfer process for the catalytic system governed by kinetics other than a first order law. But it was foumd in chapter 2 that the selectivity decreases more rapidly with increasing catalyst size for the reactions which follow the Langmuir-Hinshelwood model than a first order reactions system. The present chapter is concerned with the effect of reaction rate forms on the selectivity in a consecutive reaction system, together with the effectiveness factor.

The results are interpreted in terms of the distrubution profile of reactivity inside a catalyst pellet and it makes it possible to predict the selectivity for various kinds of reaction rate forms in comparison with the selectivity for a first order reaction system.

5-2 Statement of Problems

The systems assumed in the analysis are as follows:

1) The reaction is consecutive as, $A \xrightarrow[R_1]{k_1} B \xrightarrow[R_2]{k_2} C$.

2) The catalyst is a spherical pellet and a simple pore model is applied.

3) The system is isothermal .

The basis differential equations are given by

$$D_e \left(\frac{d^2P_A}{dr^2} + \frac{2}{r}\frac{dP_A}{dr}\right) = R_1 \tag{5-1}$$

$$D_e \left(\frac{d^2P_B}{dr^2} + \frac{2}{r}\frac{dP_B}{dr}\right) = -R_1 + R_2 \tag{5-2}$$

with boundary conditions

$$\text{at } r = R, \quad P_A = P_{AS} \qquad P_B = 0 \tag{5-3}$$

$$\text{at } r = 0, \quad \frac{dP_A}{dr} = \frac{dP_B}{dr} = 0 \tag{5-4}$$

The boundary condition of $P_{BS} = 0$ corresponds to the limiting selectivity as the conversion of a reactant approaches zero. As shown previously, the selectivity is not affected by the mixing characteristic in a reactor.

There are various kinds of rate expressions for solid catalyzed reactions but the rate expressions which follow the Langmuir-Hinshelwood model are adopted owing to their vast utility and the clear conceptions relating to the reaction mechanism. The three cases involving different adsorbed apecies, that is, a reactant, an intermediate product and a final product, were considered. They are listed in Table 5-1, with the modulus defined for each case.

The range for computations were taken as follows, whcih are correspondent to the nickel catalyzed hydrogenation of acetylene as shown in chapters 2 and 3.

$$s = 7, \quad K_i P_{AS} = 0,\ 10 \text{ and } 30, \quad M_1 = 1 \sim 50$$

The above systems are solved numerically by means of a digital computer.

5-3 Computational Results

5-3-1 Effectiveness Factor

The results are shown in Fig.5-1. In cases 1 and 2, the asymtotic solutions are available when M_1 is large.

Case 1 $$E_1 = 3/M_1 \tag{5-5}$$

Case 2 $$E_1 = \frac{3}{M_1} \frac{\sqrt{2\,(1 + K_A P_{AS})\,(K_A P_{AS} - \ln(1 + K_A P_{AS}))}}{K_A P_{AS}} \tag{5-6}$$

These asymtotic solutions are shown by the dotted lines A, B_1 and B_2 in Fig.5-1. As expected, they coincide well with the computational results in the region of $M_1 > 20$.

5-3-2 Selectivity

Fig. 5-2 shows the results.

It is observed that:

1) The selectivity S^o is regarded as unity when modulus is smaller than unity and it decreases as modulus increases, until it converges to a limiting value.

2) The four cases give the different decreasing rate of the selectivity with increasing modulus and the different limiting selectivity.

3) The selectivity in Case 2 is always lowest and those in Cases 3 and 4 are larger than in Case 1.

The limiting selectivity at large values of M_1 is derived analytically in Case 1 and it is also derived in Case 2, provided that the value of $K_A P_{AS}$ is sufficiently larger than unity, as already shown in chapter 2.

5-4 Interpretation of Computational Results in Terms of Profile of Reactivity inside a Catalyst

In order to present a physical interpretation to the computational results, the distribution of the apparent rate constant is considered. The apparent rate constant is defined by R_1/P_A or R_2/P_B so that it is a coefficient which is equal to the rate constant in the case of a first order reaction. The apparent rate constant in each case and its profile inside a catalyst pellet is described below.

Case 1 $k_{iapp} = k_i$, which is constant inside a catalyst.

Case 2 $k_{iapp} = k_i/(1 + K_A P_A)$, which increases monotonically towards the pellet center.

Case 3 $k_{iapp} = k_i/(1 + K_B P_B)$, which decreases towards the pellet center when modulus is not so large and has a minimum value at a certain position when modulus is large

Case 4 $k_{iapp} = k_i / (1 + K_C P_C)$, which decreases monotonously towards the pellet center.

The examples of their profiles are shown in Fig.5-5 and the corresponding profiles of concentrations are shown in Figs.5-3 and 4. For the two cases, the average reaction rates of a reactant are almost same but their selectivities are much different from each other owing to the different profiles of k_{iapp}. It should be noted that the ratio of the apparent rate constants of the two step reactions, as assumed in this analysis, is always constant. The effect of the distribution profile of k_{iapp} inside a catalyst is easily interpreted. Namely, the concentration of a reactant decreases with depth of penetration but the concentration of an intermediate product increases, so that the change in k_{iapp} inside the catalyst affects R_2 more strongly than R_1. These system are equivalent to a first order reaction system where the distribution of activity exist in a catalyst, no matter what the cause is.

In summary, it is demonstrated that when k_{iapp} increases towards the pellet center, the selectivity is lower than that in a first order reaction system and vice versa.

Though the expression is qualititative, it is very useful for variety of catalytic systems. Some examples are shown below.

1) A second order reaction system ($R_1 = k_1 P_X P_A$ $R_2 = k_2 P_X P_B$)

k_{iapp} ($= k_i P_X$) decreases towards pellet center so that the selectivity is larger than a first order reaction system of the same modulus. Similar predictions may be possible for the other kinetic expressions.

2) The effect of non-homogeneous deactivation proceeding in a catalyst

Shell or core-progressive mechanism for deactivation gives an extreme example of the distribution of activity in a catalyst. The results obtained in Chapter 3 that the former mechanism decreases the selectivity and the latter increases it are well interpreted from this point of view.

4) This way of consideration on selectivity may also give a good suggestion for a beeter designing of polyfunctional catalysts.

5-5 Summary

The effect of intraparticle mass transfer upon the selectivity in a consecutive reaction system is analyzed for the reactions which follow the Langmuir-Hinshelwool model. As a result, the selectivity under the influence of the mass transfer depends significantly on the rate forms of reactions. The selectivity at the same modulus is in respect ot the adsorbed species , in the following order:

reactant < no adsorption (forst order reaction) < intermediate product

$\lessgtr$ final product

The results are interpreted systematically in terms of the profile of k_{iapp} in a catalyst pellet. The criterion by which the selectivity is predicted in comparison with the system of first order reactions was introduced .

Table 5-1

	Adsorbed component	Rate expression		Modulus : M_1
Case 1		$R_1=k_1p_A$	$R_2=k_2p_B$	$R\sqrt{\frac{k_1}{D}}$
Case 2	A	$R_1=\frac{k_1p_A}{1+K_Ap_A}$	$R_2=\frac{k_2p_B}{1+K_Ap_A}$	$R\sqrt{\frac{k_1}{D(1+K_Ap_{As})}}$
Case 3	B	$R_1=\frac{k_1p_A}{1+K_Bp_B}$	$R_2=\frac{k_2p_B}{1+K_Bp_B}$	$R\sqrt{\frac{k_1}{D}}$
Case 4	C	$R_1=\frac{k_1p_A}{1+K_Cp_C}$	$R_2=\frac{k_2p_B}{1+K_Cp_C}$	$R\sqrt{\frac{k_1}{D}}$

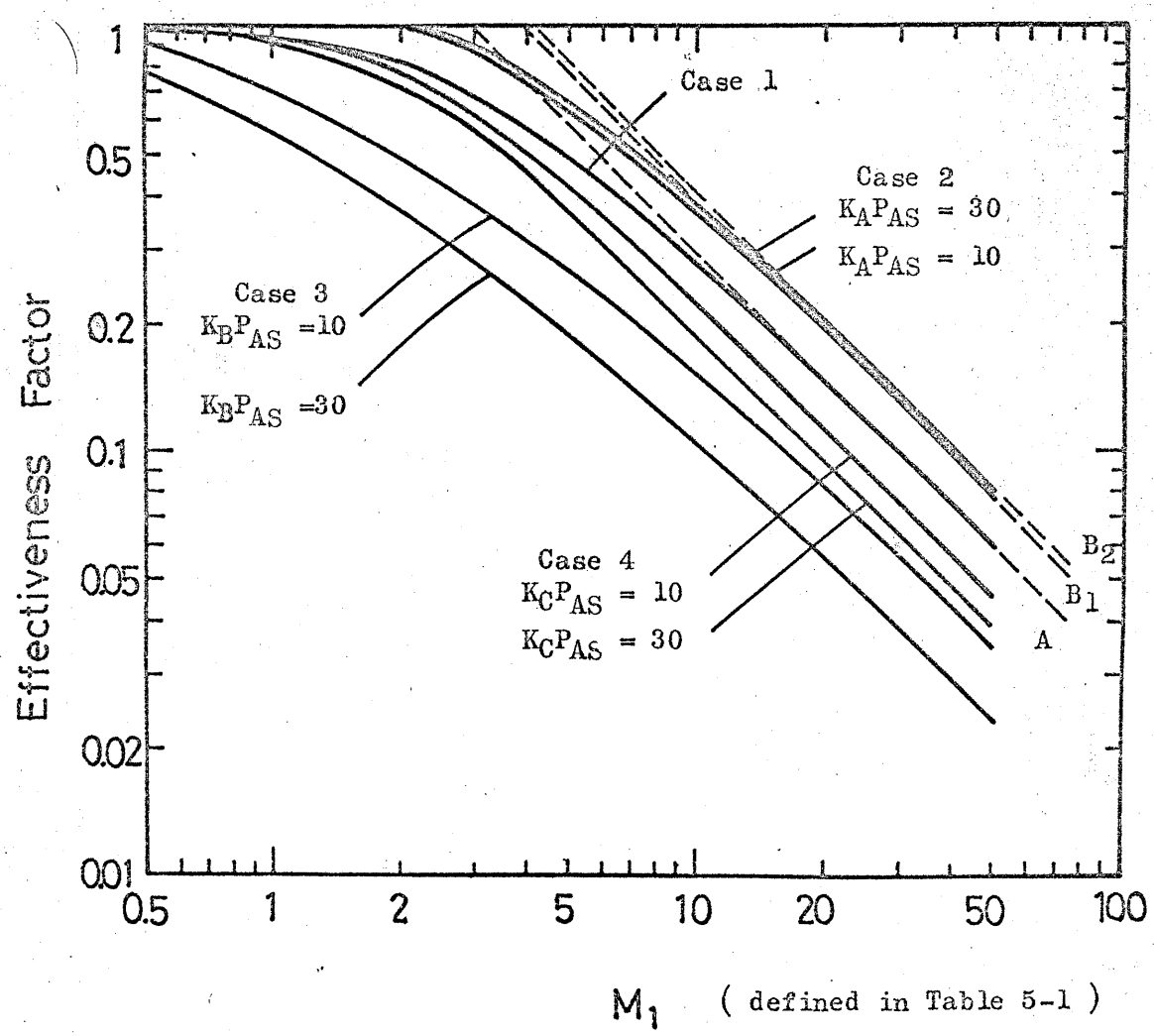

Fig.5-1 Relations between Effectiveness Factor and Modulus

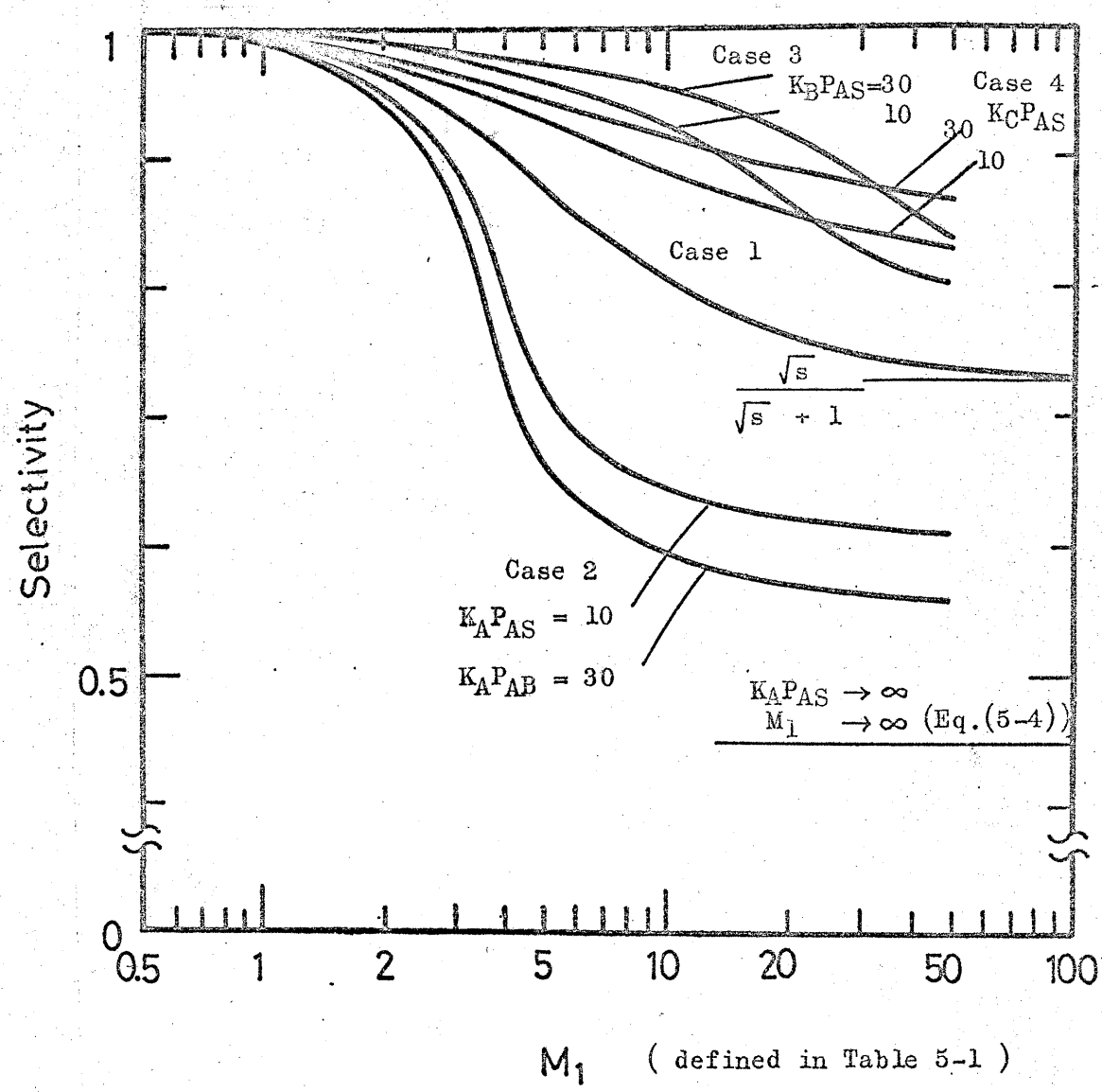

Fig.5-2 Relations between Selectivity S^o and Modulus (s = 7)

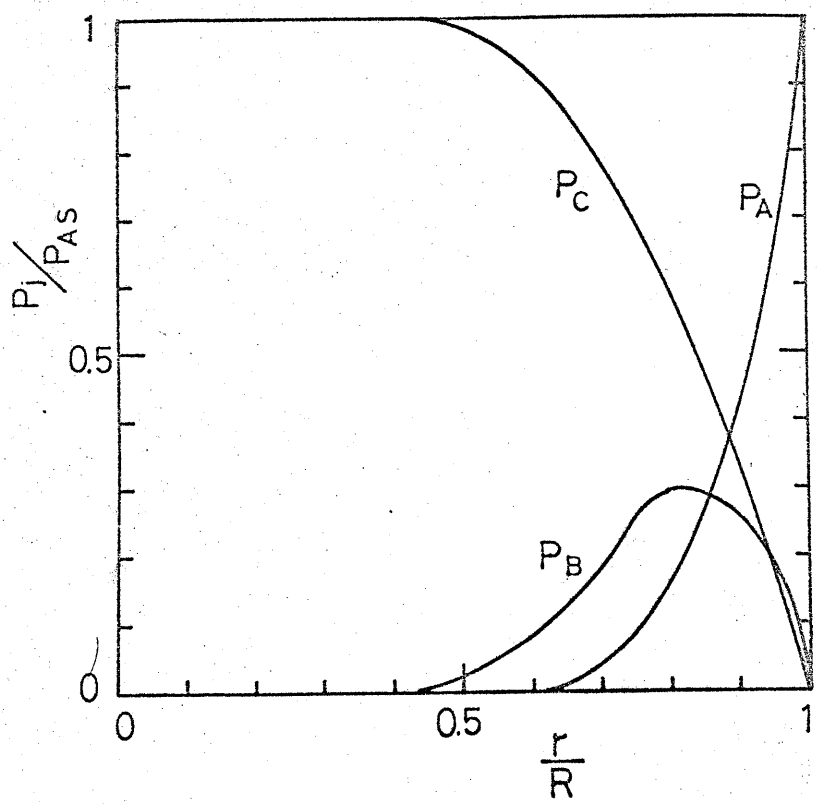

Fig. 5-3

An Example of Concentration Profiles

Case 2

$K_A P_{AS} = 30$

$M_1 = 5$

$S^o = 0.656$

$\overline{R_1} = 5.68$

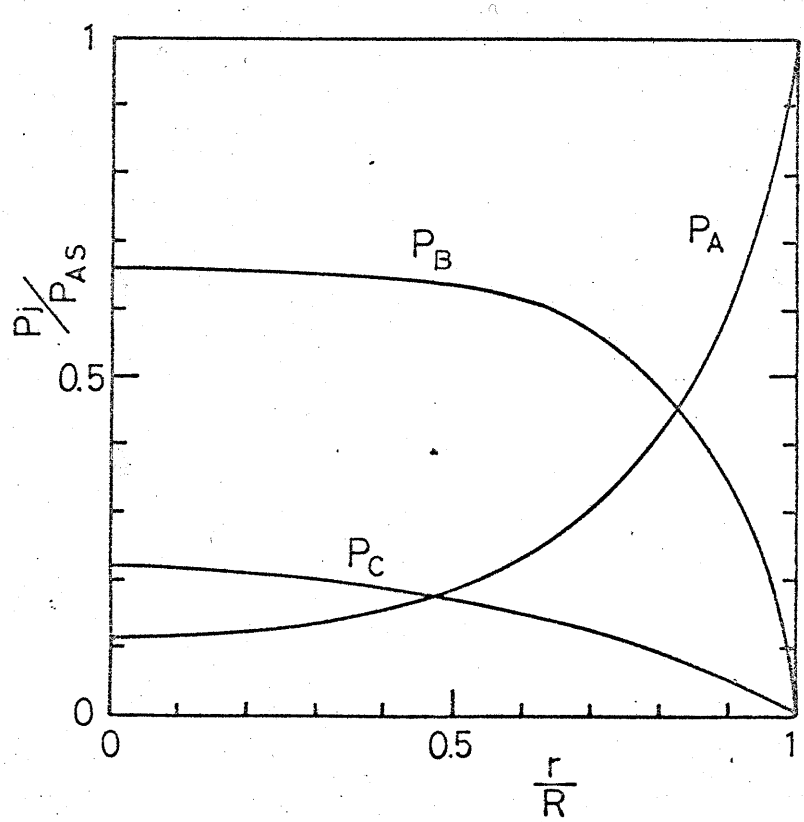

Fig.5-4

An Example of Concentratio Profiles

Case 4

$K_C P_{AS} = 30$

$M_1 = 10$

$S^o = 0.918$

$\overline{R_1} = 6.42$

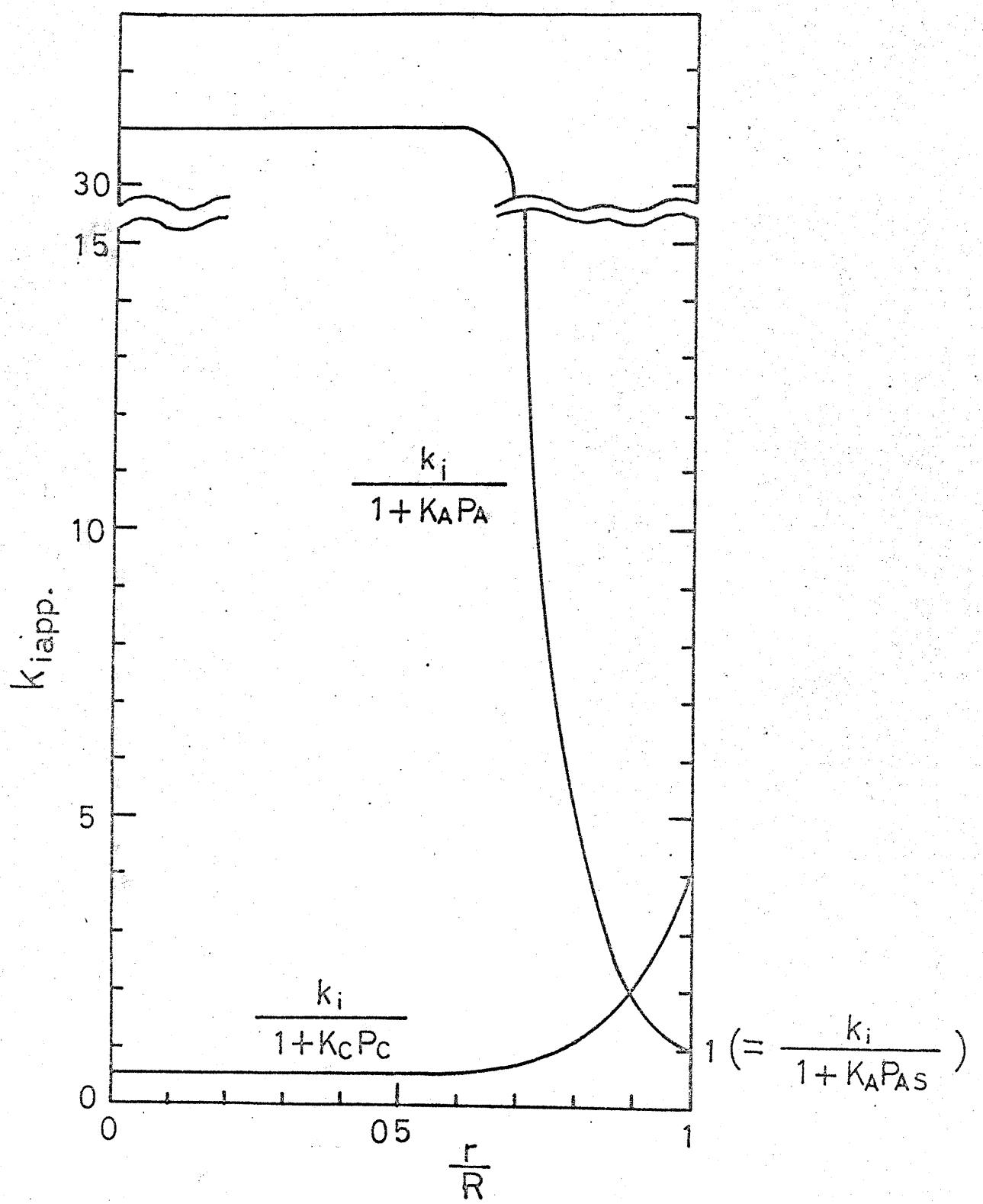

Fig.5-5 Profiles of Apparent Rate Constant $(= \frac{k_i}{1 + K_i P_i})$

The profiles correspond to the concentration profiles as shown in Figs.5-3 and 5-4.

Chapter 6 Effect of Hydrodynamic Flow through Porous Catalysts upon Effectiveness Factor

6-1 Introduction

The effect of intraparticle mass transfer on solid catalyzed reactions have been studied extensively. In these studies, it is usual that the mass transfer is assumed to be characterized by diffusion and/or the mass flow from a volume change in reactions. The catalyst pellet in a practical reactor such as a packed bed, however, is exposed to a longitudinal pressure gradient resulting from a flow resistance in the reactor. There must be some hydrodynamic flow through the pores of the catalyst. The effect of the flow on catalytic behavior has so far not been paid attention to, possibly owing to its insignificance in usual porous catalysts under ordinary operating conditions. It wll be possible, however, to promote the intraparticle mass transfer rate by making use of the inside flow for a catalyst having larger pores than usual and to raise the effectiveness factor of large sized catalysts which would otherwise be very poor. As a result, the use of large sized catalysts of high activity will lead to the decrease in the flow resistance and reactor volume.

Hydrodynamic flow through porous material has been studied extensively and they are well reviewed in some books.[C-6,M-11] According to them, the flow is determined by permeability of the material and the pressure distribution at the exterior surface of the material. The flow, however, has not been investigated under the occurence of chemical reactions.

The central subjects in the present chapter are:

1) to evaluate the flow rate through catalyst pellets placed in a reactor. knowing the porous structure of the catalyst and the operating conditon,
2) to analyze the rate of reaction under a given flow rate and
3) to give some practical examples where it is advantageous to made use of the inside flow.

6-2 Theoretical Analysis of Solid Catalyzed Reaction under the Combined Gradients of Composition and Pressure

In order to get the outlone of the effect of the hydrodynamic flow upon the rate of a reaction on the catalyst in a flow reactor, the following assumptions are made:

1) A cylindrical catalyst pellet is placed in parallel with the surrounding stream.

2) Pressure distribution at the exterior surface of the catalyst, which defines the boundary conditions for the basic differential equations determining the flow through the pellet, is assumed as the pressure is of the same value at the upper and the bottom plain of the cylinder and its gradient is constant at the side plain.

3) The film resistance between the pellet surface and the ambient fluid is not considered.

4) The pellet is isotropic in permeability.

Combining Darcy's law and the continuity equation for an incompressible fluid under the assumption of isotropy in permeability yields the following Laplase equation for the distribution of the pressure inside the pellet.

$$\nabla^2 p = 0 \qquad (6\text{-}1)$$

Eq.(6-1) is easily solved with the boundary conditions given by the second assumption and from the resultant pressure distribution, the flow through the pellet is obtained in cylindrical co-ordinates as

$$u_z = u_{in} \ (\text{ constant }), \quad u_\theta = u_r = 0 \qquad (6\text{-}2)$$

The system where a first order irreversible reaction takes place with the hydrodynamic flow and diffusion is expressed as

$$D_e \left(\frac{\partial^2 P_A}{\partial r^2} + \frac{1}{r}\frac{\partial P_A}{\partial r} + \frac{\partial^2 P_A}{\partial z^2} \right) - u_{in}\frac{\partial P_A}{\partial z} - k_1 P_A = 0 \qquad (6\text{-}3)$$

with boundary conditions

$$\text{at } z = 0 \quad P_A = P_{AS}, \qquad \text{at } z = L \quad P_A = P_{AS}, \quad \text{at } r = R \quad P_A = P_{AS} \tag{6-4}$$

These boundary conditions were taken instead of Dankwerts' type, considering the rapid mixing in a packed bed reactor comparing to that in a catalyst.

The solution of these equations are given by*

$$a'' = \sum_{n=1}^{\infty} \frac{2m_1^2 J_0(j_n x)}{J_1(j_n)\, j_n\, (j_n^2 + m_1^2)} \left(\frac{e^{\lambda_2} - 1}{e^{\lambda_1} - e^{\lambda_2}} e^{\lambda_1 y} - \frac{e^{\lambda_1} - 1}{e^{\lambda_2} - e^{\lambda_1}} e^{\lambda_2 y} + 1 \right) \tag{6-5}$$

where,

$$m_1 = R\sqrt{\frac{k_1}{De}}, \quad a'' = \frac{P_{AS} - P_A}{P_{AS}}, \quad x = r/R, \quad y = z/L_p, \quad PeB = (u_{in} L_p)/De$$

$$\omega = R/L_p, \qquad \lambda_{\substack{1\\2}} = \frac{PeB \pm \sqrt{PeB + 4(j_n^2 + m_1^2)/\omega^2}}{2} \tag{6-6}$$

and J_0 (or 1) represent zero (or first) order Bessel function and j_n is the root of $J_0(j_n) = 0$.

According to the usual definition, the effectiveness factor is represented as

$$E_1 = \frac{\int_0^1\int_0^1 k_1(1 - a'')\, x\, dx\, dy}{\int_0^1\int_0^1 k_1\, x\, dx\, dy} \tag{6-7}$$

Substituting Eq.(6-5) into Eq.(6-7) yields

$$E_1 = 1 - \sum_{n=1}^{\infty} \frac{4\, m_1^2}{j_n^2\, (j_n^2 + m_1^2)} \left(1 + \frac{(e^{\lambda_1} - 1)\,(e^{\lambda_2} - 1)}{e^{\lambda_1} - e^{\lambda_2}} \left(\frac{1}{\lambda_1} - \frac{1}{\lambda_2} \right) \right) \tag{6-8}$$

The effectiveness factor is determined by the Thiele modulus m_1, PeB representing the relative significance of flow and diffusion to the total

* Detailed derivation is presented in Appendix 6.

rate of mass transfer and ω, the ratio of the radius of the height of the cylinder. Fig.6-1 shows the relation of E_1 to m_1 for various values of PeB, ranging from 0 to 2000. As expected, the effectiveness factor increases as PeB becomes large. The curve for PeB/ m_1 = 0 is equivalent to that of the case where the mass transfer process is characerized by diffusion alone.

6-3 Experiments

6-3-1 Reaction system.

The following ion exchange reaction was carried out.

$$\text{R-H} + \text{KCl} \rightleftharpoons \text{R-K} + \text{HCl} \qquad (6\text{-}9)$$

R-H represents the acid form of Dowex-50 cation exchange resin employed in the reaction and R-K the form replaced by potassium ion. This is not a real solid catalyzed reaction but regarded as a model for it because the solid phase remains unaltered in the physical characteristics in the course of the reaction. A certain decided amount of the resin of the diameter from 0.6 to 0.8 mm$^{\phi}$ is wrpped with a nylon cloth so as to yield a spherical pellet of 10 mm$^{\phi}$. When the pellet is dipped in water, the resin swells to yield a very hard sphere of about 11 mm$^{\phi}$. The resultant pellet is regarded as an example of a solid catalyst of a rough pore structure. Before the reaction operation was begun, the pellet was treated by hydrochloric acid of 1 N. Under the condition, the resin is of its acid form completely so that Eq.(6-9) is considered to be an irreversible reaction where KCl and HCl are respectively a reactant and a product.

6-3-2 Equipments

Fig.2 shows the schematic diagram of the apparatus. The impulse responce method was employed for the rate study, which yielded a lot of information on the flow pattern in the reactor adding to the reaction rate. The apparatus comprises a tubular reactor packed with the resin pellets previously mentioned,

a flow line of carrying fluid, an arrangement for the injection of the impulse of KCl or HCl and an arrangement for measuring their concentrations.

The reactor and the flow line are made of 40 mm poly-vinylchloride tubing and packed with 4 mm glass beads up and down the resin bed to make the velocity distribution of the carrying stream uniform through the cross section of the pipe. City water was used as the carrying fluid and its electric conductivity was stabilized by adding a decided small amount of hydrochloric acid. Aconcentration profile closely resembling the delta function was created by the injection arrangement shown in Fig.6-2. A six-way brass valve was made to contain a decided amount of sample in a sample tube and force it out ot the mouthpiece which was specially designed so as to distribute the injected species uniformly through a thin cross section.

The measurements of the concentrations were made by electric conductivity detection. Platinum probes were equipped at the inlet and the outlet of the resin bed and connected to the conventional electric circuitry. The linear dependency of the electric conductivity on the concentration of HCl or KCl was examined in the range of the experiments. The relative sensitivity of HCl to KCl, d, was proved to be 3.0 in accord with the value in handbooks.

6-3-3 Experimental Procedures and Results

The concentrations of HCl and KCl solutions were adjusted to be of the same electric conductivity. Their pulses were injected at the reactor inlet several times in turn at a constant rate of carrying stream. Reproducibility of the concentration profiles at the inlet and the reponses at the outlet was proved clearly.

Some portion of KCl injected disappears by the reaction yielding the same amount of HCl. The relative electric conductivity of the reactor outlet to the inlet, therefore, becomes $(1 + (d - 1) X)$, where X designates the conversion of KCl. On the other hand, HCl is inactive in the system and the

electric conductivity remains unaltered. The conversion of KCl is calculated from the reponse as a following way.

$$S_{KCl,inlet} = S_{HCl,\ outlet} \ (= S_{HCl,inlet}) \qquad (6\text{-}10)$$

$$S_{KCL,outlet} = S_{KCl,inlet} \ (1 + (d - 1) X) \qquad (6\text{-}11)$$

Here, $S_{i,j}$ represents the peak area of the response at the position j for the injection of the component i. Eliminating $S_{KCl,inlet}$ from the equations yields

$$X = (S_{KCl,outlet} - S_{HCl,outlet}) / S_{HCl,outlet} \ (d - 1) \qquad (6\text{-}12)$$

Thus, the conversion of KCl is determined by the response curves of KCl and HCl at the reactor outlet.

A set of the impulse responses is shown in Fig.6-3.

The conversion of KCl in the fluid portion flowing out of the reactor at a definite value of residence time, X_τ, is represented by Eq.(6-13) as same as Eq.(6-12).

$$X_\tau = (h_{KCl,outlet} - h_{HCl,\ outlet}) / h_{HCl,\ outlet} \ (d - 1) \qquad (6\text{-}13)$$

Here, $h_{i,j}$ designates the height of the response at a given residence time.

In the example in Fig.6-3, $X_\tau < 5\%$, when $\tau < 5$ sec., $X_\tau = 5$ to 100% when $\tau = 5$ to 13 sec. and $X_\tau = 100\%$, when $\tau > 13$ sec.. The residence time may be composed of the two terms. That is, $(L_R - L_T) / u_{out}$ and L_{in} / u_{in}, where L_R and L_T respectively the length of the reactor and the total path inside the pellet through whcih the fluid portion flowed. The former of the two terms corresponds to the residence time in the main stream and the latter to that in the pellet. u_{in} may be much smaller than u_{out} so that the total residence time becomes longer with increasing L_{in}. Based on the

consideration, the high conversion at $\tau > 13$ sec. in comparison to the low conversion at $\tau < 5$ sec. is proved to be the result of the longer and more efficient contact of the fluid portion with the solid interior surface. Thus, the tailing part of the reponse demonstrates that the flow through thr pellet actually occurs and plays an important role in the reaction rate.

The conversion of KCl were measured at different rates of the carrying stream. The results are shown in Fig.4 in terms of FX, which corresponds to the reaction rate, versus Reinolds number defined as $(u_{out} D_p)/\nu$.

6-4 Analyses

In the preceding sections, the effect of the flow through the porous pellets on the reaction rate was examined experimentally and the phenomenological interpretation to the impulse response was given . Here, the experimental results in Fig.6-4 are analyzed quantitatively.

1) maximum reaction rate in the absence of the flow through the pellet

The rate of the reaction controled by mass transfer between the pellet surface and the ambient fluid is obtained by $R_1 = k_L C_b$. k_L and C_b are respectively the mass transfer coefficient and the bulk concentration of a reactant. k_L was estimated from Yagi and Wakao correlation.

$$Sh = 2 + 1.45\, Sc^{\frac{1}{3}}\, Re^{\frac{1}{2}} \qquad Re < 100$$

$$Sh = 2 + 0.9\, Sc^{\frac{1}{3}}\, Re^{0.6} \qquad Re > 100 \qquad (6\text{-}14)$$

Under the assumption of a plug flow reactor, the conversion of a reactant was extimated at each flow rate. The results are shown in Fig.6-4 as FX_{film}. This rate gives the maximum one in the absence of the inside flow. Its comparison with the experimental results clearly shows that the effect of the flow upon the reaction rate is significant, in particular at large values of Re.

The theoretical analysis in 6-2 assumed the absence of a film resistance. In order to compare the experiments with the analysis, the reaction rate is divided into two parts, one of which is the reaction on the exterior surface (FX_{film}) and the other is the reaction on the interior surface ($FX - FX_{film}$). The latter contribution should be compared to the analysis.

2) estimation of the flow velocity within pellets, u_{in}

The flow through porous material is determined by the pressure distribution at the exterior surface of the pellet and the permeability of the pellet. A simple analysis based on the following assumptions is employed here.

1) The average longitudinal pressure gradient in a reactor is impressed on each catalyst pellet.
2) Each pellet is considered to be a small packed bed of fine particles, in which the Kozeny-Carman relationship is applied to the pressure drop.

The average longitudinal pressure gradient in a reactor is determined by the Kozeny- Carman relationship.

$$\frac{\Delta p}{L_R} = \frac{f\, u_{out}^2\, \rho\, (1 - \varepsilon_R)}{g\, \phi\, D_p\, \varepsilon_R^3} \qquad (6\text{-}15)$$

where f represents friction factor and it is determined by

$$f = 5 / Rem \qquad Rem < 2$$

$$f = 5/Re + 0.4/(Rem)^{0.1} \qquad (6\text{-}16)$$

$$Rem = \frac{\phi\, D_p\, u_{out}\, \rho}{\mu\, 6\, (1 - \varepsilon_R)}$$

For each catalyst,

$$\frac{\Delta p_{in}}{D_p} = \frac{f_{in}\, u_{in}^2\, (1 - \theta)}{g\, \phi\, d_{in}\, \theta^3} \qquad (6\text{-}17)$$

where d_{in} and θ designate respectively the diameter of the particles constituting the pellet and the porocity of the pellet.

Combining Eqs.(6-15) and (6-17) under the first assumption that $\frac{\Delta p}{L_R} = \frac{\Delta p_{in}}{D_p}$ yields

$$\frac{f\, u_{out}^2}{Dp} = \frac{f_{in}\, u_{in}^2}{d_{in}} \qquad (6\text{-}18)$$

where the values of shape factor and porocity are assumed to be equal for the reactor and the pellet:

Based on the Eq.(6-18), u_{in} is determined by u_{out}, D_p , d_{in} and Eq.(6-16) ich gives f as a finction of u. In general, this equation cannot be solved explicitly and required some itterations as to u_{in} and f_{in}. When the flow through the pellet is in laminar flow range, however, u_{in} is represented explicitly as,

$$u_{in} = \frac{f\,\rho}{30\,(1-\varepsilon_R)\mu}\,\frac{d_{in}^2}{D_p}\,u_{out}^2 \qquad (6\text{-}19)$$

This equation shows that u_{in}/u_{out} increases with increasing u_{out}, because f varies in a fractional order in respect to u_{out} ,as expressed in power law.

3) determination of the rate constant of the reaction

The ion exchange reaction on the solid surface is so rapid that the total rate is controled by mass transfer. The rate constant appearing in the Thiele modulus, therefore, should be replaced by the mass transfer rate constant within the pellet. That is, $(k_L a)_{in}$,where a_{in} represents the interior surface area per unit volume of a catalyst pellet. k_L was determined from Yagi and Wakao correlation for the flow rate u_{in} and the particle size d_{in}.

4) determination of PeB and m_1

In order to compare the experiments with the theoretical analysis , the spherical pellets employed in the experiments were approximated by a cylinder of

which diameter and height are of the same length. Then, PeB and m_1 are respectively defined by Eqs.(6-20) and (6-21).

$$PeB = \frac{u_{in}\,(2R)}{D_e} \tag{6-20}$$

$$m_1 = R\sqrt{\frac{(k_L a)_{in}}{D_e}} \tag{6-21}$$

Thus, the value of the effectiveness factor, E_1, is estimated for each operating condition from Fig.6-1 so that the overall rate constant in unit volume of the reactor, $(1 - \varepsilon_R)\,(k_L a)_{in}\,E_1$ is given. The line shown in g.6-5 represents the reaction rate on the interior surface estimated by such procedure. The close agreement of the line with $(FX - FX_{film})$ demonstrates the validity of the above analysis based on the flow through the pellet.

The values of the main parameters are listed in Table 6-2.

6-5 Comparison of the Reactor Involving Hydrodynamic Flow through a Catalyst with Usual Reactors

In this section, the flow reactors involving the inside flow through the catalysts are designed for a given reaction or adsorption process and compared with the usual reactors where the intraparticle mass transfer is characterized by diffusion alone. Relative merits of the reactors are judged by their volume and the total pressure drop to give a same conversion of a reactant at a fixed rate of the reactant flow.

Problem 1

Design a reactor for a solid catalyzed liquid phase reaction. The rate of the reaction is assumed to be given by the relation that m_1 is unity for the catalyst size of 1 mm. The following three types of catalysts are considered. Two of them are the usual porous catalyst and the remaining is of a rough pore structure and involves the inside flow.

catalyst 1 a fine particle of D_p = 1 mm. , of which effectiveness factor is almost unity since $m_1 = 1$

catalyst 2 a pellet of D_p = 20 mm., of which effectiveness factor is 0.15 since m_1=20

catalyst 3 a pellet of D_p = 20 mm., which is an aggregate of fine particles of 1 mm$^{\phi}$.

The reactor was assumed to be of a plug flow type and the desired conversion to be 90%. For the catalysts 1 and 2, the conservation equation in the reactor as $-F\frac{dP_A}{dl} = k_1 P_A$ is easily solved for a corresponding rate constant of the reaction and the reactor length and the pressure drop are determined. The design of the reactor packed with catalyst 3 was carried out by estimating the velocity of the inside flow, PeB and m_1 and employing the charts in Fig.6-1.

The results are shown in Fig.6-6, where the reactor length and the pressure drop are plotted to the superficial velocity of the flow in the reactor.

As to the reactor length, catalyst 1 is superior to catalyst 2 owing to the higher effectiveness factor. In the region that u is larger than 1.5×10^2 m/hr, the length for catalyst 3 is $1/(1 - \varepsilon_R)$ times that for catalyst 1, indicating that the pellet effectiveness factor is unity due to the rapid inside flow. In other words, the catalyst volume required is much the same for the two catalysts but the increased void fraction for catalyst 3 causes the slight expansion of the reactor. When u becomes smaller than 1.5×10^2 m/hr, the decrease of the inside flow makes the effectiveness factor lower than unity and leads to the increase of the required volume of catalysts, compared to catalyst 1.

As to the pressure drop, the reactor of catalyst 1, whose length is shortest, gives far the largest of the three, as the result of a high flow

resistance of fine particles. The pressure drop for catalyst 3 is about one fifth of catalyst 2 in the region of $u > 1.5 \times 10^2$ m/hr, corresponding to the relative length of the reactor.

Thus, it is obvious that catalyst 3 is always superior to catalyst 2 which is of the same size but not involving the inside flow. Furthermore, catalyst 3 is more advantageous than catalyst 1, at least in the region of $u > 1.5 \times 10$ m/hr, where the pellet effectiveness factor of catalyst 3 is unity.

In practice, the enormous pressure drop may make it impossible to operate such fine particles as catalyst 1 in the region. Then, only the possibility to use them is to decrease the superficial velocity and increase the cross section of the reactor. For example, the same capacity and pressure drop as catalyst 3 at $u = 1.5 \times 10^2$ m/hr. is realized by operating catalyst 1 at $u = 2.7 \times 10$ m/hr. This decrease in the flow velocity corresponds to five times the cross section of the reactor. The large cross section may be disadvantageous, adding to the fact that the handling of fine particles is often troublesome in practical industries.

In summary, it may be stated that the effect of the inside flow realizes the high activity of fine particles and the small pressure drop for large pellets simultaneously.

Problem 2

Design a reactor for a solid catalyzed liquid phase reaction, where the overall rate of the reaction is controled by a film resistance. The following four types of catalysts are considered.

catalyst 1 a fine particle of $D_p = 1$ mm.

catalyst 2 a pellet of $D_p = 5$ mm.

catalyst 3 a pellet of $D_p = 20$ mm.

catalyst 4 a pellet of D_p = 20 mm., which is an aggregate of fine particles of D_p = 1 mm.$^{\phi}$

The desired conversion was assumed to be 90% as same as the first problem. The mass transfer coefficient through the liquid film is estimated from Yagi and Wakao correlation, Eq.(6-14). The procedure of designing the reactor of catalyst 4 is much the same as described in 6-4.

The results are shown in Fig. 6-7.

First, catalysts 1, 2 and 3 are compared to one another. The pressure drop not so varied among them. The main difference is the reactor length and it is concluded that catalyst 1, fine particle, is far the best.

The relative merits of catalysts 1 and 4 are not so clear as the first problem, because the superiority is reversed with the pressure drop and the reactor length. They should be examined in individual cases.

Problem 3

There is a problem of practical importance, in close connection with the second problem. That is a design of an adsorption column for the removal of impurities or the recovery of useful species from a fluid stream by means of solid adsorbents. The operation is necessarily unsteady-state and the behavior of the column , as represented by a break through, is obtained by solving partial differential equations in respect to time and positions. Such problem has been treated by many investigators[M-10)] but the approach by Kawasoe[K-)] was reffered to here. In his analysis, the intraparticle mass transfer resistance and the film resistance were taken into consideration under the assumption of rapid equilibration for a linear adsorption isotherm.

According to it , the overall transfer coefficient based on a simple pore model, $K_F a$, is represented as

$$\frac{1}{K_F\, a} = \frac{1}{\dfrac{15\, D_e\, (1 - \varepsilon_R)}{R^2}} + \frac{1}{k_L\, a} \qquad (6\text{-}22)$$

where a is the exterior surface area of the adsorbents per a unit volume of the column. The first term of the right side of Eq.(6-22) corresponds to the intraparticle resistance and the second term to the film resistance.

Noting that $k_L = Sh\, D/\, 2R$, $D_e = \theta D/\tau$ and $a = \dfrac{3\,(1 - \varepsilon_R)}{R}$, Eq.(6-22) becomes

$$\frac{1}{K_F\, a} = \frac{1}{15\, D\, \theta (1 - \varepsilon_R)/\, \tau R^2} + \frac{1}{1.5\, D\, (1 - \varepsilon_R)\, Sh/\, R^2} \qquad (6\text{-}23)$$

Substituting the possible values as $\varepsilon_R = 0.4$, $\theta = 0.4$ and $\tau = 4$ into Eq.(6-23) yields

$$\frac{1}{K_F\, a} = \frac{1}{0.9\, D/\, R^2} + \frac{1}{0.9\, D\, Sh/\, R^2} \qquad (6\text{-}24)$$

For example, let the case of $u = 1.5 \times 10^2$ m/hr be considered on the basis of Eq.(6-24). The pellet effectiveness factor of catalyst is about unity, according to the results of the second problem. Therefore, Sherwood number for the inside flow and the fine particles constituting the pellel, 13.5, is to be aken as Sh in Eq.(6-24). Sh for catalyst 1 at the same superficial velocity is 73. It is concluded that the film resistance is negligible in Eq.(6-24). It indicates that the behavior of the column such as a break-through is not dependent on the film resistance but on the intraparticle resistance, which is equal in these two catalysts. The only difference between the catalysts is therefore, in the pressure drop. Catalyst 4 gives about one-sixtieth of the pressure drop for catalyst 1. Furthermore, it is obvious from Eq.(6-24) that the large sized adsorbent without the inside flow is disadvantageous by causing the significant increase of the transfer resistance.

Thus, the effect of the inside flow in the three examples has been cleared. It is remarkable in particular for the first and the third problems. The characteristics common to them is that the process is subject to the intraparticle mass transfer effect. The large sized pellet involving the inside flow realizes much the same activity of the small size, when the flow is fast enough to raise the pellet effectiveness factor up to unity, and eliminates the high flow resistance of fine particles.

It shoud be noted that the most intersting aspect of the inside flow is its preferable tendency at a high velocity of a reactant stream, that is, a large capacity of the equipment. It is suggestive for the solution of the most urgent problem encountered in the recent industries, the removal of poisonous species from the waste water or gas discharged from the factories.

Though the interest has been focused on the liquid-solid systems in this paper, the conception may be extended to the gas-solid systems. The effect of the inside flow, however, may become significant at a larger scale of the solid such as a pellet of 20 cm composed of 5 mm of catalyst pellets, owing to the rapid diffusion in conparison with the liquid phase.

7-6 Summary

The effect of the hydrodynamic flow through porous catalysts exposed to the pressure gradient in a reactor upon the behavior of a single catalyst and of the reactor was investigated in this chapter. Reports of this type of study have apparently not been published to date.

In the first place, theoretical treatment of a solid catalyzed reaction accompanied with the hydrodynamic flow and diffusion was given. The effectiveness factor, by which the results were represented, is determined by PeB , the Thiele modulus and the shape factor of the pellet.

The rate study of the ion exchange reaction was carried out employing the

pellet of 11 mm$^{\phi}$ composed of the cation exchange resin of 0.6 ~ 0.8 mm , which was regarded as a catalyst of a very rough pore structure. The results indicated that the flow through the pellet actually occured and brought about a signficant increase in the reaction rate, in particular at high flow rates in the reactor. The results were analyzed quantitatively and interpreted comprehensively on the basis of the theoretical analysis presented here.

The comparison of the reactor involving such inside flow with that of usual porous catalyst demonstrated that the inside flow leads to a high activity equal to fine catalyst particles and a small flow resistance. Furthermore, its preferable tendency at large flow rates may give a powerful means to the urgent problem in recent industries, the purification of the waste water or gas discharged from factories which frequently demands the equipments of large catacity.

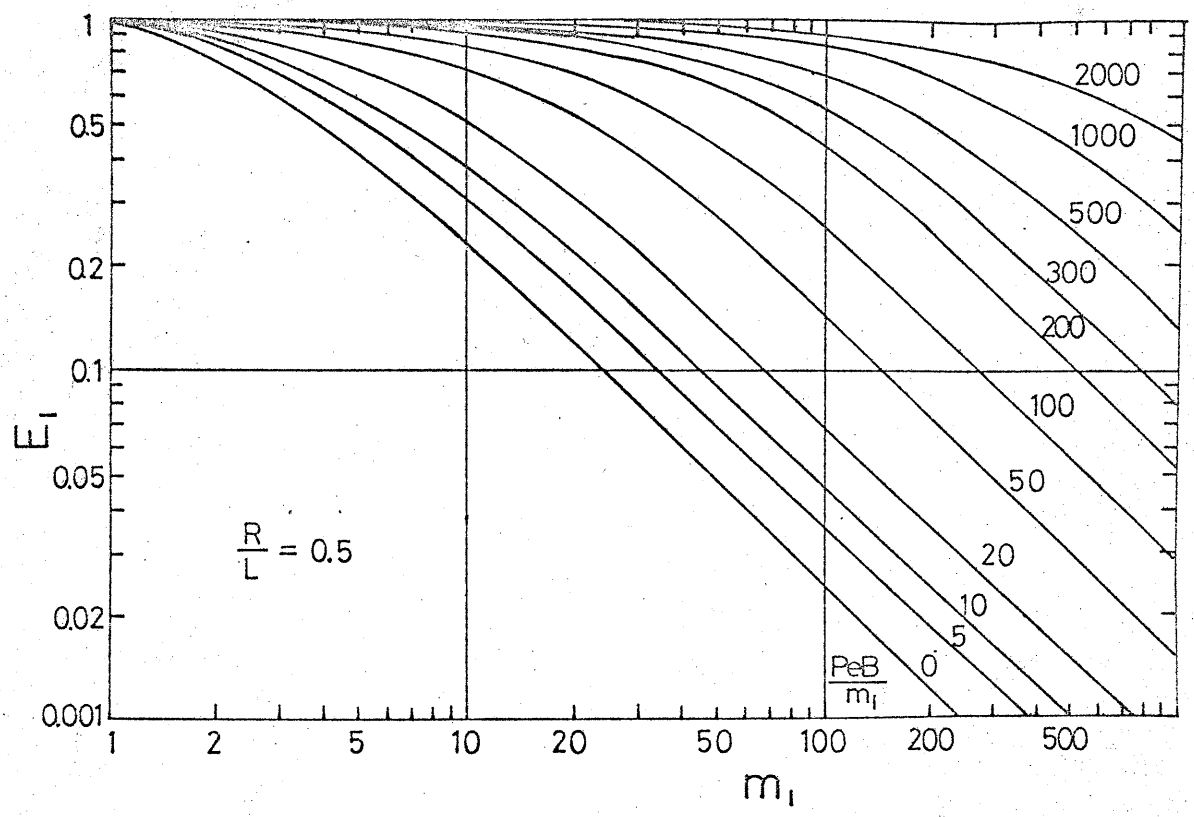

Fig.6-1 Effectiveness Factor under the Combined Effects of Hydrodynamic Flow and Diffusion

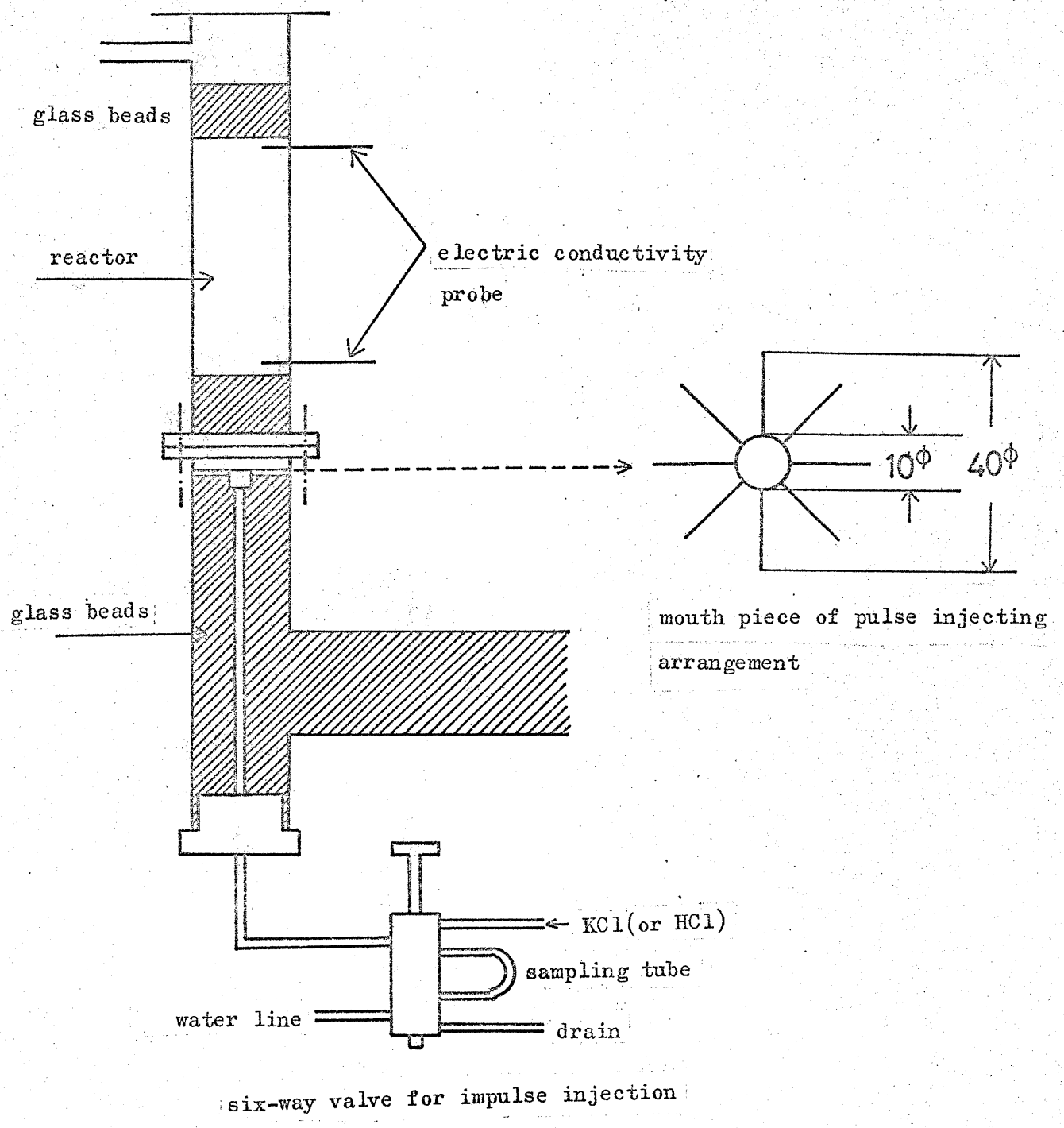

Fig.6-2 Main Parts of the Apparatus

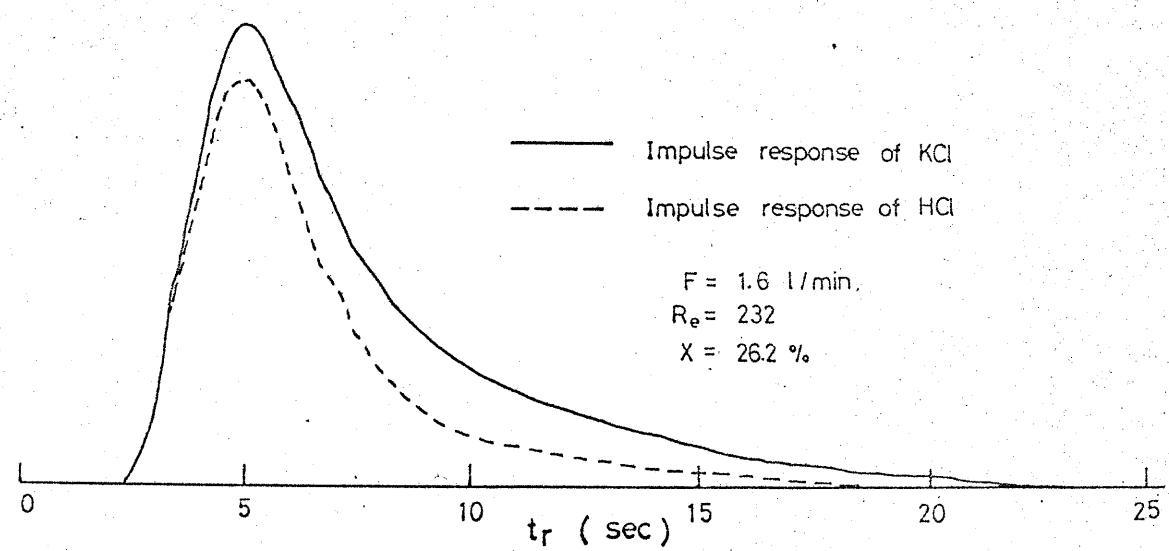

Fig.6-3 An Example of a Set of Impulse Responses

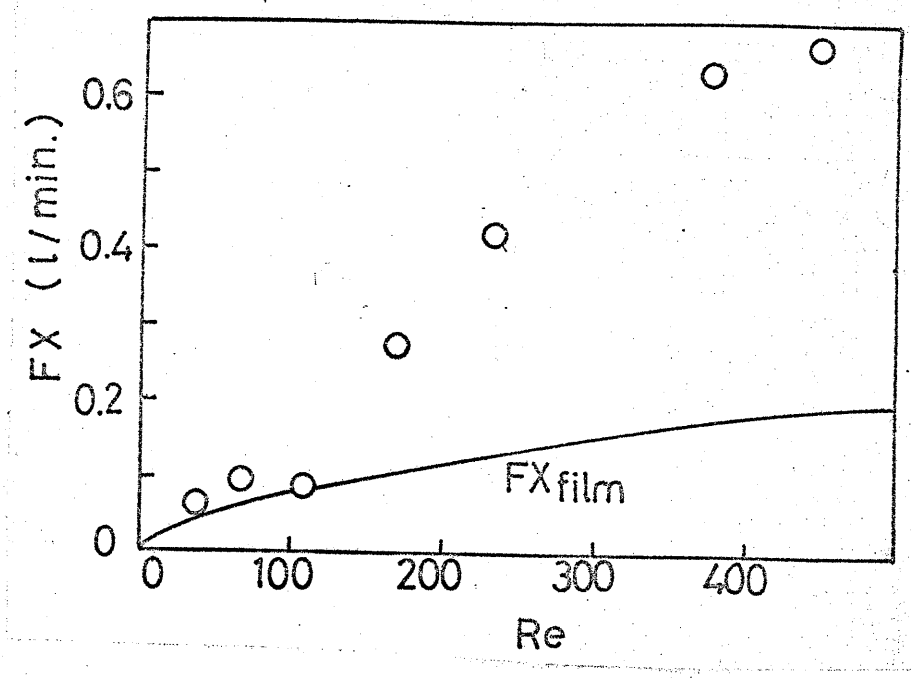

Fig.6-4 Relation of Reaction Rates to Reinolds Number

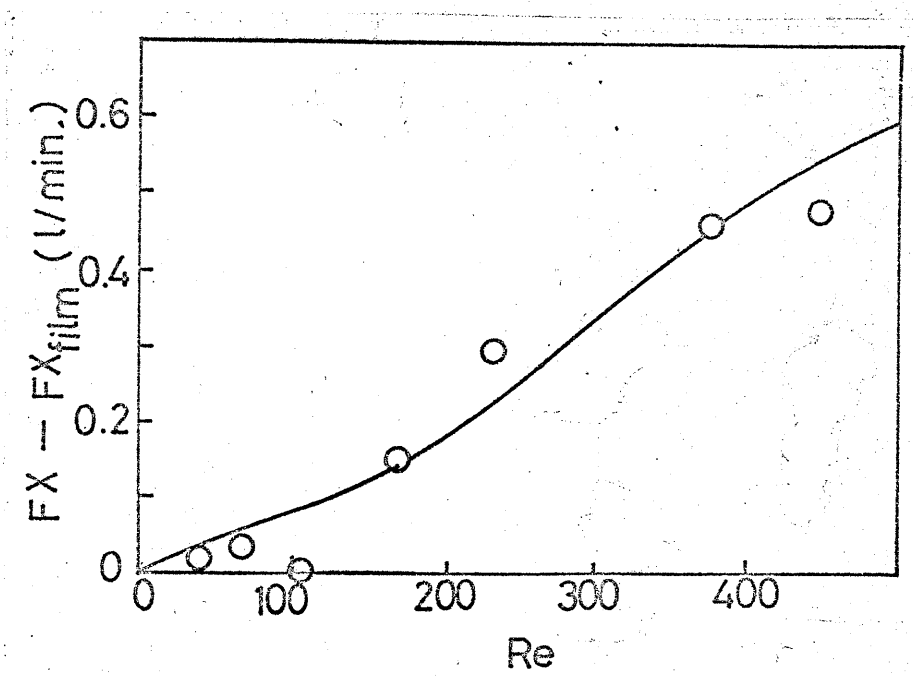

Fig.6-5 Comparison of Experimental Results with Theoretical Ones

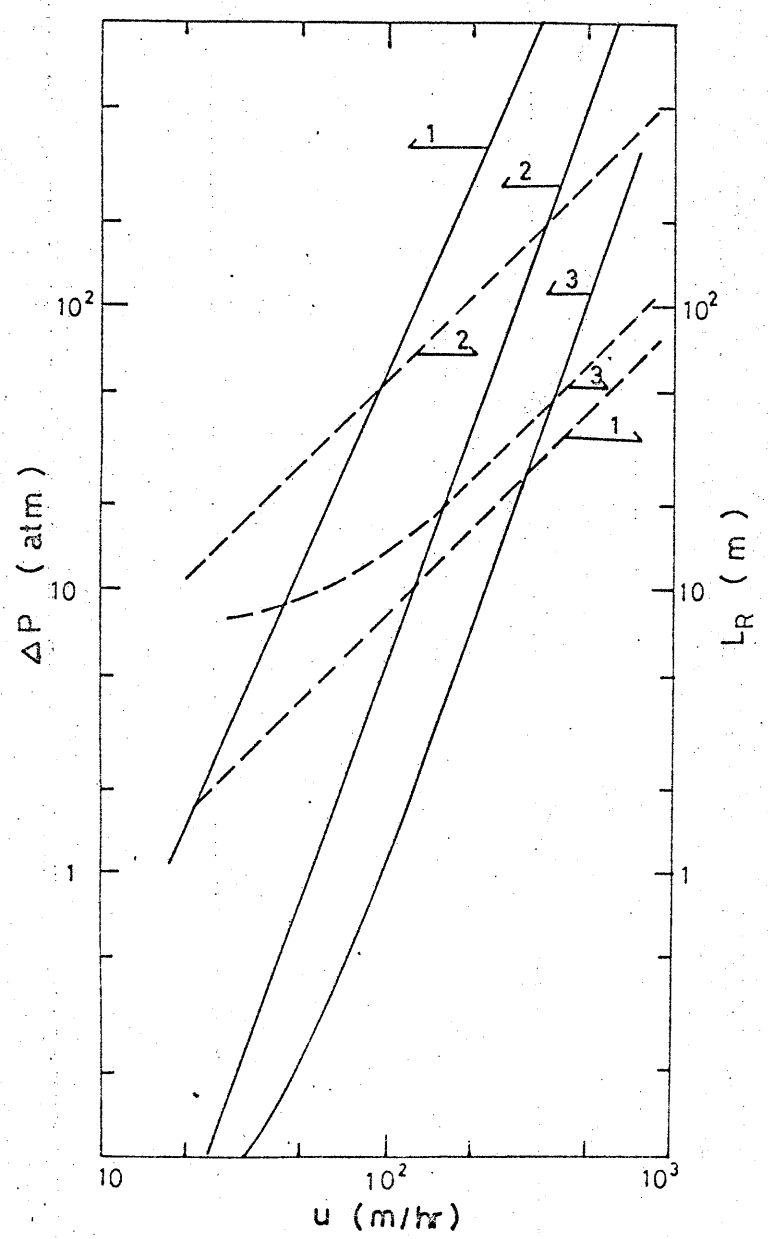

Fig.6-6 Comparison of the Reactor Involving the Inside Flow with Usual Reactors

1 a fine particle of D_p = 1 mm.

2 a pellet of D_p = 20 mm.

3 a pellet of D_p = 20 mm., composed of fine particles of D_p = 1 mm.

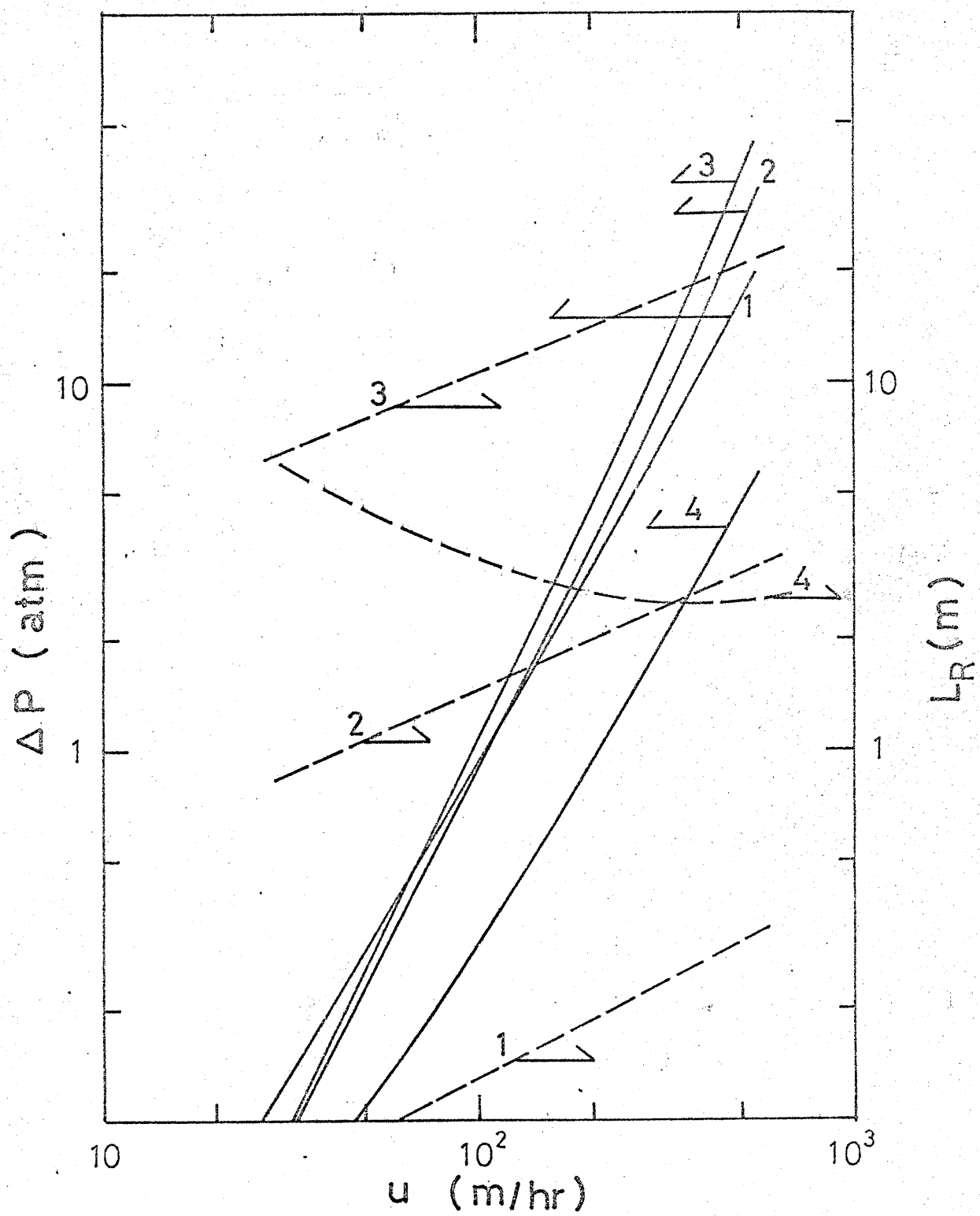

Fig.6-7 Comparison of the Reactor Involving the Inside Flow with Usual Reactors (mass transfer controle)

1 a fine particle of D_p = 1 mm.

2 a pellet of D_p = 5 mm.

3 a pellet of D_p = 20 mm.

4 a pellet of D_p = 20 mm., composed of fine particles of D_p = 1 mm.

Chapter 7 Fixed Bed Reactor of Supported Liquid Phase Catalysts

7-1 Introduction

The discovery of various liquid phase catalysts, frequently containing tranditional metal complex, urged the recent development of the industrial processes employing them. One of the successful examples is found in the process for conversion of olefin to aldehyde by the use of palldium complex, famous as the Wacker-Höchst process. The advance in the field of metal complex catalyst will produce an increasing number of useful reactions in the future. However, the present industrial equipments for such homogeneous reactions in the liquid phase, usually gas-bubbling type reactor, involve many problems difficult to solve mechanical problems such as the corrosion of the wall of the equipments, catalyst loss by entrainment and so on, and reaction engineering problems, such as back-mixing in the reactor and the difficulty in the prediction or the control of the reaction. The holding system of liquid phase catalysts as shown in this chapter, that is, the stationary bed of the porous materials containing a liquid phase catalyst in their pores, will eliminate the disadvantages otherwise encountered.

However, a new problem will be posed for the system, that is, the use of the ordinary sized porous material may result in low activity or low selectivity owing to a significant mass transfer effect. According to the author, it is one of the main reasons why the system has not become of practical use in industry, despite of the fact that it has already been suggested in 1935. The information on the solid catalysts obtained in the preceding chapters will give a hint for this problem. The high activity of the commercial nickel catalyst employed in the studies are caused by the dispersion of the active parts as the microparticles within the catalyst pellet and the rapid diffusion through macropore. Provided that the liquid phase catalyst is dispersed as small liquid particles within a porous material, the rapid diffusion through the empty pores may eliminate the mass transfer resistance and present high activity.

Supported liquid phase catalyst was first proposed by Moravec et al.[M- ,) and the recent studies of Rony[R- ,) and Acres et al.[A-) made some theoretical and experimental contribution in this fields. These studies, however, paid no attension to the problem stated above and adding to it, the effects of system parameters on the behavior of the catalyst were not elucidated. Furthermore, application of the system has been retricted to essentially non-volatile liquid phase catalyst.

In the present work, the catalyst system is applied to the conversion of ethylene to acetaldehyde by so-called Wacker-Höchst process. The main purposes of the study are listed below.

1) Examining the stability of the activity of the catalyst
2) Kinetic study of the supported liquid phase catalyst in comparison with a bubble column reactor
3) Applying the theory of the effectiveness factor to the catalyst system
4) Realization of the dispersion of the liquid phase catalyst within a porous material and analyzing such system

7-2 Reaction

Since the pioneering work was undertaken by Schmidt et al.[S-), the reaction of ethylene to acetaldehyde catalyzed by the hydrochloric acid solution of $PdCl_2$ and $CuCl_2$ has been investigated by many researchers from different point of views. The mechanism of the reaction and the variables affecting the rate are gradually being elucidated.

The reaction involves the conversion of ethylene to acetaldehyde accompanied with the reduction of palladium ion, oxidation of the resulting metalic palladium by cupric chloride and reoxidation of cuprous chloride with oxygen. After all, $PdCl_2$ functions as a catalyst. According to the recent book,) the rate of the overall reaction is expressed as Eq.(7-5).

$$C_2H_4 + PdCl_2 + H_2O \longrightarrow CH_3CHO + Pd + 2HCl \quad (7\text{-}1)$$

$$Pd + 2CuCl_2 \longrightarrow PdCl_2 + 2CuCl \quad (7\text{-}2)$$

$$2CuCl + \tfrac{1}{2}O_2 + 2HCl \longrightarrow 2CuCl_2 + H_2O \quad (7\text{-}3)$$

$$C_2H_4 + \tfrac{1}{2}O_2 \longrightarrow CH_3CHO \quad (7\text{-}4)$$

$$R_1 = \frac{k_1 \left[Pd^{2+}\right] \left[C_2H_4\right]}{\left[Cl^-\right]^2 \left[H^+\right]} \quad (7\text{-}5)$$

7-3 Fixed Bed Reactor of Supported Liquid Phase Catalyst

7-3-1 Equipments and Operating Conditions

The apparatus employed in the experiments is shown schematically in Fig.7-1. A reactor of glass tube of 10 mm I.D. and a pre-saturator, which is a small bubble column contactor filled with hydrochloric acid solution of the same concentration as the catalyst solution, are placed in a thermo-stated vessel. The use of the pre-saturator keeps the solvent of catalyst solution from vaporizing. A distillatory apparatus was connected to the outlet of the reactor in order to remove most of water vapor from the effluent gas, which was neccesary for a reliable analysis of the composition by means of gas chromatography.

The composition of the reacting gas is (N_2 61% O_2 37% C_2H_4 2.3%), total flow rate in the reactor is about 22 to 27 cm^3/min., and reaction temperature is 70°C, unless otherwise stated.

7-3-2 Preparation of Supported Liquid Phase Catalyst

The catalyst solution is usually of the same composition ($PdCl_2$ 5.64 mmol/l, $CuCl_2$ 0.1 mol/l, HCl 0.06 mol/l). The composition was selected in the range where the three steps of the reaction system, Eqs. (7-1), (7-2) and (7-3), balance to one another so that metalic palladium didn't deposit.

Porous glass supplied by the Tokyo Shibaura Electric Co.Ltd, whose pore diameter is smaller than 50 Å, and the porous alumina pellet named FCC supplied by the FujimiKemmazai Kogyo Co. Ltd., whose average pore diameter is about 10 μ, are employed as carrier materials of the catalyst solution. The use of chemically inactive materials is important for the system. In reality, some other porous materials affected significantly the catalyst solution.

Owing to the high ionization potential, palladium ion is easy to lose the charge by the contact with other metals so that carrier materials must be cleaned from impurities. They were treated by hydrochloric acid solution and then pure water at boiling temperature for several hours, heated and dried in a vacuum. Then, the catalyst solution was added by vacuum in the carrier materials. The catalyst pellet was proved to contain 0.25 gm. of catalyst solution per 1 gm. of carrier material, by the decrease in the weight when dried up and by means of colorimetric determination of palladium ion in the solution in which a decided amount of the catalyst pellets is soaked. The content of the catalyst solution clearly shows that the whole pore volume is filled with it.

7-3-3 Experimental results

1) Stability of catalytic activity

As shown in Fig. 7-2, the catalytic activity remains almost constant in the course of the reaction. The rate constant k_1 was calculated assuming a first order reaction respecting to the concentration of ethylene in the catalyst solution .

$$k_1 = \frac{-K \ln (1 - X)}{W/F} \qquad (7\text{-}6)$$

$$F = F^0 \frac{760}{760 - P_{H_2O,T_{reactor}}} \frac{T_{reactor}}{T_{room}} \qquad (7\text{-}7)$$

Here, K and W represent respectively the gas-liquid partition coefficient of the reactant and the total volume of the catalyst solution contained in the catalyst

pellets in the reactor. F and F^o are the volumetric flow rate at the inlet of the pre-saturator and in the reactor.

2) Kinetic studies

Figs. 7-3 and 4 show that $R_1 \propto P_{C_2H_4} P_{O_2}^{0}$, in accord with the results by the bubble column reactor shown later and by many other investigators. Fig.7-5 shows that $k_1 \propto [Pd^{2+}]^{0.57}$, where the change in the concentration of $[Cl^-]$ is negligible. Activation energy of the reaction is 9.57 kcal/mol from Fig.7-6. Here, the change in solubility of ethylene with temperature was taken into account.

The dependency of the rate on the concentration of palladium ion and the observed activation energy differ from those obtained by the bubble column reactor in which the mass transfer effect is eliminated. The differences may be caused by poor effectiveness factors of the catalyst pellet employed in these experiments and they are discussed in detail later.

3) Effect of pellet size and carrier material on catalytic activity

Fig.7-7 shows the rate constants for different sized catalysts, ranging from 30 μ to 5 mm. Catalytic activity is strongly influenced by pellet size and the trend may be explained by the effectiveness factor. They are discussed later on the basis of the intrinsic rate constant of the reaction and the effective diffusion coefficient within the carrier material.

7-4 Bubble Column Reactor

The same apparatus was employed, except that the fixed bed reactor was replaced by a glass tube (I.D. 10 mm) equipped with a mouthpiece of glass filter at the bottom, from which the reacting gas mixture was bubbling into the catalyst solution. Fig.7-8 shows the rate constants for different values of

the concentration of palladium ion and of the total flow rate. Each family of the same total flow rate converges to a limiting rate constant, represinting that the rate-controling step shifts from mass transfer to homogeneou reaction. For example, in the case of $[Pd^{2+}]$ = 5.64 mmol/l, the total rate is controled by the homogeneous reaction if the flow rate is more than 40 ml/min.. Under the condition, the gas phase is dispersed in the liquid phase as bubbles smaller than 1 mm and the volume ratio of the former to the latter is more than 45%.

The kinetic studies are carried out in the reaction controling range .

Fig.7-9 and 10 respectively show that $k_1 \propto [Pd^{2+}]^{0.83}$ and $R_1 \propto P_{C_2H_4}$. The true activation energy of hthe reaction is proved to be 14.7 kcal/mol from Fig.7-11 where the rate constants are expressed by k_1^o ($= \frac{k_1 [Cl^-]^2 [H^+]}{[Pd^{2+}]}$) instead of k_1, eliminating the effects of the composotion of the catalyst solution and comparing the present data with the results by other investigators. In each literature, a value of k_1^o was calculated at one oprating condition and plotted in the figure by a small circle and the line is drawn so as to represent the activation energy and the temperature range which the experiments coveredd.

7-5 Effective diffusion Coefficient in the Liquid Phase Supported in the Porous Materials

KCl solution of 1 mol/l was supported by the carrier materials in much the same fashion as the catalyst pellet was prepared. The resultant pellets was soaked in the pure water being agitated by a nagnetic stirrer and controled within 0.5°C. The diffusion rate of KCl from the pellets into the water was measured by the increase in the electric conductivity of the water. The effective diffusion coefficient was estimated by the comparison of the measured diffusion rate with the theoretical one.) Some examples of the desorption curves are shown in Fig. 7-13. It should be noted that the effective diffusion coefficient is defined as D/τ instead of $\theta D/\tau$ as usually defined in a gas-solid system, The tortuosity factor was proved to be 7.0 for the porous glass

and 1.3 for the porous alumina.

The effective diffusion coefficient of ethylene at the reaction temperature ($70^{o}C$) was estimated in the following way. Potassium chloride and ethylene are of almost the same molecular diffusivity in water at $20^{o}C$. Activation energy of the viscosity of water is 5.06 ($0^{o}C$), 3.42 ($50^{o}C$) and 2.8 ($100^{o}C$) in kcal/mol. Activation energy of diffusion may be equivalent to that of viscosity though the sign is reversed. To be sure, the observed activation energy for the porous glass, 4.9 kcal/mol , in the range of 5 to $35^{o}C$, agrees well with that for viscosity at $0^{o}C$, 5.06 kcal/mol. Based on the consideration, the effective diffusion coefficient of ethylene at $70^{o}C$ was estimated by the extrapolation of the experimental result at $25^{o}C$ assuming the activation energy to be 3.42 kcal/mol.

$$D_e = 6.56 \times 10^{-6} \quad cm^2/sec \quad \text{(the porous glass)}$$

$$De = 3.18 \times 10^{-5} \quad cm^2/sec \quad \text{(the porous alumina)}$$

7-6 Analyses

The reaction has been proved to follow a first order law in respect to the concentration of ethylene,and the intrinsic rate constant and the effective diffusion coefficient have been obtained. The Thiele modulus, therefore, can be determined for each size of the catalyst. Fig.7-14 shows the experimental effectiveness factor (= $k_{lobs} / k_{lintrinsic}$) versus the modulus. The experimental results agrees well with the theoretical relation between the effectiveness factor and the modulus. It should be noted that the effectiveness factors for the two different carrier materials coincide with each other when the difference in their effective diffusion coefficients is considered.

The apparent difference of the activation energy and the rate dependency on Pd^{2+} in the supported liquid phase catalyst from the intrinsic reaction may be caused by the poor effectiveness factor of the catalyst. Under the condition where the kinetic studies were made, the effectiveness factor can be approximated by $3/m_1$. Therefore,

$$R_{lobs} = k_{lobs} \left[C_2H_4\right] = k_1E_1 \left[C_2H_4\right] = 3\sqrt{\frac{k_1D_e}{R}}\left[C_2H_4\right] \quad (7\text{-}8)$$

On this relation, the apparent activation energy for the supported liquid phase catalyst is:

$$E_{obs} = (E_d + E_a) / 2 = (14.7 + 3.42) / 2 = 9.1 \text{ kcal/mol}$$

This prediction agrees well with the experimental observation (9.57 kcal/mol).

The apparent dependency of the rate on $\left[Pd^{2+}\right]$ may be expressed as:

$$k_{lobs} = \propto k_1^{\frac{1}{2}} \propto \left[Pd^{2+}\right]^{\frac{0.83}{2}} = \left[Pd^{2+}\right]^{0.42}$$

The agreement of this prediction with the experimental result, $\left[Pd^{2+}\right]^{0.57}$, is not so good, though they coincide qualititatively with each other. This disagreement may be understood, when the following fact is considered. When the catalysts were put into the reactor at an elevated temperature, a very small amount of catalyst solution oozed from the pellets, possibly to yield small liquid particles at the contact points between the pellets. The reaction in the small particles may not be ignored in the region of the high concentration of Pd^{2+}, because the pellet effectiveness factor is very small.

Thus, it is demonstrated that the apparent difference in the kinetics is caused by the poor effectiveness factor of the supported liquid phase catalyst.

7-7 Dispersion of a Catalyst Solution within a Carrier Material

From an industrial point of view, high activity and high selectivity are desired in general. They are frequently attained by operating a catalyst under a high effectiveness factor. In the catalyst system treated here, the effectiveness factor becomes unity at the pellet size as small as about 50 . This size is , however, not of practical use for a fixed bed reactor. The small effectiveness factor, in spite of the rather slow rate of the depletion of the reactant, is resulted from the small diffusibility in the liquid phase and the poor solubility of the reactant in the catalyst solution. Such problem will arise in general for this type of catalyst. The author intends to eliminate the significant mass transfer resistance by the dispersion of the active catalyst solution within the carrier material.

Catalyst solution is supported in pores by the balance of surface tension with gravitational force. The gravitational force is proportional to the mass of the solution (volume of the pore), but on the other hand the surface tension to the length of the interface (diameter of the pore). As a result, the solution contained in larger pores is more easily removed by the increase of the gravitational force.

Based on the consideration, the supported liquid phase catalysts were put in a centrifugal separator. When an appropriate centrifugal force is added, the catalyst solution in larger pores will be removed but that in smaller pores will still remain. In reality, a pore structure is not an assembly of cylindrical pores but may be regarded as the void spaces between a large number of fine particles. Consequently, the catalyst solution will be contained in the void space near the contact points of the particles, when the centrifugal force is added to them. That is exactly what was intended.

Fig.7-15 shows the relation between the fraction of catalyst solution in the total pore volume, ε°, and the time that the centrifugal force was added to

the catalyst, for several values of the velocity of revolution of the centrifugal separator. The content of the catalyst solution becomes almost constant within a minute, representing a rapid equilibration.

Whether or not the solution in a pore of the radius r is removed will be examined by the following way. Assuming that a cylindrical pore is located perpendicularly to the centrifugal force, the force balance equations is expressed as

$$2\pi r \alpha \cos\theta = \pi r^2 l \rho L (2\pi n)^2 \qquad (7\text{-}9)$$

where l is the pore length, α and ρ are respectively the interface tension and the density of the solution, θ is the contact angle between the solution and the interior wall of the pore, L is the length of the arm of the centrifugal separator and n is the velocity of revolution in r.p.m..

Eq.(7-9) leads to

$$r_{critical} = \frac{\alpha \cos\theta}{2\pi^2 \rho L n^2 l} \qquad (7\text{-}10)$$

If the radius of a pore is smaller than $r_{critical}$, the solution in the pore won't be removed at all, but for the parger pores, some portion of the solution will be removed. Of course, the practical situation becomes much more complicated owing to a complex pore structure. In order to get the approximate value of $r_{critical}$ in the present system, each value is substituted into Eq.(7-10), assuming that the pore length is equal to the diameter of the pellet as considered and that n is 1000 r.p.m..

Then, Eq.(7-10) gives

$$r_{critical} = 6.4\ \mu \qquad (7\text{-}11)$$

This value agrees in the order with the average pore size for the porous alumina, indicating that the pore structure is competent for the control

of the content of the catalyst solution by this method. On the other hand, the catalyst solution supported by the porous glass was not removed at all, even at the high velocity of revolution as 3000 r.p.m.. This is because its average pore diameter is as small as 50 Å. Porous materials of such pore structure are not competent for this type of catalyst.

It should be also noted that the use of a carrier material of too rough pore structure may result in flowing out of some portions of the catalyst solution, when the catalyst pellets are packed in a reactor, by the force of gravity for the height of the reactor. Such phenomenon was actually observed for the porous material supplied by the Norton Co. Ltd., whose average pore diameter is about an order of 1 mm.

The activity of the catalyst of which content of the catalyst solution was controled by the treatment shown above was measured. The porous alumina pellet of 10 mm. was employed as a carrier. The results are shown in Fig.7-16, in which the effectiveness factor is defined as the observed activity relative to the possible activity for the content of the catalyst solution under a reaction controling condition. The effectiveness factor increases with the decrease in the content of the catalyst solution and becomes unity at $\varepsilon^{\circ} = 0.4$, indicating that the effective size of the particles of the catalyst solution dispersed in the pellet becomes smaller than 50 . In Fig.7-16, $(\varepsilon^{\circ} E_1 / E_{1,\ \varepsilon^{\circ}=1})$ is also plotted as a function of ε°. This represents the average activity per unit volume of the catalyst pellet relative to that in the case where whole pore volume is filled with the catalyst solution. It increases with decreasing content of the catalyst solution and becones eight times the activity at $\varepsilon^{\circ} = 1$. In the region of $\varepsilon^{\circ} < 0.4$, it decreases linearly in respect to ε°, representing that the catalyst solution functions under a reaction controling condition.

The catalyst structure is a typical example to which the micro-macropore model is properly applied. The Thiele modulus of the catalyst pellet is given by

$$m_1' = R\sqrt{\frac{\varepsilon k_1' \rho_1}{D_M}} \qquad (2\text{-}17)$$

Let the case of $\varepsilon^\circ = 0.4$ be considered. The effectiveness factors of the microparticles are unity on the above considerations. The volume ratio of the microparticles to total catalyst volume ε is $\theta\varepsilon^\circ = (0.4)\ (0.4) = 0.16$. The diffusion coefficient in the macropore, which is the empty pores in this case, may be considered to be about 2×10^{-2} cm2/sec. The intrinsic rate constant k_1' is 8×10^{-2} sec^{-1} from Fig.7-8. Substituting these values into Eq.(2-17) gives $m_1' = 0.4$. The effectiveness factor of the macropore is ,therefore, unity in this case. Furthermore, it is predicted that the increase in the pellet size up to 2.5 cm doesn't reduce activity.

Thus, it is demonstrated that the effectiveness factor and the activity of the catalyst pellet is increased by the treatment by means of a centrifugal separator and that they may be easily controled by the velocity of revolution. These may be of practical importance not only for a simple reaction as shown here but also for a complex reaction system.

7-8 Summary

This chapter is concerned with the liquid phase catalyst supported by a porous material, the stationry bed of which will eliminate various difficulties emcountered in the ordinary industrial equipments for gas-liquid catalytic reactions, gas-bubbling type. While the proposal of this type of catalyst was made as far as 35 years ago, most of their important aspects were not elucidated yet as cleared in the introduction. They are investigated systematically in this chapter.

The stable operation observed in the experiments for the conversion of ethylene to acetaldehyde by Wacker-Hochst process proved clearly the applicability of the catalyst system to the process, despite of the high vapor pressure

of the catalyst solution. The parameters affecting the activity and the apparent kinetics of the catalyst were analyzed based on the true kinetics obtained by the rate study by a bubble column reactor and the measured effective diffusion coefficient in the liquid phase supported by the porous material. It was concluded that the homogeneous reaction in the catalyst solution is not affected at all by being supported in pores and that the apparently different kinetics observed in the experiments are die to the poor effectiveness factor of the catalyst.

As expected beforehand, the difficulty posed for this type of catalyst was its low activity at the ordinary sized carrier material, resulted from a signigicant diffusion resistance in the liquid phase. A centrifugal separator was proved to give a powerful means to the problem. When a centrifugal force is added to the catalyst, the catalyst solution in larger pores is removed but in smaller pores it still remains and the resultant catalyst structure allows a rapid diffusion through the empty pores. The experiments showed that the activity and the effectiveness factor of the catalyst is easily controled by the velocity of the revolution of the separator, through the content of the catalyst solution on the pore structure.

As a result, the stationary bed of this type of catalyst was proved to be superior to the bubble column reactor.

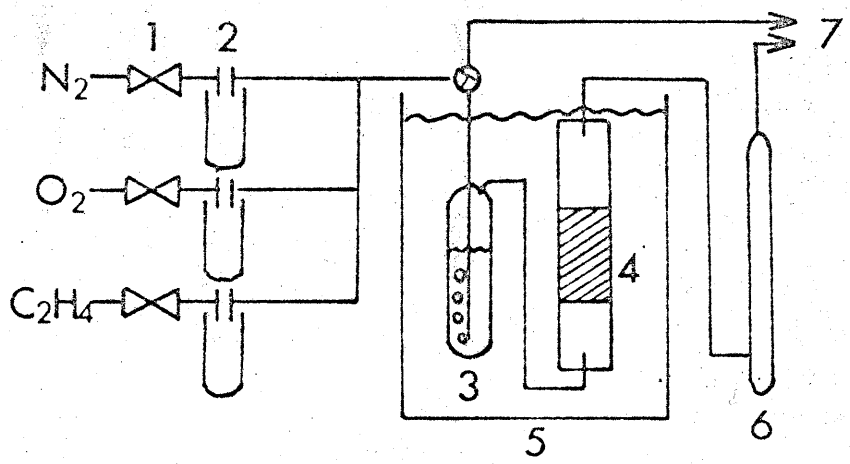

Fig. 7-1 Flow sheet of the apparatus

1 valve 2 flow meter 3 pre-saturator
4 reactor 5 thermostatic vessel 6 distilling column
7 gas fracto meter

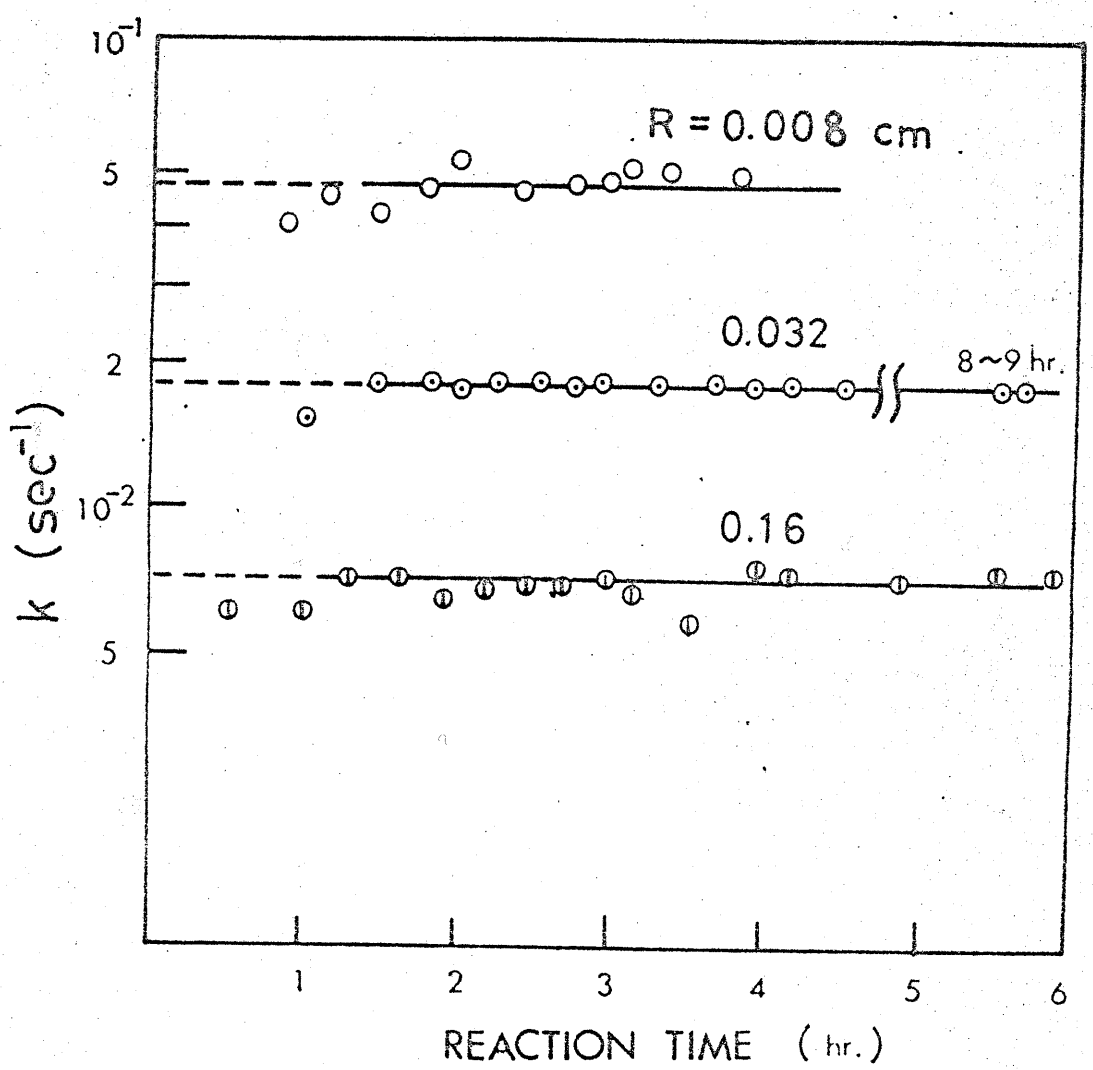

Fig. 7-2 Variation of k with time
(porous glass carrier)

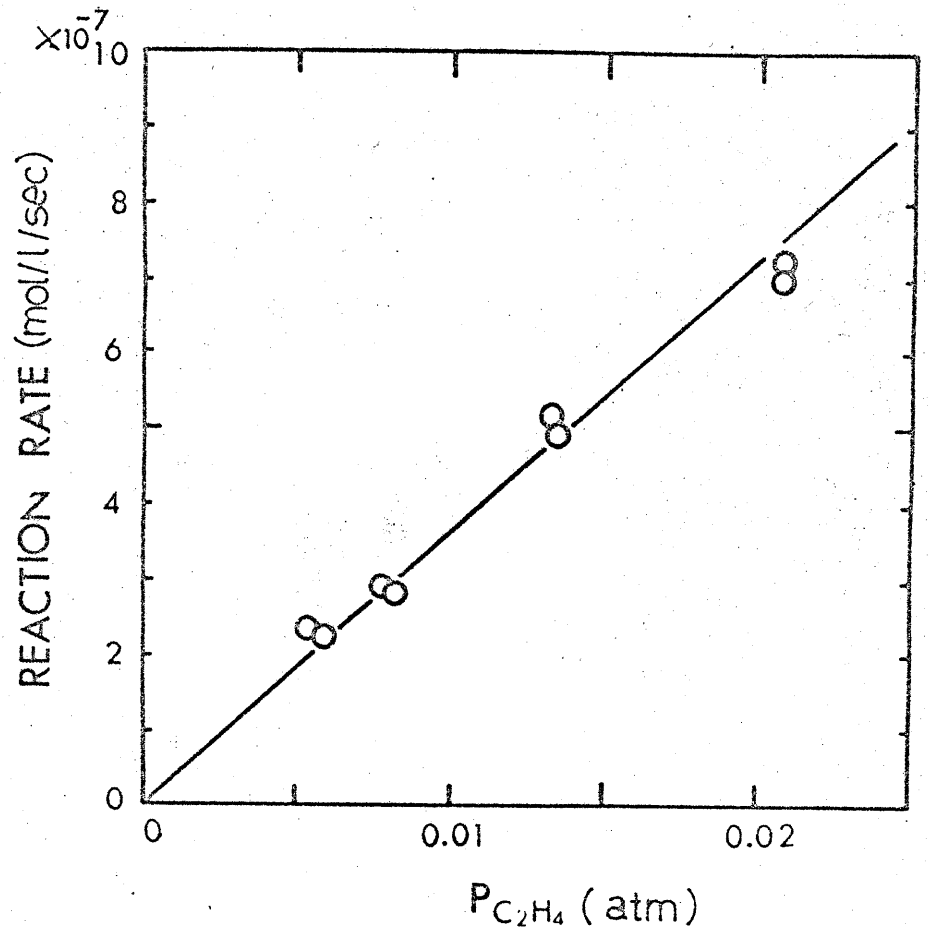

Fig.7-3 Dependence of the reaction rate on the partial pressure of ethylene

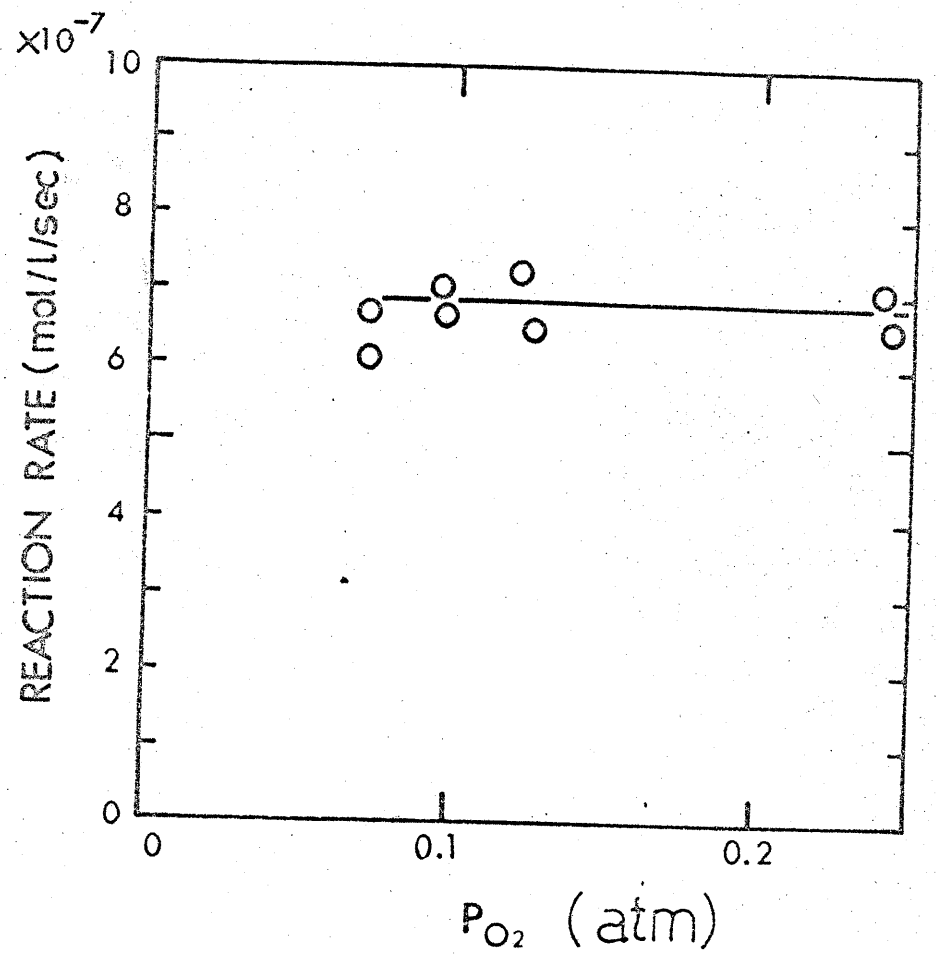

Fig.7-4 Dependence of the reaction rate on the partial pressure of oxygen

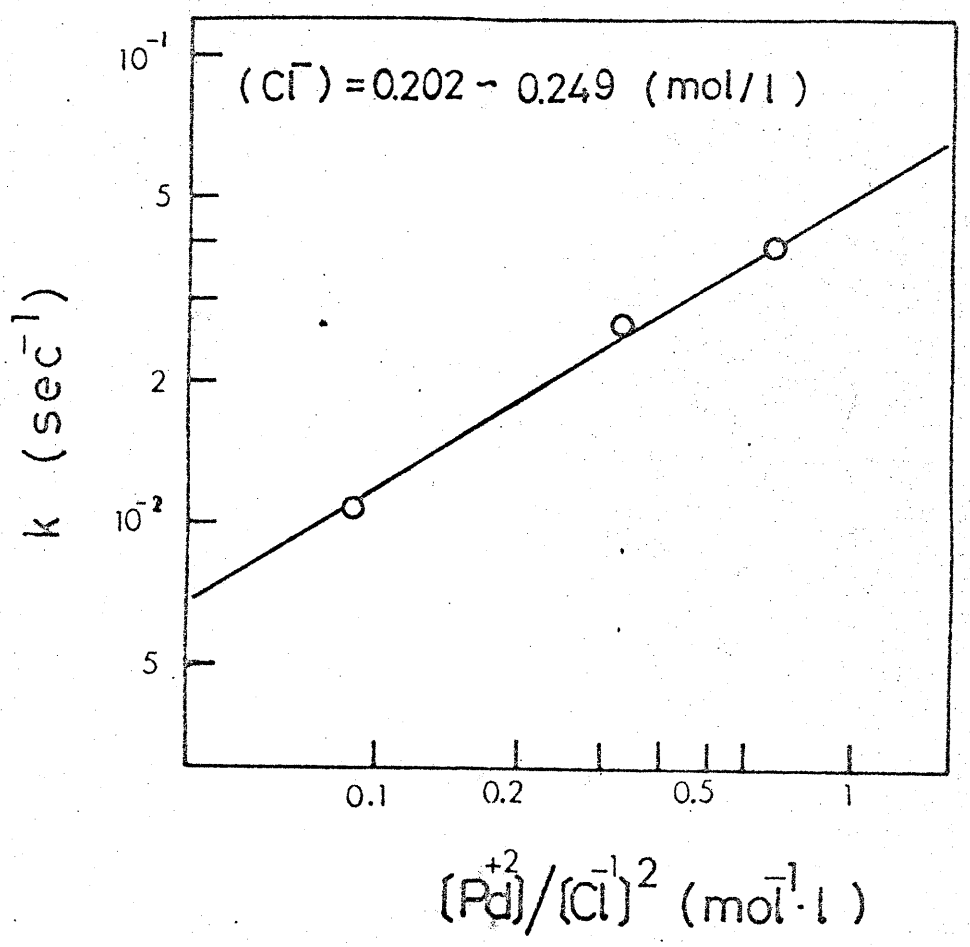

Fig.7-5 Dependence of k on the concentration of palladium

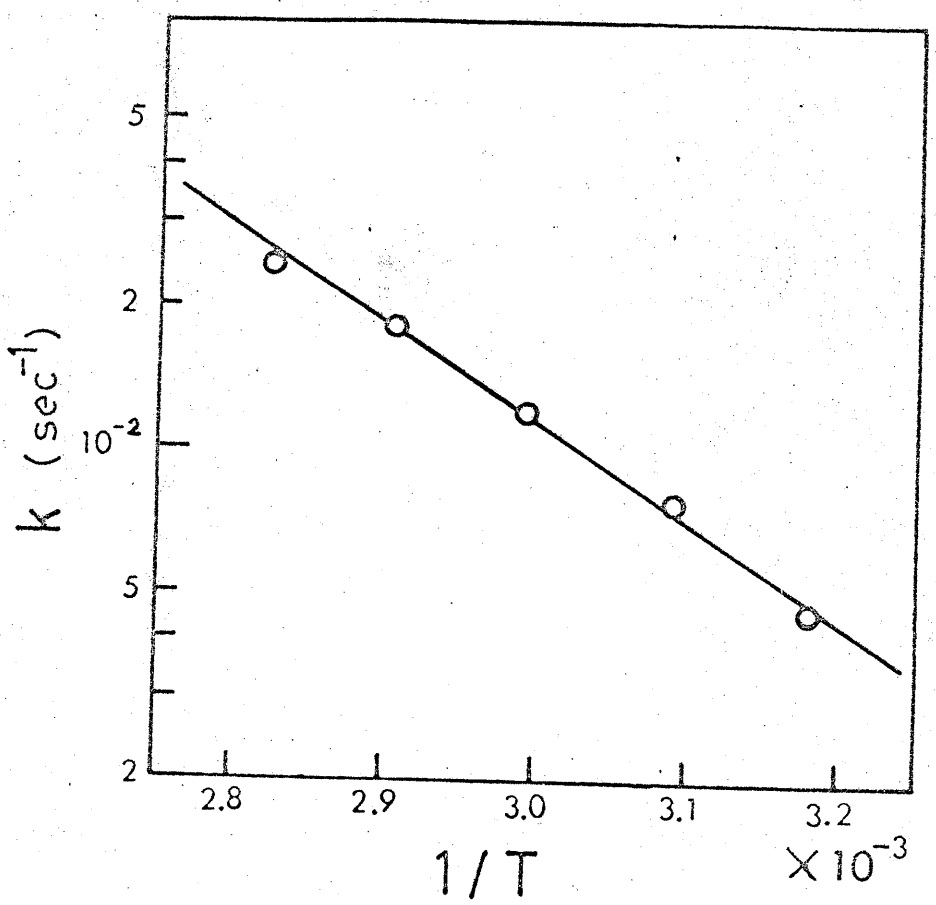

Fig.7-6 Arrhenius plot for supported catalyst

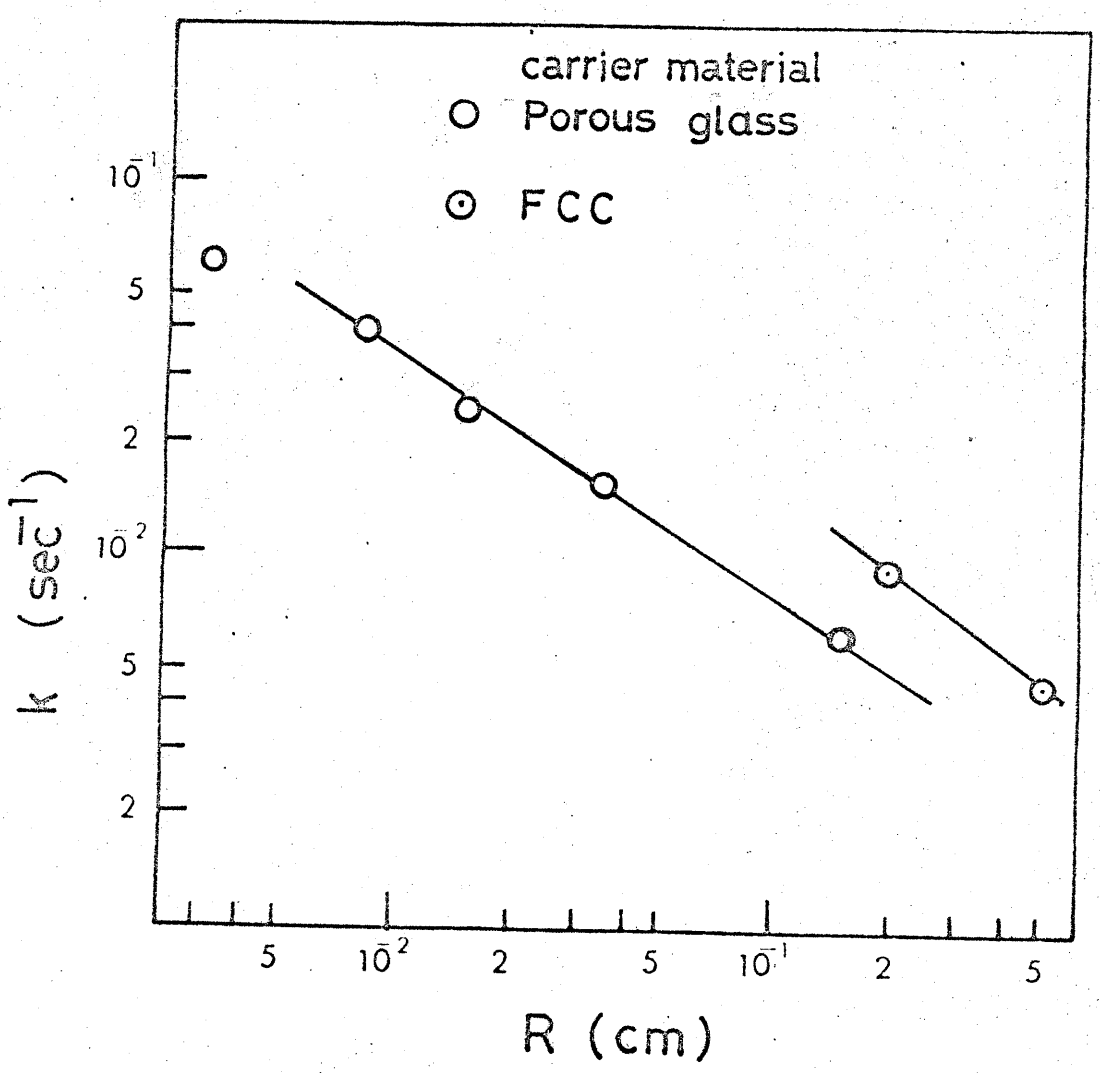

Fig.7-7 Dependence of k on the size of carrier particle

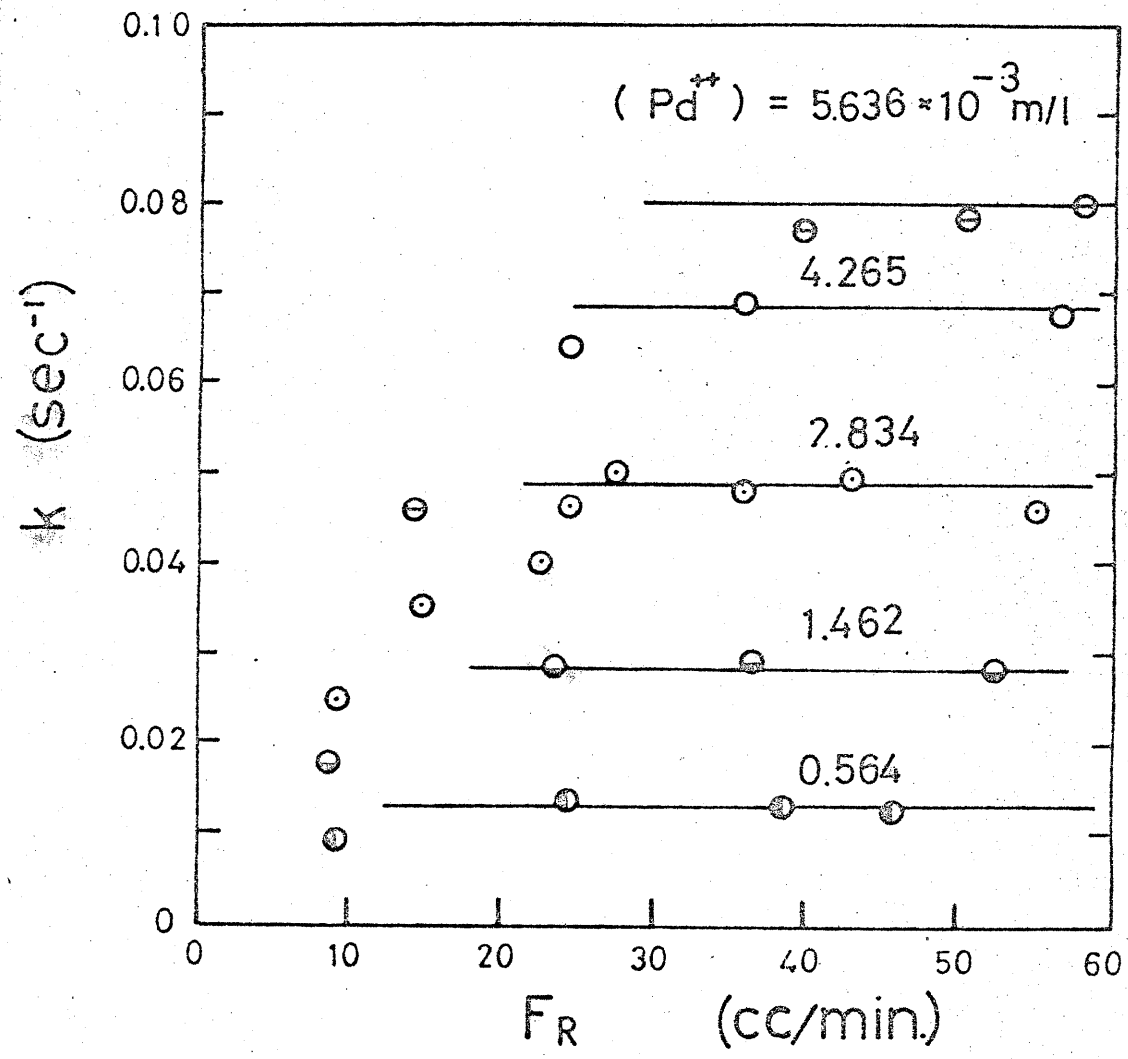

Fig.7-8 Dependence of k on the flow rate in the bubbling bed

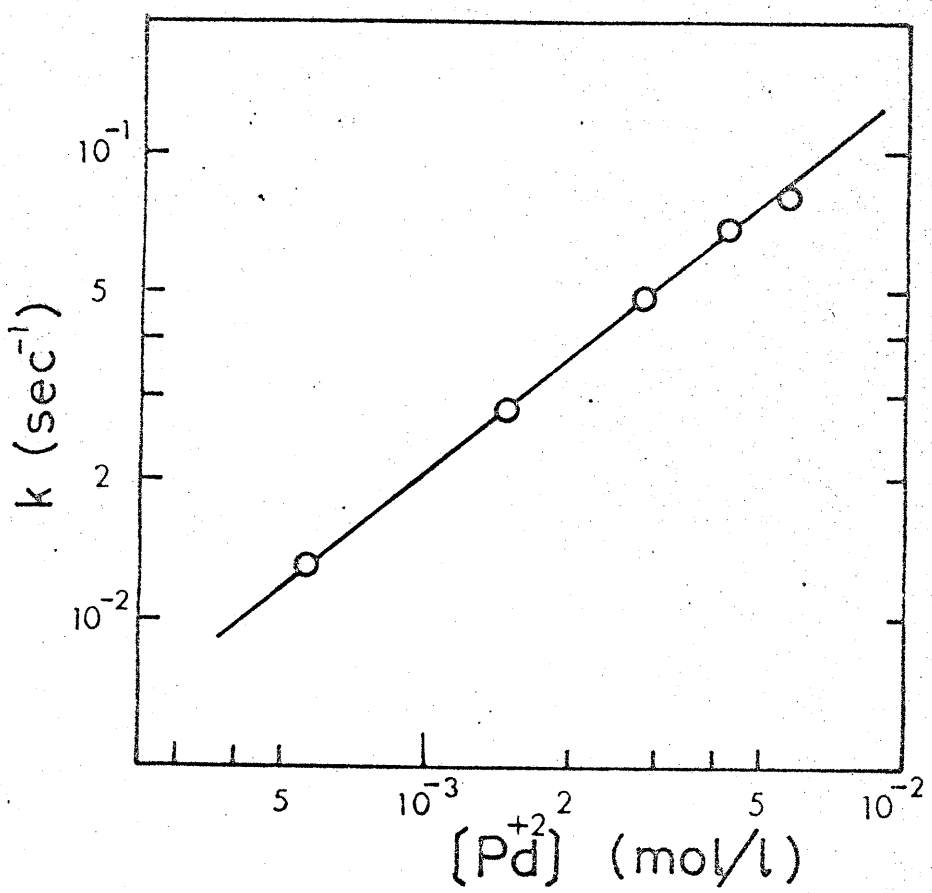

Fig.7-9 Dependence of k on the concentration of palladium

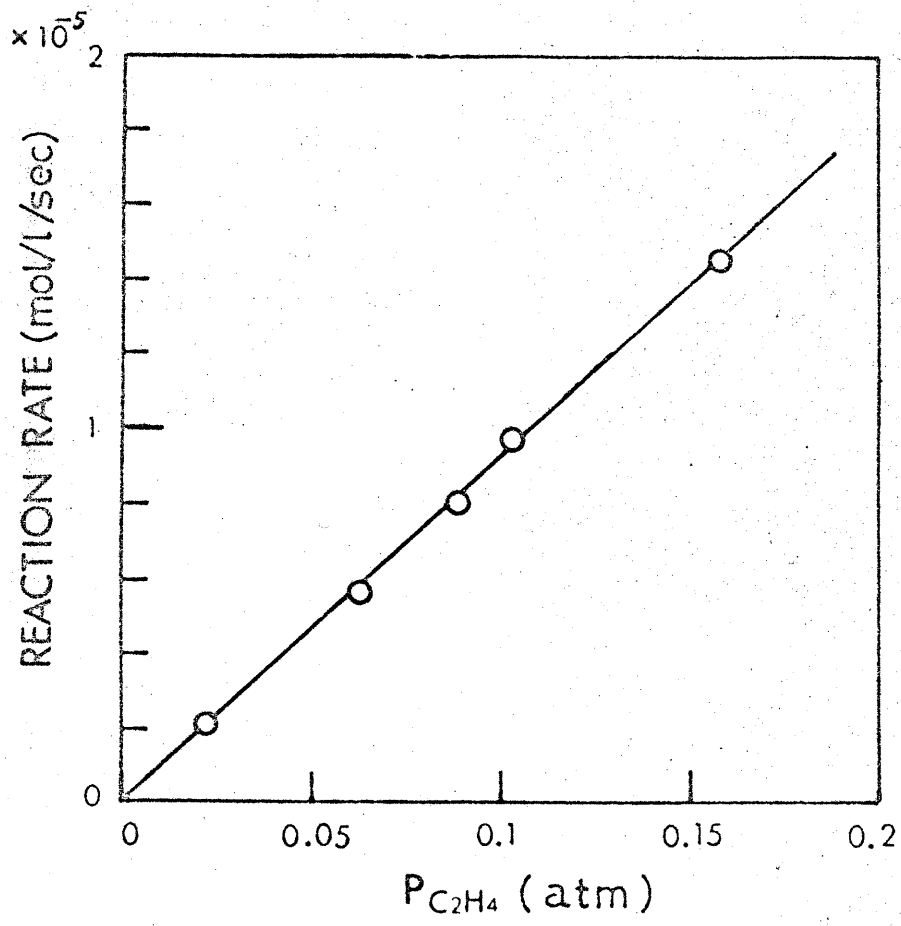

Fig.7-10 Dependence of the reaction rate on the partial pressure of ethylene

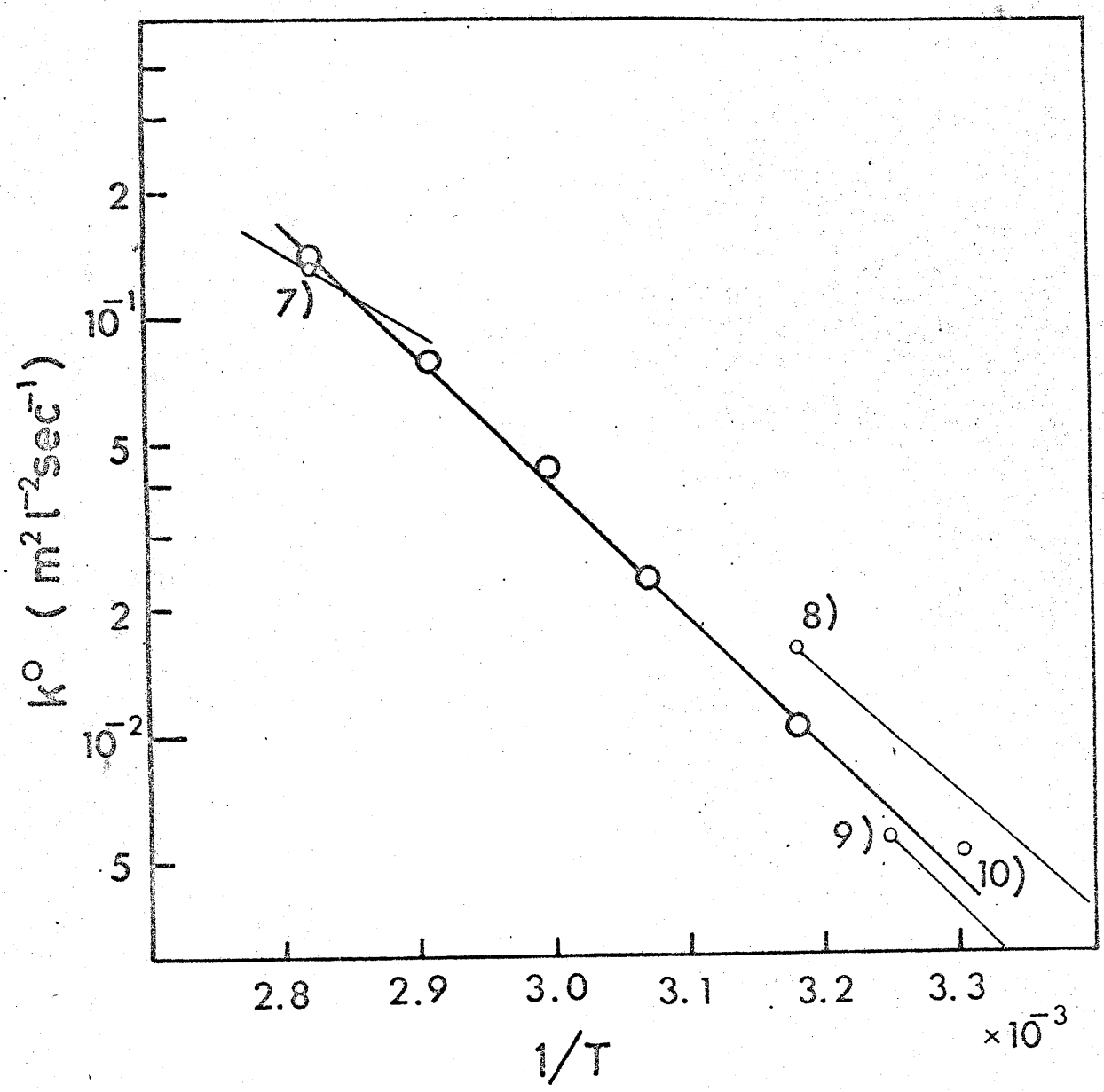

Fig.7-11 Arrhenius plot for the bubbling bed and comparison with the other works

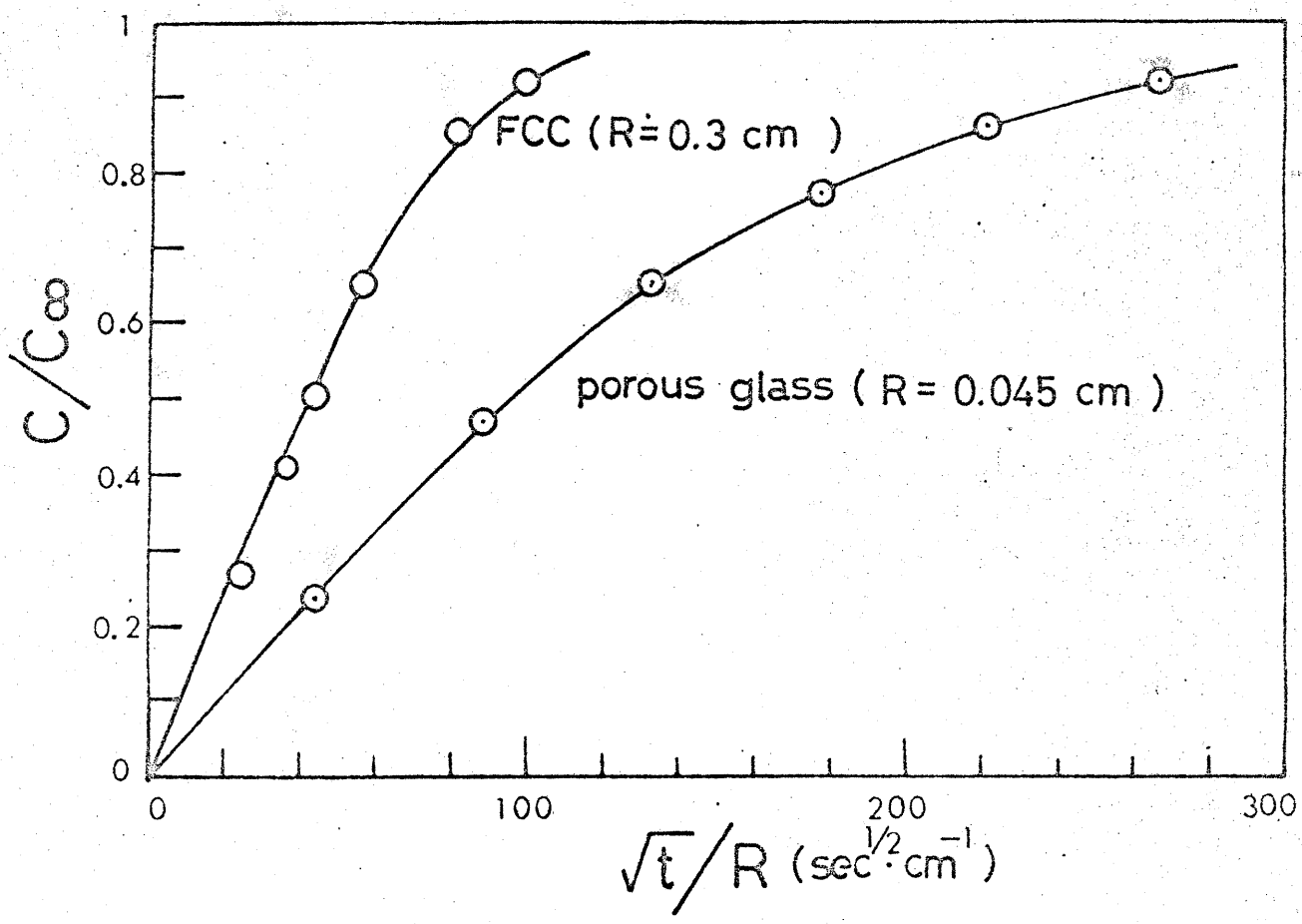

Fig.7-12 Rate of effusion from porous particles (25°C)

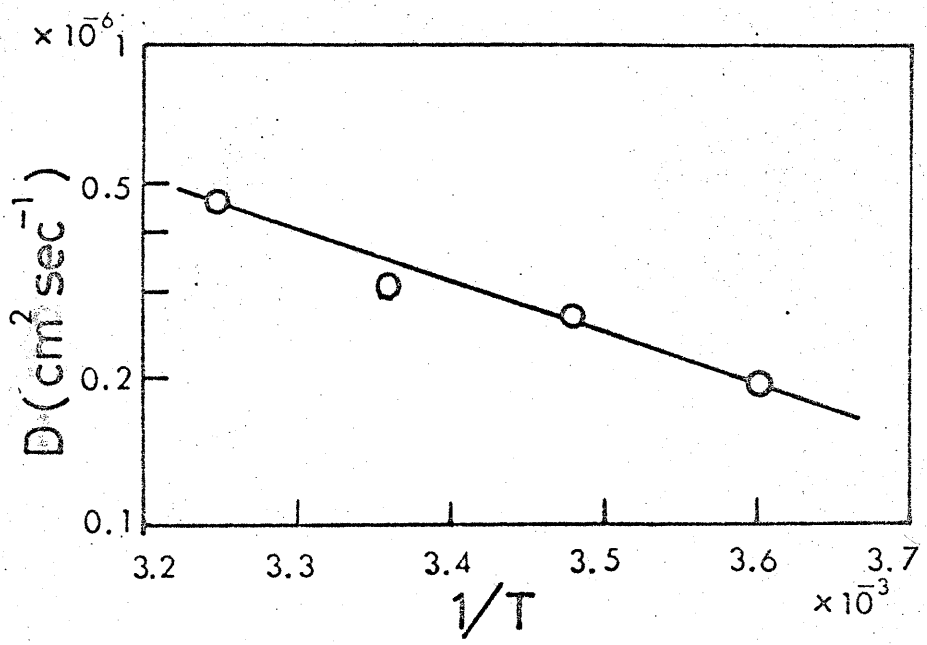

Fig.7-13 Dependence of diffusion coefficient of porous glass on temperature

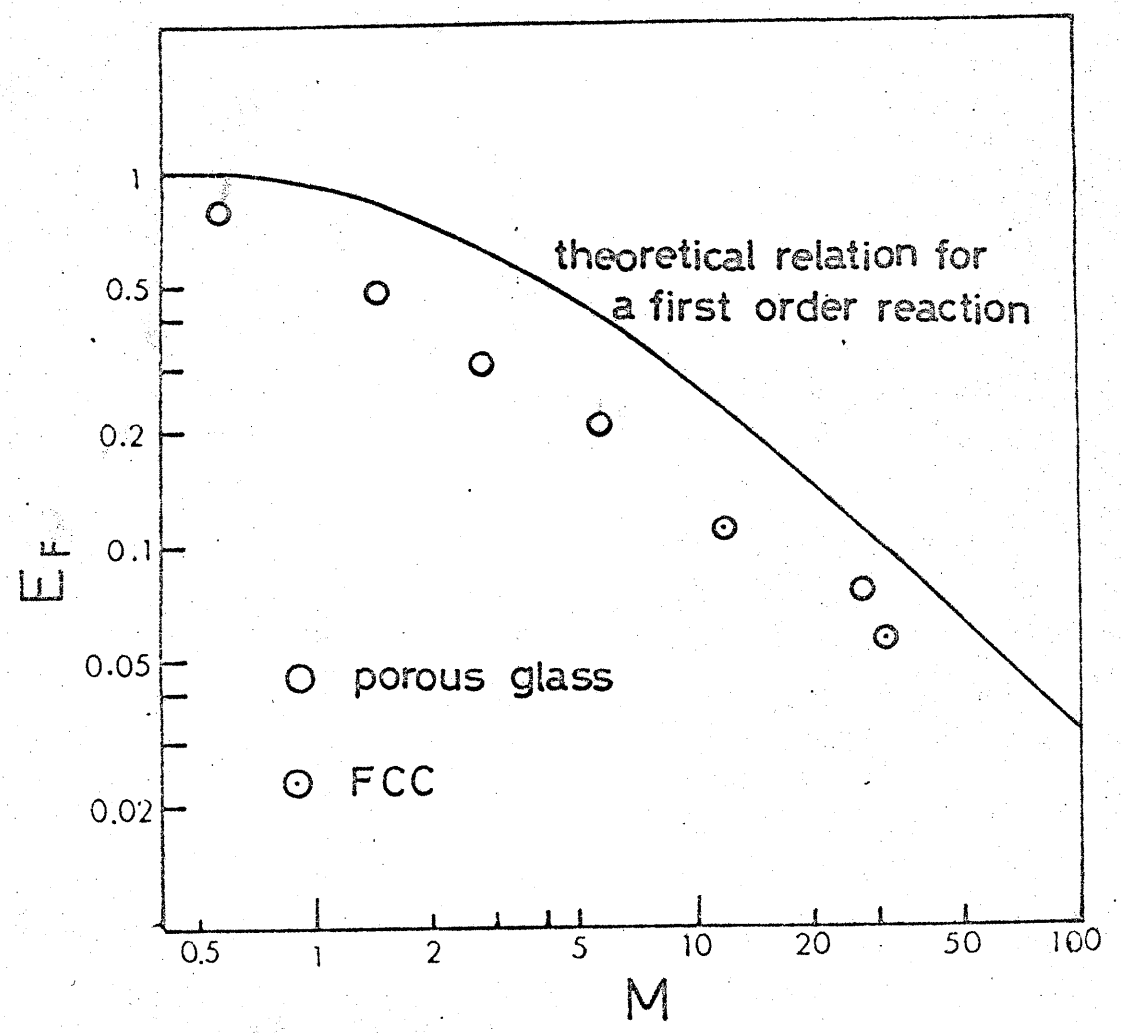

Fig.7-14 Relation between observed effectiveness factors and estimated moduli

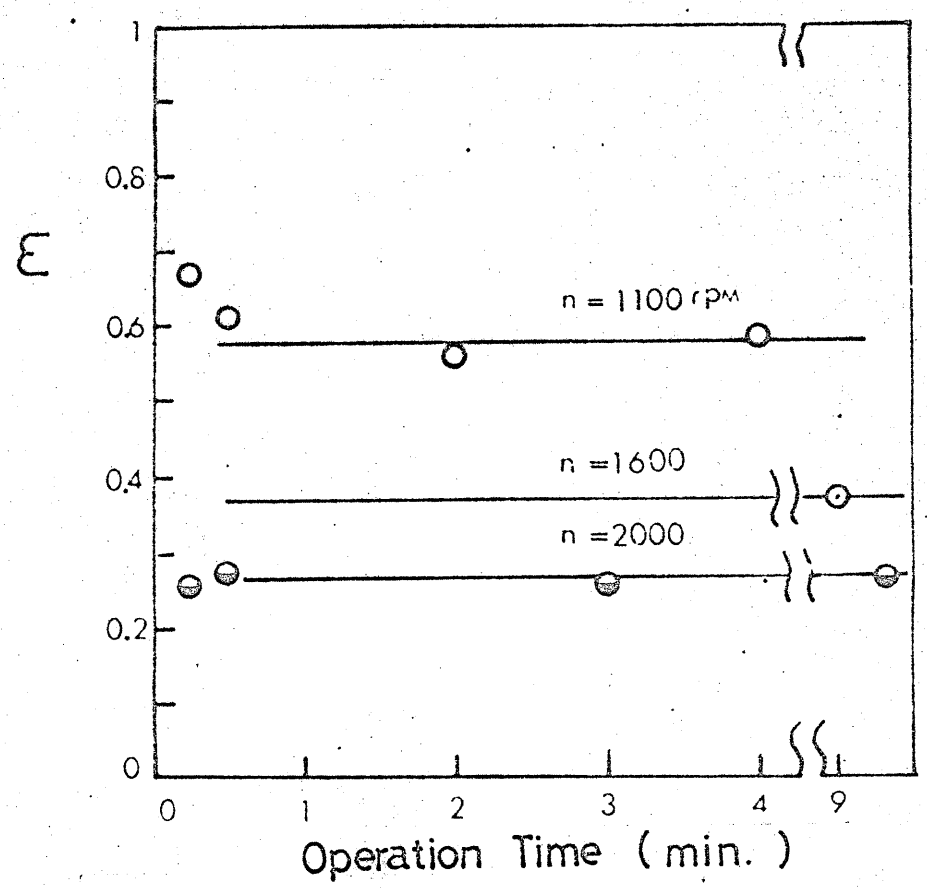

Fig.7-15 Dependence of hold up of liquid on operation time of a centrifugal separator (FCC R = 0.5 cm)

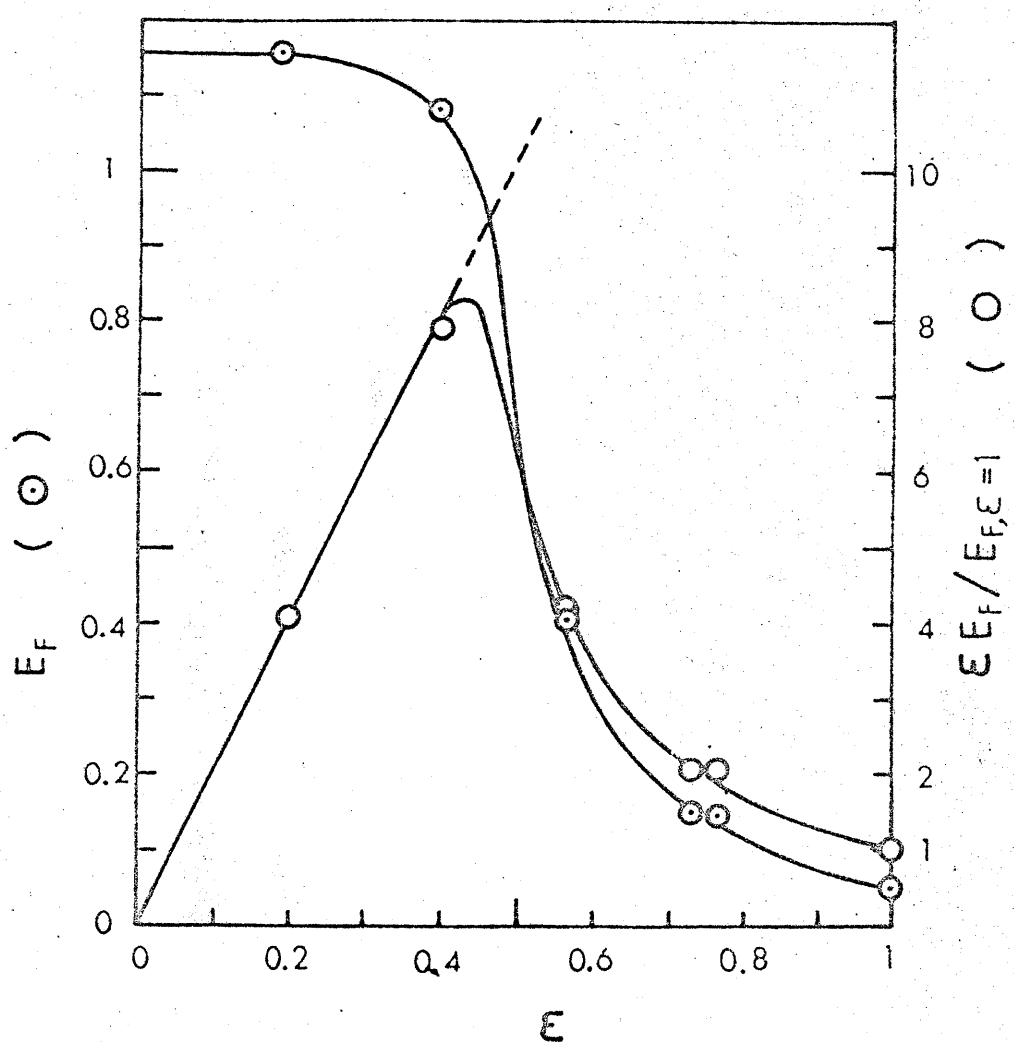

Fig.7-16 Dependence of effectiveness factor and specific activity of a catalyst particle on hold up of catalyst solution

Chapter 8 Summary

This dessertation " Effect of Mass Transfer on the Behavior of a Catalyst " consists of the following 7 chapters.

In chapter 1, the historical review of the studies in this field was presented. It was pointed out that the effect of mass transfer on activity, one of the most important factors in the industrial solid catalyst, is being elucidated and systematized by a large number of the studies from the theoretical and experimental viewpoints. On the contrary, the other two factors of selectivity and time change of the catalytic behavior have not been investigated sufficiently and in particular there have been few experimental investigations. A systematical approach supported by experiments is now required in these fields. It was also pointed out that the model for the solid catalyzed reaction employed in nost of the studies should be reconsidered on the basis of the more detailed examination of the porous structure of the actual catalyst.

On these survey, the experimental and theoretical studies on the consecutive hydrogenation of acetylene on a supported nickel catalyst was carried out in chapters 2 and 3.

Chapter 2 was concerned with the dependency of the selectivity of the intermediate product, ethylene, on the catalyst size. The comparison of the experimental results with the theoretical analysis based on the simple pore model and the linear kinetics represented some agreements on the qualititative trend of the selectivity to the pellet size and the conversion of the reactant. The discrepancies, however, were also observed in two points. One of them is the more rapid decrease in the selectivity with the increase in the pellet size than predicted by the basic theory. The other is that the limiting

selectivity as the conversion approaches zero never converges to unity even for the sufficiently small catalyst paticles, though it is one of the most important predictions of the basic theory. The kinetic studies elucidated that the former discrepancy is due to the catalytic rate forms of the reaction which do not follow a first otder law by the Langmuir-Hinshelwood model.

For the latter discrepancy, the micro-macropore model was proposed according to the microscopic observation of the catalyst, which proved that the catalyst is composed of the aggregated fine nickel crystals, possibly the catalytic parts, dispersed in the macroporous structure of the carrier material. The diffusion resistance for the micropore process which is not eliminated by reducing the pellet size presented the reasonable interpretation for the latter discrepancy.

In chapter 3, the attension was focused on the time change of the selectivity and the conversion with deactivation of the catalyst. In the first place, the time change for the three models of the deactivation mechanism, homogeneous poisoning, shell poisoning and core poisoning, was analyzed on the basis of the simple pore model and the linear kinetics, representing the remarkable difference in the tendency of the time change among these deactivation mechanisms. The experimental results suggested clearly the shell-progressive mechanism, which was correspondent to the deactivation by some poisoning species produced from the reactant, acetylene, as proved by the other experiments. As expected, the difference of the experimental results from the simple analysis were interpreted comprehensively when the micro-macropore model based on the kinetics which follow the Langmuir-Hinshelwood model is considered with a slight modification for the deactivation process. Particularly, the quantitative analysis for the fine catalyst particles for which the macropore effectiveness factor is unity, demonstrated clearly the rationlity of the micro-macropore model, by its close agreement with the

experiments. These experimental study was carried out for the two different batches of the catalyst of the same brand. The most important point is that the different selectivities at the beginning of the operation and the different tendencies of the time change for these two groups are explained simultaneously and quantitatively by the only difference in the micropore modulus.

By the studies in cahpters 2 and 3, it is demonstrated that the catalytic process follows the micro-macropore model based on the two step consecutive reactions governed by the Langmuir-Hinshelwood mechanism.

In chapter 4, the effect of mass transfer on a consecutive reaction system was studied from the viewpoint different from chapter 2 and 3. It was shown that the effect not only decreases the selectivity but also changes the apparent reaction scheme. This was proved by finding the fact that the three cases, 1) a consecutive reaction system affected by the diffusion process in the micropore and the macropore 2) a consecutive and parallel reaction system affected by the macropore diffusion process and 3) a consecutive and parallel reaction system safe from the mass transfer effect, present the apparently equivalent relations between the selectivity and the conversion. It means that the observed reaction scheme doesn't necessarily reflect the real one. Detailed evaluation of the transfer effect is necessary to determine the real reaction scheme. It is possible that some of the apparent schemes of the complex reactions which has been reported so far are the results of the transfer effect. The sufficient information of the transfer processes, however, are frequently difficult to obtain. The three criteria was proposed, by which the applicability of the first model involving the micro-macropore structure is examined based on the apparent kinetic data. The analysis of the synthesis of ethylene oxide by these criteria showed that this system id interpreted comprehensively as the consecutive reaction system influenced by the diffusion processes in the micropore and the macropore, while it has been considered

to be a typical example of consecutive and parallel reaction systems by the apparent kinetic measurements.

The results of chapters 2,3 and 4 indicate that this type of investigation into the transfer process for many complex reactions systems is required for the studies in this field to be systematized. It may give a powerful means to the deeper interpretation and the improvement of the selectivity, giving a clear boundary between the mass transfer effect and the intrinsic catalytic reaction.

Chapter 5 presented the first reported study of the selectivity in a consecutive reaction system for the reaction rate forms other than a first order law. Owing to the vast applicability for the solid catalyzed reaction and the experimental results in chapter 2, the rate forms were assumed to follow the Langmuir-Hinshelwood mechanism. For the three cases involving the different adsorbed species, the reactant, the intermediate product and the final product, the selectivity was calculated numerically. The results were compared to each other, together with the first order system, indicating the remarkable difference in the dependency of the selectivity on the modulus of the catalyst. The selectivity for a same value of modulus is in respect to the adsorption species, in the following order

reactant < no adsorption (first order reaction) < omyrt,rfosyr ½tpfivy

$\lessgtr$ final product

The interpretation of the results from the viewpoint of the distribution profile of the apparent rate constant for the hypothetical first order law within the catalyst presented the generalized law on the selectivity. It is that the increasing profile of the apparent rate constant towards the pellet center, lead to t lower selectivity compared with the uniform profile encountered in the [illegible] order [illegible] and vice versa.

in the first order reactions under an isothermal condition and vice versa.

Chapters 6 and 7 are the results of the contemplation on the results of the preceding chapters.

In chapter 6, the hydrodynamic flow caused by the longitudinal pressure gradient in a reactor was first paid attention to as a mass transfer mechanism in a solid catalyst. In the first place, theoretical analysis was given for a first order reaction under the combined effect of the diffusion and the hydrodynamic flow, representing the reasonable augumentation of the effectiveness factor with increasing velocity of the flow. Next, the experiments carried out for the liquid phase ion exchange reaction on the oion exchange resin of very rough pore structure demonstrated the remarkable effect of the hydrodynamic flow and the results agreed well with the theoretical analysis. The relative merits of the reactor involving the hydrodynamic flow to the reactor of the usual porous catalysts were discussed by designing each reactor for a given conversion and capacity. It was shown clearly that the hydrodynamic flow makes it possible to reduce the volume of a reactor and the flow resistance to the greatest extent, by the high activity of the large catalyst pellet whichwould not been obtained otherwise. The most teresting point is its more preferable tendency at large flow rates in the reactor, which may give a powerful means to the urgent problem in the recent industries, the purification of the waste water or gas discharged from the factories.

Chapter 7 were concerned with the stationary bed of the liquid phase catalyst supported in the porous material as a better operation of gas-liquid catalytic reactions, which may eliminate the various problems encountered in the usual bubble column reactor. The behavior of this type of catalyst has not been elucidated yet, though its proposal was made a long time ago. The experiments for the conversion of ethylene to acetaldehyde by Wacker-Hochst process assured the stable operation of the stationary bed. The activity of different sezed carrier material and the observed kinetics were analyzed

the stable operation of the stationary bed. The activity of different sized carrier material and the observed kinetics were analyzed by the application of the effectiveness factor on the basis of the experimental determination of the intrinsic rate constant and the effective diffusivity. As expected beforehand, the use of the ordinary size of the carrier material led to very poor effectiveness factor owing to the diffusion resistance in the liquid phase. This problem was solved by the treatment of the supported liquid phase catalyst under the field of the centrifugal force, which removes catalyst solution in larger pores to present the empty pore for the rapid diffusion in a gas phase. The activity of the catalyst is able to be raised by the treatment until the effectiveness factor reaches unity. Furthermore, the activity is controled with ease by the velocity of revolution of the centrifugal separator.

Thus, the stationary bed of this type of catalyst may become a reactor superior in the activity, the mixing characteristics and the controllability to the bubble column reactor.

Nomenclature

A	reactant
a	exterior surface area of pellets per unit volume of reaction
a'	P_A / P_{AI}
a"	$(P_{AS} - P_A) / P_{AS}$
a	interior surface area per unit volume of porous pellet
B	intermediate product in a consecutive reaction system or product in simple reaction
b'	P_B / P_{AI}
C	final product in consecutive reaction system
C_D	concentration of poisoning deposits on interior surface of catalyst
C_j	concentration of j-component
D	molecular diffusion coefficient
D_e	effective diffusion coefficint for porous material
D_K	effective diffusion coefficint for microparticle
D_M	effective diffusion coefficint for macropore
D_p	diameter of catalyst pellet
d	relative sensitivity of HCl to KCl on electric conductivity probe
d_{in}	diameter of fine particles constituting pellet
E	E_1 / E_2
E_a	activation energy of reaction
E_d	activation energy of diffusion
E_i	effectiveness factor relating to k_i based on simple pore model
E_i'	effectiveness factor for catalyst pellet based on micro-macro pore model
E'	E_1' / E_2'
E_{Hi}, E_{Sai} E_{Sbi}, E_{Ci} E_{il}	effectiveness factors defined in chapter 3 (Table 3-1)

E_H, E_{Sa}, E_{Sb}, E_C	ratio of two effectiveness factors defined in chapter 3 (Table 3-1)
F	volumetric flow rate in reactor
F^o	volumetric flow rate given by Eq.(7-7)
f	friction factor for the flow in packed bed, given by Kozeny-Carman relationship
g	acceleration of gravity
ΔH	heat of reaction
$[j]$	concentration of j-component in liquid phase
K	gas-liquid partition coefficint
K_F	overall mass transfer coefficint given by Eq.(6-22)
K_j	adsorption equilibrium constant of j-component in Langmuir-Hinshelwood type of reaction rate form
k_1	rate constant for reaction of A
k_2	rate constant for consecutive reaction of B
k_i'	rate constants for a consecutive reaction system defined for micro-macropore model
k_i^o	$= k_i P_{H_2}$; rate constant involving partial pressure of hydrogen
$k_{iapp.}$	apparent rate constant defined in chapter 5-4
k_L	mass transfer coefficient through liquid film
L	radius of microparticle
L_p	height of cylindrical pellet
L_R	reactor length
l	longitudinal coordinate
M_1	modulus defined in chapter 5 (Table 5-1)
m_i	modulus based on simple pore model
m_i'	modulus for macropore in micro-macropore model

m_L	modulus for Langmuir-Hinshelwood type of reaction rate (p.29)
m_{il}, m_{io} m_i', m_{is}' m_{il}', m_{is}	modulus defined in chapter 3 (Table 3-1)
P_j	partial pressure of j-component
PeB	dimensionless number representing relative significance of flow through pores to diffusion ; $u_{in}L_p / De$
p	pressure
Δp	pressure drop
R	radius of pellet
R_i	rate of the reaction A→B (i=1) ; rate of the reaction B→C (i=2)
Re	Reinolds number defined as uDp / ν
Rem	Reinolds number defined as $\frac{\phi D_p u}{6(1-\varepsilon_R)\nu}$
r	radial co-ordinate
S	selectivity defined as ratio of intermediate product formed to reactant consumed
S^o	limiting selectivity as X approaches zero
S_p	selectivity for plug flow reactor
S_m	selectivity for back-mix reactor
Sc	Schmidt number ; ν / D
Sh	Sherwood number ; $D_p k_L / D$
s	k_1 / k_2
s'	k_1' / k_2'
T	temperature
t	time
u, u_{out}	superficial velocity in reactor ; subscript out is used to distinguish it from u_{in}
u_{in}	velocity of flow through porous material

V	total volume of catalyst solution in reactor
W	total volume of catalyst pellets in reactor
w	volume of catalyst pellets in unit length of reactor
X	conversion of reactant ; $(P_{AI} - P_A) / P_{AI}$
x	dimensionless radial co-ordinate ; r/L or r/R
y	dimensionless longitudinal co-ordinate ; z/L_p
z	longitudinal co-ordinate in cylindrical co-ordinates

Greek letter

α	constant defined by $= 1 - \alpha C_D$
γ	ratio of consecutive and parallel reaction defined by reaction scheme B (chapter 4)
ε	fraction of catalyst volume occupied by microparticle
ε_R	void fraction in packed bed
ε°	fraction of pore volume occupied by catalyst solution
θ	porocity
μ_i	modulus for microparticle
μ_{10}	modulus of non-deactivated microparticle for Langmuir-Hinshelwood type of reaction form
ν	kinematic viscosity
ρ	density
σ	surface tension
τ	contact time in reactor
τ	tortuosity for porous material
τ_c	dimensionless contact time in reactor

ϕ	degree of deactivation
ϕ	shape factor for pellet
λ	effective thermal conductivity in the solid catalyst
λ	characteristic root for linear second differential equation
ω	ratio of radius to height in cylindrical pellet
η_i	effectiveness factor for microparticle
η	η_1 / η_2

Subscript

0	reffers to value based on the initial rate constant, k_{i0} or k_{i0}'
A	reffers to reactant
B	reffers to intermediate product
i (=1or2)	reffers to the reaction A B (1) or B C (2)
S	reffers to value at exterior surface of catalyst pellet
I	reffers to value at reactor inlet
obs	reffers to value observed experimentally
R	reffers to reactor

Superscript

'	reffers to value based on the intrinsic reaction in microparticles ; rate constant of deactivated catalysts in chapter 3

References

A - 1 Acreres, G. J. K., Bond, G. C., Cooper, P. J., Dawson, J. A., J. Catalysis, 6 139('66)

A - 2 Akehata, T., Namkoong, S., Kubota, H., Shindo, M., Can. J. Chem. Eng. 39 127('61)

A - 3 Andersen, J. B., Chem. Eng. Sci., 18 147('63)

A - 4 Andersen, J. B., Chem. Eng. Sci., 20 587('65)

A - 5 Andersen, R. B., Whitehouse, A. M., Ind. Eng. Chem. 53 1011('61)

A - 6 Andrianova, T. I., Todes, D. M., Zh. Fiz. Khim 30 522('56)

A - 7 Aris, R., Chem. Eng. Sci., 6 262('57)

A - 8 Aris, R., Ind. Eng. Chem. Fundamentals, 20 587('65)

A - 9 Austin, L. G., Walker, P. R., Jr., A. I. Ch. E. Journal 9 303('63)

B - 1 Balder, J. R., Petersen, E. E., Chem. Eng. Sci., 23 1287('68)

B - 2 Barnett, L. G., Weaver, R. E. C., Gilkson, M. M., A. I. Ch. E. Journal 7 211('61)

B - 3 Beecher, R., Voorhies, A., Jr., Eberly, P., Jr., Ind. Eng. Chem. Res. and Dev. 7 203('68)

B - 4 Beek, J., A. I. Ch. E. Journal 7 350('61)

B - 5 Beek, O., Smith, A. E., Wheeler, A., Proc. Roy. Soc. (London) A177, 62('40)

B - 6 Bischoff, K. B., A. I. Ch. E. Journal 11 351('65)

B - 7 Bischoff, K. B., Chem. Eng. Sci., 22 525('67)

B - 8 Bischoff, K. B., Chem. Eng. Sci., 23 451('68)

B - 9 Blue, R. W., Holn, V. C. F., Regier, R. B., Fast, E., Heckelsberg, L., Ind. Eng. Chem., 44 2710('52)

B - 10 Bokhoven, C., Raayen, W., J. Phys. Chem., 58 471('54)

B - 11 Bond, G. C., J. Chem. Soc. 2705('58)

B - 12 Bond, G. C., Mann, R. S., J. Chem. Soc. 4738('58)

B - 13 Bond, G. C., 'Catalysis by metal' Academic Press. London('62)

B - 14 Butt, J. B., A. I. Ch. E. Journal, 11 106('65)

B - 15 Butt, J. B., Chem. Eng. Sci., 21 275('66)

C - 1 Carberry, J. J., A. I. Ch. E. Journal, 7 350('61)

C - 2 Carberry, J. J.. A. I. Ch. E. Journal, 8 557('62)

C - 3 Carberry, J. J., Chem. Eng. Sci., 17 675('62)

C - 4 Carberry, J. J., Gorring, R. C., J. Catalysis, 5 529('66)

C - 5 Chu, C., Hougen, O. A., Chem. Eng. Sci., 17 167('62)

C - 6 Collins, R. E., 'Flow of Fluids through porous meterial' Reinhold Pub. Coop., New York ('61)

C - 7 Coughlin, R. W., A. I. Ch. E. Journal, 13 1031('67)

C - 8 Crank, J., 'Mathematics of Diffusion' p90('56)

C - 9 Canningham, R. A., Carberry, J. J., Smith, J. M., A. I. Ch. E. Journal 11 636('65)

D - 1 Damköler, G., 'Der Chemie Ingenieur' Vol. III p430. Akademische Verlangsgesellshafl M. B. H., Leipzig ('37)

D - 2 Damköler, G., Z. Ekktrochem., 42 846('36)

D - 3 Damköler, G., Z. Phys. Chem. A193 16('43)

D - 4 Dozono, T., Shiba, T., Bull. Jap. Pet. Inst. 5 8('63)

F - 1 Farkas, A., Farkas, L., J. Ame. Chem. Soc., 60 22('38)

G - 1 Gupta, V. P., Douglas, W. J. M., Can. J. Chem. Eng., 45 117('67)

G - 2 Gunn, D. J., Chem. Eng. Sci., 21 383('66)

G - 3 Gunn, D. J., Chem. Eng. Sci., 22 1439('67)

H - 1 Henry, P., J. Ame. Chem. Soc., 86 3246('64)

H - 2 Hightower, J. W., J. Catalysis, 7 298('67)

H - 3 Hirasa, K., dissertation, Univ. of Tokyo, Jap. ('66)

H - 4 Hoogschagen, J., Ind. Eng. Chem., 47 906('55)

H - 5 Hougen, O. A., Watson, K. M., 'Chemical Process Principles' Part III p999, Wiley, New York ('48)

H - 6 Hutching, J., Carberry, J. J., A. I. Ch. E. Journal 12 20('66)

H - 7 Hudgias, R. R., Chem. Eng. Sci., 23 93('68)

I - 1 Irving, J. P., Butt, J. B., Chem. Eng. Sci., 22 1859('67)

J - 1 Johnson, M. F., Kreger, W. E., Erickson, H. Ind. Eng. Chem., 49 283('57)

K - 1 Kano, H., Kuezuka, K., Kogyo Kagaku Zashi (Japan), 61 1157('58)

K - 2 Kasaoka, S., Sakata, Y., Misaki, K., Kagaku Kogaku (Japan) 30 153('66)

K - 3 Kawazoe, K., dissertation, Univ. of Tokyo, ('66)

K - 4 Komiyama, H., Inoue, H., J. Chem. Eng. Japan, 1 142('68)

K - 5 Komiyama, H., Inoue, H., J. Chem. Eng. Japan, 2 163('69)

K - 6 Komiyama, H., Inoue, H., J. Chem. Eng. Japan, 3 117('70)

K - 7 Komiyama, H., Inoue, H., J. Chem. Eng. Japan, 3 206('70)

K - 8 Komiyama, H., Inoue, H., Shokubai (Japan) 13 143p ('71)

K - 9 Komiyama, H.,Inoue,H.,Meeting of the Soc. Chem. Eng. Japan,Sapporo,August ('71)

K - 10 Kubota, H., Shindo, M., Kagaku Kogaku (Japan) 20 11('56)

K - 11 Kubota, H., Shindo, M., Akehata, K., Hayashi, E., Kagaku Kogaku (Japan) 23 284('59)

L - 1 Lewis, J. R., Taylor J. S., J. Ame. Chem. Soc., 60 877('38)

L - 2 Love, K. S., Emett, P. H., J. Ame. Chem. Soc., 63 3297('41)

M - 1 Marshall, W. R., Jr., Pigford, R. L., 'The Application of Differential Equations to Chemical Engineering Problens', Published by Univ. Delaware

M - 2 Masamune, S., Smith, J. M., A. I. Ch. E. Journal 12 384('66)

M - 3 Maxted, E. B., 'Adv. in Cat.' Vol. III p129

M - 4 Miller, D. N., Kirk, R. S., A. I. Ch. E. Journal, 8 183('62)

M - 5 Miller, F. W., Deans, H. A., A. I. Ch. E. Journal, 13 45('67)

M - 6 Mingle, J. O., Smith, J. M., A. I. Ch. E. Journal, 7 243('61)

M - 7 Mitsutani, A., Tanaka, K., Bull. Jap. Pet. Inst. 5 8('63)

M - 8 Moravec, R. Z., Schelling, W. T., Oldenshaw, C. F., Brit., Pateut. 511, 556('39) Chem. Ab., 35, 6103('41)

M - 9 Moravec, R. Z., Schelling, W. T., Oldenshaw, C. F., Can. Patent 396, 994 ('41) Chem. Ab., 35, 6103('41)

M - 10 Murakami, Y., Masuda, M., Kobayashi, T., Hattori, T., Shokubai (Japan) 7 296('65)

M - 11 Muskat, M., 'Flow of Homogeneous Fluid thorough Porous Media' ('37)

O - 1 Olson, J. H., Ind. Eng. Chem. Fundamentals 7 185('68)

O - 2 Otani, S., Wakao, N., Smith, J. M., A. I. Ch. E. Journal 10 130('64)

O - 3 Otani, S., Smith, J. M., J. Catalysis, 5 332('66)

O - 4 Otake, T., Kunugida, E., Suga, K., Kogyo Kagaku Zashi (Japan) 68 58('65)

O - 5 Orzechowski, A., Mac Cormack, Can. J. Chemistry, 32 388('54)

P - 1 Pasquon, I., Dente, M., J. Catalysis, 1 508('62)

P - 2 Petersen, E. E., Chem. Eng. Sci., 17 987('62)

P - 3 Petersen, E. E., Chem. Eng. Sci., 20 587('65)

P - 4 Petersen, E. E., Friedly, J. C., Devogelaue, R. J., Chem. Eng. Sci., 19 683('64)

P - 5 Petersen, E. E., 'Chemical Reaction Analysis' Prentice-Hall ('65)

P - 6 Prater, C. D., Chem. Eng. Sci. 8 284('58)

P - 7 Prater, C. D., Lago, R. M., 'Adv. in Cat.' Vol. III, Acadmic Press., ('51)

R - 1 Rao, R. M., Smith, J. M., A. I. Ch. E. Journal 10 293('64)

R - 2 Rao, R. M., Wakao, N., Smith, J. M., Ind. Eng. Chem. Fundamentals, 3 127('64)

R - 3 Rester, S., Aris, R., Chem. Eng. Sci., 24 793('69)

R - 4 Rester, S., Jonven, J., Aris, R., Chem. Eng. Sci., 24 1019('69)

R - 5 Roberts, G. W., Satterfield, C. N., Ind. Eng. Chem. Fundamentals, 4 288('65)

R - 6 Rony, P. R., J. Catalysis, 6 139('66)

R - 7 Rony, P. R., Chem. Eng. Sci. 23 1021('68)

S - 1 Sada, E., Wen, C. Y., Chem. Eng. Sci., 22 559('67)

S - 2 Sagara, M., Masamune, S., Smith, J. M., A. I. Ch. E. Journal, 13 1226('67)

S - 3 Saltan, D. I., White, R. R., Chem. Eng. Prog. Symp. Series, No. 4 48 59('52)

S - 4 Satterfield, C. N., Sherwood, T. K., 'The Role of Diffusion in Catalysis' Addison-Wesley, Cambridge, Mass

S - 5 Schmidt, J., Hafner, W., Jira, R., Seldmeier, J., Sieber, R., Ruttinger,R., Kojer, H., Angew. Chem., 71 176('59)

S - 6 Schneider, P., Mitschka, P., Chem. Eng. Sci. 21 455('66)

S - 7 Schneider, P., Mitscka, P., Chem. Eng. Sci. 24 1725('69)

S - 8 Sheridan, J., J. Chem. Soc. 133 301('45)

S - 9 Sheridan, J., J. Chem. Soc. 373('44)

S - 10 Shilson, R. E., Amundson, N. R., Chem. Eng. Sci., 13 226('61)

S - 11 Shilson, R. E., Amundson, N. R., Chem. Eng. Sci., 13 237('61)

S - 12 Shokubai Kogaku Koza, 'Shokubai Busseiron' (Japan)

S - 13 Smith, N. L., Amundson, N. R., Ind. Eng. Chem., 43 2157('51)

S - 14 Stern, E. W., 'Catalysis Review' p73. Editted by Heiuewan, ('68)

S - 15 Suga, K., Morita, V., Kunugida, E., Otake, T., Kogyo Kagaku Zashi (Japan) 136('67)

T - 1 Tabata, M., Yoshida, F., Kiryu, T., Kogyo Kagaku Zashi (Japan) 70 136('67)

T - 2 Takeuchi, M., Kubota, H., Shindo, M., Kagaku Kogaku (Japan) 30 523('66)

T - 3 Thiele E. W., I. E. C., 31 916('39)

T - 4 Tinkler, J. D., Metzner, A. B., Ind. Eng. Chem., 53 663('61)

T - 5 Tinkler, J. D., Pigford, R. L., Chem. Eng. Sci., 15 326('61)

V - 1 Vargaftik, M. N., Moiseev, J. I., Sirkin, Ya. K., Dokl. Akad. Nauk., SSSR 147 399('62)

W - 1 Waguer, C., Z. Physik. Chem., A193 1 ('43)

W - 2 Wakao, N., Selwood, P. W., Smith, J. M., A. I. Ch. E. Journal, 8 478('62)

W - 3 Wakao, N., Fujishiro, F., Kagaku Kogaku (Japan) 30 745('66)

W - 4 Wakao, N., Smith, J. M., Ind. Eng. Chem. Fundamentals, 3 123('64)

W - 5 Wakao, N., Yamazaki, T., Yamada, N., Kagaku Kogaku (Japan) 30 159('66)

W - 6 Wan, S. W., Ind. Eng. Chem., 31 916('39)

W - 7 Weekman, V. W. Jr., J. Catalysis, 4 260('65)

W - 8 Weekman, V. W. Jr., J. Catalysis, 5 44('66)

W - 9 Wei, J., J. Catalysis, 1 526('62)

W - 10 Wei, J., J. Catalysis, 1 538('62)

W - 11 Weisz, P. B., Prater, C. D., 'Adv. in Cat.' Vol. 7 Academic Press. New York('54)

W - 12 Weisz, P. B., Swegler, E. W., J. Phys. Chem., 59 823('55)

W - 13 Weisz, P. B., Chem. Eng. Prog. Symp. Ser. No. 25 55 29('59)

W - 14 Weisz, P. B., Z. Physik, Chem. Neue Folge, 11 1('57)

W - 15 Weisz, P. B., Hicks, J. S., Chem. Eng. Sci. 17 265('62)

W - 16 Wheeler, A., 'Catalysis' P. H. Emett, ed., Vol. 2 Reinhold, New York, ('55)

W - 17 Wicke, E., Brötz, W., Chem. Ind. Tech., 21 219('49)

W - 18 Wurzbacker, G., J. Catalysis, 5 476('66)

Z - 1 Zeldowitsch, J. B., Acta Physicochim., (U. R. S. S.), 10 583('39)

Ø - 1 Østergaard, K., Chem. Eng. Sci., 18 259('63)

ACKNOWLEDGEMENT

The author would like to acknowledge the continuing guidances and encouragements of Prof. H.Inoue.

He also wishes to express his thanks to assoc.Prof. E.Ohshima, Dr. H.Matsuyama and Dr. T.Furusawa for valuable discussion and to Miss M.Namiki and Mr. M.Komiyama for typing the manuscript.

Appendix 1 The Selectivity in a Consecutive Reactions System

——— Simple Pore Model ———

The steady state conservation equations in a single catalyst in which the consecutive reactions, $A \longrightarrow B \longrightarrow C$, take place under the condition stated in chapter 2-2 are written as follows.

$$D_e \left(\frac{d^2 P_A}{dr^2} + \frac{2}{r}\frac{dP_A}{dr} \right) = k_1 P_A \tag{1}$$

$$D_e \left(\frac{d^2 P_B}{dr^2} + \frac{2}{r}\frac{dP_B}{dr} \right) = -k_1 P_A + k_2 P_B \tag{2}$$

The boundary conditions for Eqs.(1) and (2) are given by

$$\text{at } r = R, \quad P_A = P_{AS} \quad \text{and} \quad P_B = P_{BS} \tag{3}$$

$$\text{at } r = 0, \quad \frac{dP_A}{dr} = 0 \quad \text{and} \quad \frac{dP_B}{dr} = 0 \tag{4}$$

The above equations are reduced to dimensionless forms as

$$\frac{d^2 a}{dz^2} + \frac{2}{z}\frac{da}{dz} = m_1^2 a \tag{5}$$

$$\frac{d^2 b}{dz^2} + \frac{2}{z}\frac{db}{dz} = -m_1^2 a + m_2^2 b \tag{6}$$

$$\text{at } z = 1, \quad a = 1 \quad \text{and} \quad b = \frac{P_{BS}}{P_{AS}} \tag{7}$$

$$\text{at } z = 0, \quad \frac{da}{dz} = 0 \quad \text{and} \quad \frac{db}{dz} = 0 \tag{8}$$

$$\text{where} \quad a = \frac{P_A}{P_{AS}}, \quad b = \frac{P_B}{P_{AS}}, \quad z = \frac{r}{R}, \quad m_i = R\sqrt{\frac{k_i}{D_e}} \tag{9}$$

Setting $x = az$ and $y = bz$ yields

$$\frac{d^2 x}{dz^2} = m_1^2 x \tag{10}$$

$$\frac{d^2 y}{dz^2} = -m_1^2 x + m_2^2 y \tag{11}$$

$$\text{at } z = 1, \quad x = 1 \quad \text{and} \quad y = \frac{P_{BS}}{P_{AS}} \tag{12}$$

at $z = 0$, $x = 0$ and $y = 0$ (13)

The solution of Eq.(10) is

$$x = C_1 e^{m_1 z} + C_2 e^{-m_2 z} \tag{14}$$

where C_1 and C_2 are constants of integration.

Determining C_1 and C_2 by the boundary conditions (12) and (13) and substituting them into Eq.(14) yields

$$x = \frac{\sinh (m_1 z)}{\sinh m_1} \tag{15}$$

It is easily known that Eq.(11) has a particular solution

$$y = - \frac{m_1^2}{m_1^2 - m_2^2} x = - \frac{s}{s - 1} x \tag{16}$$

where $s = k_1 / k_2$.

The solution of Eq.(11) is therefore represented as

$$y = C_3 e^{m_2 z} + C_4 e^{-m_2 z} - \frac{s}{s - 1} \frac{\sinh (m_1 z)}{\sinh m_1} \tag{17}$$

C_3 and C_4 are determined by the boundary conditions (12) and (13) and as a result Eq (17) becomes

$$y = \left(\frac{s}{s - 1} + \frac{P_{BS}}{P_{AS}} \right) \frac{\sinh (m_2 z)}{\sinh m_2} - \frac{s}{s - 1} \frac{\sinh (m_1 z)}{\sinh m_1} \tag{18}$$

From Eqs.(15) and (18), the concentration profiles in the catalyst are represented as

$$a = \frac{P_A}{P_{AS}} = \frac{\sinh (m_1 z)}{z \sinh m_1} \tag{19}$$

$$b = \frac{P_B}{P_{AS}} = \frac{1}{z} \left(\frac{s}{s - 1} + \frac{P_{BS}}{P_{AS}} \right) \frac{\sinh (m_1 z)}{\sinh m_2} - \frac{s}{s - 1} \frac{\sinh (m_1 z)}{\sinh m_1} \tag{20}$$

According to the definition, effectiveness factor is given by

$$E_1 = \frac{4\pi R^2 D_e \left.\frac{dP_A}{dr}\right]_{r=R}}{\frac{4}{3}\pi R^3 \; k_1 P_{AS}} = \frac{3}{m_1^2} \left.\frac{da}{dz}\right]_{z=1} \tag{21}$$

From Eq.(19),

$$\left.\frac{da}{dz}\right]_{z=1} = m_1 \coth m_1 - 1 \tag{22}$$

Substituting Eq.(22) in Eq.(21) yields

$$E_1 = \frac{3}{m_1} \left(\coth m_1 - \frac{1}{m_1} \right) \tag{23}$$

In this thesis, the selectivity for a single catalyst is defined as

$$S = \frac{-4\pi R^2 D_e \left.\frac{dP_B}{dr}\right]_{r=R}}{4\pi R^2 D_e \left.\frac{dP_A}{dr}\right]_{r=R}} = \frac{-\left.\frac{db}{dz}\right]_{z=1}}{\left.\frac{da}{dz}\right]_{z=1}} \tag{24}$$

From Eq.(20),

$$-\left.\frac{db}{dz}\right]_{z=1} = -\left(\frac{s}{s-1} + \frac{P_{BS}}{P_{AS}}\right)\left(m_2 \coth m_2 - 1\right) + \frac{s}{s-1}\left(m_1 \coth m_1 - 1\right) \tag{25}$$

Substituting Eqs.(22) and (25) into Eq.(24), the selectivity is represented as

$$S = \frac{s - 1/E}{s-1} - \frac{1}{sE} \frac{P_{BS}}{P_{AS}} \tag{26}$$

where

$$E = E_1/E_2 \;, \quad E_2 = \frac{3}{m_2} \left(\coth m_2 - \frac{1}{m_2} \right) \tag{27}$$

Thus, a single catalyst process has been solved.

The mass balances of A and B in a plug flow reactor, in which the above single catalyst process proceeds, are written as

$$-F \frac{dP_A}{dl} = \text{rate of A per unit length of the reactor} \tag{28}$$

$$-F\frac{dP_B}{dl} = \text{rate of B per unit length of the reactor} \tag{29}$$

where l and F represent respectively the longitudinal co-ordinate in the reactor and the volumetric flow rate.

Substituting Eqs.(22) and (25) with some modifications in Eqs (28) and (29) yields

$$F\frac{dP_A}{dl} = -wk_1E_1P_A \tag{30}$$

$$F\frac{dP_B}{dl} = w\left(k_1E_1 \frac{s - 1/E}{s - 1} P_A - k_2E_2P_B \right) \tag{31}$$

where w represents the volume of the catalyst pellets packed in a unit length of the reactor.

Assuming that $P_{BS} = 0$ at the reactor inlet, the boundary conditions for Eqs.(30) and (31) are

$$\text{at } l = 0 , \qquad P_A = P_{AI} \quad \text{and} \quad P_B = 0 \tag{32}$$

The solution of Eq.(30) with the boundary condition (32) is

$$\frac{P_A}{P_{AI}} = e^{-(wk_1E_1/F)\, l} \tag{33}$$

The conversion of A at an arbitrary position in the reactor is therefore given by

$$X = \frac{P_{AI} - P_A}{P_{AI}} = 1 - e^{-(wk_1E_1/F)\, l} \tag{34}$$

Substituting Eq (33) in Eq.(31) yields

$$F\frac{dP_B}{dl} = w\left(k_1E_1 \frac{s - 1/E}{s - 1} P_{AI}\, e^{-(wk_1E_1/F)\, l} - k_2E_2P_B \right) \tag{35}$$

The solution of Eq.(35) with the boundary condition (32) is

$$\frac{P_B}{P_{AI}} = \frac{s}{s - 1}\left(e^{-(wk_2E_2/F)\, l} - e^{-(wk_1E_1/F)\, l} \right) \tag{36}$$

Combining Eqs.(33) and (36), the selectivity defined as $\frac{P_B}{P_{AI} - P_A}$ is given by

$$S = \frac{s}{s-1} \; \frac{e^{-(wk_2E_2/F)\,l} - e^{-(wk_1E_1/F)\,l}}{1 - e^{-(wk_1E_1/F)\,l}} \tag{37}$$

Eq.(37) describes the selectivity in terms of the position in the reactor. Eliminating l in Eq.(37) by the relation of (34), it becomes

$$S = \frac{(1-X)^{1/sE} - (1-X)}{X\,(1-1/sE)} \; \frac{s - 1/E}{s-1} \tag{38}$$

Thus, the selectivity is obtained as a function of s, E and X.

$\dfrac{(1-X)^{1/sE} - (1-X)}{X\,(1-1/sE)}$ in Eq.(38) becomes unity when X approaches 0, so that the selectivity at X=0 is given by

$$S^{o} = \frac{s - 1/E}{s-1} \tag{39}$$

The conservation equations for a backmix reactor, which the same catalytic process takes place, are written as

$$F\,(P_{AI} - P_A) = Wk_1E_1P_A \tag{40}$$

$$F\,P_B = W\left(k_1E_1 \frac{s}{s-1} P_A - k_2E_2P_B\right) \tag{41}$$

where W represents the total volume of the catalyst pellets in the reactor.

From Eq.(40), the concentraion of A in the reactor and the conversion of it are given by

$$\frac{P_A}{P_{AI}} = \frac{1}{1 + \tau k_1E_1} \tag{42}$$

$$X = \frac{\tau k_1E_1}{1 + \tau k_1E_1} \tag{43}$$

where $\tau = W/F$.

Substituting Eq.(42) into Eq.(41) leads to

$$\frac{P_B}{P_{AI}} = \frac{1}{1 + \tau k_2E_2} \; \frac{\tau k_1E_1}{1 + \tau k_1E_1} \; \frac{s - 1/E}{s-1} \tag{44}$$

,so that the selectivity is given by

$$S = \frac{1}{1 + \tau k_2 E_2} \frac{s - 1/E}{s - 1} \tag{45}$$

Combining Eqs.(43) and (45) yields

$$S = \frac{1}{1 + \frac{X}{1 - X} \frac{1}{sE}} \frac{s-1/E}{s-1} \tag{46}$$

Setting X = 0 in Eq.(46), it becomes

$$S^o = \frac{s - 1/E}{s - 1} \tag{47}$$

Eqs.(46) and (47) represent the selectivity in a backmix reactor.

Appendix 2 The Selectivity in a Consecutive Reactions System

Micro-macropore Model

The conservation equations in a micropaticle, in which the consecutive reactions $A \xrightarrow{k_1'} B \xrightarrow{k_2'} C$ take place, are written as

$$D_K \left(\frac{d^2P_A^o}{dr^2} + \frac{2}{r}\frac{dP_A^o}{dr} \right) = k_1' P_A^o \tag{1}$$

$$D_K \left(\frac{d^2P_B^o}{dr^2} + \frac{2}{r}\frac{dP_B^o}{dr} \right) = -k_1' P_A^o + k_2' P_B^o \tag{2}$$

with boundary conditions

$$\text{at } r = L, \quad P_A^o = P_A \quad \text{and} \quad P_B^o = P_B \tag{3}$$

$$\text{at } r = 0, \quad \frac{dP_A^o}{dr} = 0 \quad \text{and} \quad \frac{dP_B^o}{dr} = 0 \tag{4}$$

where P_i^o represents the partial pressure within the microparticle.

Owing to the similarity of the above equations to Eqs.(1) ~ (4) in Appendix 1, the solution for the microparticle process is obtained on the analogy of Appendix 1.

The average rate of A inside a microparticle is given by

$$\frac{3}{L} D_K \left.\frac{dP_A^o}{dr}\right]_{r=L} = \frac{3P_A}{L^2} D_K \left.\frac{da^o}{dz^o}\right]_{z^o=1} \tag{5}$$

where a^o and z^o represent respectively P_A^o/P_A and r/L.

On the analogy of Eq.(22) in Appendix 1,

$$\left.\frac{da^o}{dz^o}\right]_{z^o=1} = \mu_1 \coth \mu_1 - 1 \tag{6}$$

where $\mu_1 = L\sqrt{\dfrac{k_1'}{D_K}}$.

Eq.(5) therefore becomes

$$\text{rate of A} = k_1' \eta_1 P_A \tag{7}$$

where

$$\eta_1 = \frac{3}{\mu_1}\left(\coth \mu_1 - \frac{1}{\mu_1} \right) \tag{8}$$

Similarly, the average rate of B is represented as

$$\text{rate of B} = -\frac{s' - 1/\eta}{s' - 1} k_1' \eta_1 P_A + k_2' \eta_2 P_B \tag{9}$$

where

$$\eta_2 = \frac{3}{\mu_2}\left(\coth\mu_2 - \frac{1}{\mu_2}\right), \quad \mu_2 = L\sqrt{\frac{k_2'}{D_K}}$$

$$\eta = \eta_1/\eta_2, \quad s' = k_1'/k_2' \tag{10}$$

On the basis of Eqs.(7) and (9) and the assumption that the microparticles are distributed uniformly in the catalyst pellet, the conservation equations in the pellet are written as

$$D_M\left(\frac{d^2P_A}{dr^2} + \frac{2}{r}\frac{dP_A}{dr}\right) = \varepsilon k_1' \eta_1 P_A \tag{11}$$

$$D_M\left(\frac{d^2P_B}{dr^2} + \frac{2}{r}\frac{dP_B}{dr}\right) = -\varepsilon\frac{s' - 1/\eta}{s' - 1} k_1' \eta_1 P_A + \varepsilon k_2' \eta_2 P_B \tag{12}$$

with boundary conditions

$$\text{at } r = R, \quad P_A = P_{AS} \quad \text{and} \quad P_B = P_{BS} \tag{13}$$

$$\text{at } r = 0, \quad \frac{dP_A}{dr} = 0 \quad \text{and} \quad \frac{dP_B}{dr} = 0 \tag{14}$$

where ε is the fraction of the catalyst volume occupied by the microparticles.

Rearranging Eqs.(11) ~ (14) to dimensionless forms and setting $x = az$ and $y = bz$, where $a = P_A/P_{AS}$, $b = P_B/P_{AS}$ and $z = r/R$, yields

$$\frac{d^2x}{dz^2} = m_1'^2 x \tag{15}$$

$$\frac{d^2y}{dz^2} = -\frac{s' - 1/\eta}{s' - 1} m_1'^2 x + m_2'^2 y \tag{16}$$

where $m_i' = R\sqrt{\dfrac{\varepsilon k_i' \eta_i}{D_M}}$,

$$\text{at } z = 1, \quad x = 1 \quad \text{and } y = P_{BS}/P_{AS} \tag{17}$$

$$\text{at } z = 0, \quad x = 0 \quad \text{and } y = 0 \tag{18}$$

Eq.(15) with the boundary conditions (17) and (18) is equivalent to Eq.(10) with the boundary conditions (12) and (13) in Appendix 1, so that the solution is

$$x = \frac{\sinh (m_1'z)}{\sinh m_1'} \tag{19}$$

It is easily known that Eq.(16) has a particular solution of

$$y = \frac{-\frac{s' - 1/\eta}{s' - 1} m_1'^2}{m_1'^2 - m_2'^2} x = -\frac{s'}{s' - 1} x \tag{20}$$

The solution of Eq.(16) is therefore

$$y = C_1 e^{m_2'z} + C_2 e^{-m_2'z} - \frac{s'}{s' - 1} \frac{\sinh (m_1'z)}{\sinh m_1'} \tag{21}$$

Determing C_1 and C_2 by the boundary conditions (17) and (18) leads to

$$y = \left(\frac{s'}{s' - 1} - \frac{P_{BS}}{P_{AS}} \right) \frac{\sinh (m_2'z)}{\sinh m_2'} - \frac{s'}{s' - 1} \frac{\sinh (m_1'z)}{\sinh m_1'} \tag{22}$$

Noting that $x = az$ and $y = bz$, Eqs.(14) and (22) become

$$a = \frac{P_A}{P_{AS}} = \frac{1}{z} \frac{\sinh (m_1'z)}{\sinh m_1'} \tag{23}$$

$$b = \frac{P_B}{P_{AS}} = \frac{1}{z} \left(\frac{s'}{s' - 1} - \frac{P_{BS}}{P_{AS}} \right) \frac{\sinh (m_2'z)}{\sinh m_2'} - \frac{s'}{s' - 1} \frac{\sinh (m_1'z)}{z \sinh m_1'} \tag{24}$$

The average rates of A and B inside the catalyst are derived from these concentration profiles.

$$\text{rate of A} = \varepsilon k_1' \eta_1 E_1 P_{AS} \tag{25}$$

$$\text{rate of B} = \varepsilon k_1' \eta_1 E_1 P_{AS} \frac{s' - 1/\eta E'}{s' - 1} - \varepsilon k_2' \eta_2 E_2' P_{BS} \tag{26}$$

Here ,

$$E_i' = \frac{3}{m_i'} \left(\coth m_i' - \frac{1}{m_i'} \right), \quad E' = E_1'/E_2' \tag{27}$$

From Eqs.(25) and (26), overall effectiveness factor and selectivity are given by

$$\text{overall effectiveness factor} = \varepsilon \eta_1 E_1' \tag{28}$$

$$S = \frac{s' - 1/\eta E'}{s' - 1} - \frac{1}{s'\eta E'} \frac{P_{BS}}{P_{AS}} \tag{29}$$

Thus, the single catalyst process has been solved.

In much the same way as described in Appendix 1, the conversion of A and the selectivity of B in a plug flow reactor are given by

$$X = 1 - e^{-(\varepsilon w k_1' \eta_1 E_1'/F)\,l} \tag{30}$$

$$S = \frac{(1-X)^{1/s'\eta E'} - (1-X)}{X\,(1 - 1/s'\eta E')} \quad \frac{s' - 1/\eta E'}{s' - 1} \tag{31}$$

The limit of Eq.(31) as X approaches to 0 leads to

$$S^o = \frac{s' - 1/\eta E'}{s' - 1} \tag{32}$$

Appendix 3 The Selectivity in a Consecutive Reactions System Governed by Langmuir-Hinshelwood Kinetics in which $K_A P_{AS}$ and Thiele Modulus are large

3-1 Simple pore model

In a consecutive reactions system $A \xrightarrow{R_1} B \xrightarrow{R_2} C$, the rate forms based on Langmuir-Hinshelwood model are approximated as follows, provided that $K_A P_{AS}$ is large enough compared to unity.

$$R_1 = \frac{k_1 P_A}{1 + K_A P_A} \doteqdot \frac{k_1}{K_A} \tag{1}$$

$$R_2 = \frac{k_2 P_B}{1 + K_A P_A} \doteqdot \frac{k_2 P_B}{K_A P_A} \tag{2}$$

The assumption that Thiele modulus is sufficiently large allows the spherical catalyst to be approximated by a flat plate geometry. As a result, the steady state conservation equations in a spherical catalyst, in which the above reactions take place, are written as

$$\frac{d^2 P_A}{dl^2} = k_1' \tag{3}$$

$$\frac{d^2 P_B}{dl^2} = -k_1' + k_2' \frac{P_A}{P_B} \tag{4}$$

with boundary conditions

$$\text{at } l = 0, \quad P_A = P_{AS} \quad \text{and} \quad P_B = P_{BS} \tag{5}$$

$$\text{at } P_A = 0, \quad \frac{dP_A}{dl} = 0, \quad P_B = 0 \quad \text{and} \quad \frac{dP_B}{dl} = 0 \tag{6}$$

where l represents the distance from the pellet surface and $k_i' = k_i / K_A$.

The boundary condition (6) must be satisfied simultaneously at a certain position inside the pellet, otherwise R_2 becomes infinite.

The solution of Eq.(3) with the boundary conditions (5) and (6) are given by

$$P_A = y^2 \tag{7}$$

$$\text{where } y = P_{AS}^{\frac{1}{2}} - \sqrt{\frac{k_i'}{2}}\, l . \tag{8}$$

The reaction rate of A is therefore represented as

$$\text{rate of A} = -D_e \left.\frac{dP_A}{dl}\right]_{l=0} = D_e \sqrt{2k_1'}\, P_{AS}^{\frac{1}{2}} \tag{9}$$

Noting Eqs.(7) and (8), Eq.(4) and the boundary conditions become

$$\frac{d^2P_B}{dy^2} = -2 + 2s\frac{P_B}{y^2} \tag{10}$$

$$\text{at } y = P_{AS}^{\frac{1}{2}}, \qquad P_B = P_{BS} \tag{11}$$

$$\text{at } y = 0, \qquad P_B = 0 \quad \text{and} \quad \frac{dP_B}{dy} = 0 \tag{12}$$

where $s = k_1/k_2$. (13)

Setting $y = e^t$ and $P_B = y^2 z$ converts Eq.(10) to

$$\frac{d^2z}{dt^2} + 3\frac{dz}{dt} + 2\frac{s}{s-1}z + 2 = 0 \tag{14}$$

The solution of Eq.(14) is

$$z = C_1 e^{\lambda_1 t} + C_2 e^{\lambda_2 t} - \frac{s}{s-1} \tag{15}$$

where $\lambda_{\substack{1\\2}} = \frac{1}{2}\left(-3 \pm \sqrt{1 + 8/s}\right)$. (16)

Eq.(15) and the relations $y = e^t$ and $P_B = y^2 z$ leads to

$$P_B = y^2\left(C_1 y^{\lambda_1} + C_2 y^{\lambda_2} - \frac{s}{s-1}\right) \tag{17}$$

Since $\lambda_2 < -2$, the boundary condition that $P_B = 0$ at $y = 0$ requires that $C_2 = 0$. Thus Eq.(17) becomes

$$P_B = y^2\left(C_1 y^{\lambda_1} - \frac{s}{s-1}\right) \tag{18}$$

Eq.(18) satisfies another requirement that $\frac{dP_B}{dy} = 0$ at $y = 0$.

Determining C_1 by the other boundary condition (11) leads to

$$P_B = y^2\left[\left(\frac{P_{BS}}{P_{AS}} + \frac{s}{s-1}\right) P_{AS}^{-\frac{1}{2}\lambda_1} y^{\lambda_1} - \frac{s}{s-1}\right] \tag{19}$$

The formation rate of B is given by

$$\text{rate of B} = D_e \left.\frac{dP_B}{dl}\right]_{l=0} = D_e \frac{k_1'}{2} \left(-\lambda_1 - 2\right)\frac{P_{BS}}{P_{AS}^{\frac{1}{2}}} - \lambda_1 \frac{s}{s-1} P_{AS}^{\frac{1}{2}} \quad (20)$$

From Eqs.(9) and (20), the selectivity is represented as

$$S = \frac{(-\lambda_1 - 2)\ P_{BS}/P_{AS} - \lambda_1 \frac{s}{s-1}}{2} \quad (21)$$

The limiting selectivity as X = 0 is obtained by substituting $P_{BS} = 0$ into Eq.(21). Noting Eq.(16),

$$S^o = \frac{3 - \sqrt{1 + 8/s}}{4} \frac{s}{s-1} \quad (22)$$

3-2 Micro-macropore model

The microparticle process is analogous to the system described above, provided that the diffusion coefficient D_e is replaced by that in micropore D_K. Noting Eqs.(9) and (20), the conservation equations in a catalyst pellet are written as

$$\frac{d^2P_A}{dl^2} = k_1^o\ P_A^{\frac{1}{2}} \quad (23)$$

$$\frac{d^2P_B}{dl^2} = -k_1''\ P_A^{\frac{1}{2}} + k_2'' \frac{P_B}{P_A^{\frac{1}{2}}} \quad (24)$$

with boundary conditions

$$\text{at } l = 0, \quad P_A = P_{AS} \quad \text{and} \quad P_B = 0 \quad (25)$$

$$\text{at } P_A = 0, \quad \frac{dP_A}{dl} = 0, \quad P_B = 0 \quad \text{and} \quad \frac{dP_B}{dl} = 0 \quad (26)$$

where

$$k_1^o = \frac{3\varepsilon}{R\ D_M}\sqrt{\frac{2k_1\ D_K}{K_A}}, \qquad k_1''/k_1^o = \frac{-\lambda_1 \frac{s}{s-1}}{2} \quad (27)$$

$$k_2''/k_1^o = 1 + \frac{\lambda_1}{2}$$

D_M and ε represent respectively the diffusion coefficient in macropore and the fraction of the catalyst volume occupied by the microparticles.

The boundary condition, $P_B = 0$ at $l = 0$, corresponds to the limiting selectivity at $X = 0$. The other boundary condition (26) is justified by the assumption that modulus are sufficiently large.

Multiplying Eq.(23) by $\frac{dP_A}{dl}$ and integrating it with respect to x yields

$$\left(\frac{dP_A}{dl}\right)^2 = \frac{4}{3} k_1^o P_A^{\frac{3}{2}} + C_1 \tag{28}$$

By the boundary condition (26), $C_1 = 0$. Noting that $\frac{dP_A}{dl}$ is negative, Eq.(28) leads to

$$\frac{dP_A}{dl} = -\sqrt{\frac{4}{3} k_1^o} \; P_A^{\frac{3}{4}} \tag{29}$$

The solution of Eq.(29) with the boundary condition (25) is given by

$$P_A = y^4 \tag{30}$$

where

$$y = P_{AS}^{\frac{1}{4}} - \frac{1}{2}\sqrt{\frac{k_1^o}{3}}\, l \,. \tag{31}$$

The reaction rate of A is given by

$$\text{rate of A} = -D_M \left.\frac{dP_A}{dl}\right)_{l=0} = D_M \sqrt{\frac{4k_1^o}{3}}\; P_{AS}^{\frac{3}{4}} \tag{32}$$

Substituting Eq.(30) in Eq.(24) gives

$$\frac{k_1^o}{12} \frac{d^2P_B}{dl^2} = -k_1'' y^2 + k_2'' \frac{P_B}{y^2} \tag{33}$$

The boundary conditions are reduced to

$$\text{at } y = P_{AS}, \qquad P_B = 0 \tag{34}$$

$$\text{at } y = 0, \qquad P_B = 0 \quad \text{and} \quad \frac{dP_B}{dy} = 0 \tag{35}$$

Setting $y = e^t$ and $P_B = e^{4t}\, z$, Eq.(33) becomes

$$\frac{d^2z}{dt^2} + 7\frac{dz}{dt} + 12\,(1 - k_2''/k_1^o)\,z + 12\,k_1''/k_1^o = 0 \tag{36}$$

The solution of Eq.(36) is

$$z = C_1\,e^{\lambda_1' t} + C_2\,e^{\lambda_2' t} - \frac{k_1''/k_1^o}{1 - k_2''/k_1^o} \tag{37}$$

where $\lambda_{1,2}' = \frac{1}{2}\left(-7 \pm \sqrt{1 + 48\,k_2''/k_1^o}\right)$. (38)

Substituting $e^t = y$ and $z = P_B\,e^{-4t}$ in Eq.(37) yields

$$P_B = y^4\left(C_1\,y^{\lambda_1'} + C_2\,y^{\lambda_2'} - \frac{k_1''/k_1^o}{1 - k_2''/k_1^o}\right) \tag{39}$$

Noting that $P_B = 0$ at $y = 0$ and that $\lambda_2' < -4$, it is concluded that $C_2 = 0$. Because $\lambda_1' > -3$, the boundary condition (35) is satisfied.

From the other boundary condition (34), C_1 is determined and the resulting concentration profile is represented as

$$P_B = \frac{k_1''/k_1^o}{1 - k_2''/k_1^o}\,y^4\left(P_{AS}^{-\frac{\lambda_1'}{4}}\,y^{\lambda_1'} - 1\right) \tag{40}$$

Consequently, the formation rate of B is given by

$$\text{rate of B} = D_M \left.\frac{dP_B}{dl}\right]_{l=0}$$

$$= \frac{D_M}{2}\sqrt{\frac{k_1^o}{3}}\;\frac{(-\lambda_1')\,(k_1''/k_1^o)}{1 - k_2''/k_1^o}\,P_{AS}^{\frac{3}{4}} \tag{41}$$

From Eqs.(32) and (41), the selectivity S^o is given by

$$S^o = \frac{(-\lambda_1')\,(k_1''/k_1^o)}{4\,(1 - k_2''/k_1^o)} \tag{42}$$

Substituting Eqs.(16), (27) and (38) in Eq.(42) yields

$$S^o = \frac{s}{s-1}\;\frac{7 - \sqrt{13 + 12\sqrt{1 + 8/s}}}{8} \tag{43}$$

Appendix 4 The Change in the Selectivity and the Conversion with Deactivation

Simple Pore Model

4-1 Homogeneous poisoning

The conservation equations in a catalyst pellet, in which the first order rate constants for the consecutive reactions are respectively δk_{10} and δk_{20}, are written as

$$D_e \left(\frac{d^2 P_A}{dr^2} + \frac{2}{r}\frac{dP_A}{dr} \right) = \delta k_{10} P_A \tag{1}$$

$$D_e \left(\frac{d^2 P_B}{dr^2} + \frac{2}{r}\frac{dP_B}{dr} \right) = -\delta k_{10} P_A + \delta k_{20} P_B \tag{2}$$

with boundary conditions

$$\text{at } r = R, \quad P_A = P_{AS} \quad \text{and} \quad P_B = P_{BS} \tag{3}$$

$$\text{at } r = 0, \quad \frac{dP_A}{dr} = 0 \quad \text{and} \quad \frac{dP_B}{dr} = 0 \tag{4}$$

In Appendix 1, the behavior of the backmix reactor, in which each catalyst is subject to the similar differential equations as shown above, has been solved. On the analogy of Eqs.(43) and (45) in Appendix 1, the conversion of A and the selectivity of B are represented as

$$X = \frac{\tau \delta k_{10} E_1}{1 + \tau \delta k_{10} E_1} \tag{5}$$

$$S = \frac{1}{1 + \frac{X}{1 - X}\frac{1}{sE_H}} \; \frac{s - 1/E_H}{s - 1} \tag{6}$$

where

$$E_i = \frac{3}{m_i'}\left(\coth m_i' - \frac{1}{m_i'} \right), \quad m_i' = R\sqrt{\frac{\delta k_{i0}}{D_e}}$$

$$E_H = E_1 / E_2 , \quad s = k_{10}/k_{20} \tag{7}$$

and W represents the total volume of the catalysts in the reactor.

4-2 Shell poisoning

4-2-1 model 2-b

A simple pore model as solved in Appendix 1 is applied to the core part, $0 < r < 1$. From Eqs.(22) and (25) in Appendix 1, the concentration gradients of A and B at $r = 1$ are given by

$$\left.\frac{dP_A}{dr}\right]_1 = \frac{m_{11}^2}{3l} E_{11} P_{A1} \tag{8}$$

$$\left.\frac{dP_B}{dr}\right]_1 = -\frac{m_{11}^2}{3l} E_{11} \frac{s - 1/E_1}{s - 1} P_{A1} \tag{9}$$

where

$$m_{i1} = l\sqrt{\frac{k_{i0}}{D_e}}, \quad E_{i1} = \frac{3}{m_{i1}}\left(\coth m_{i1} - \frac{1}{m_{i1}}\right), \quad E_1 = \frac{E_{11}}{E_{21}} \tag{10}$$

The conservation equations in the deactivated shell part, $1 < r < R$, are written as

$$D_e\left(\frac{d^2P_A}{dr^2} + \frac{2}{r}\frac{dP_A}{dr}\right) = \delta k_{10} P_A \tag{11}$$

$$D_e\left(\frac{d^2P_B}{dr^2} + \frac{2}{r}\frac{dP_B}{dr}\right) = -\delta k_{10} P_A + \delta k_{20} P_B \tag{12}$$

with boundary conditions

$$\text{at } r = R, \quad P_A = P_{AS} \quad \text{and} \quad P_B = P_{BS} \tag{13}$$

$$\begin{aligned} &\text{at } r = 1, \quad P_A = P_{A1} \quad \text{and} \quad \frac{dP_A}{dr} = \left.\frac{dP_A}{dr}\right]_1 \quad (\text{Eq.(8)}) \\ &\qquad\qquad P_B = P_{B1} \quad \text{and} \quad \frac{dP_B}{dr} = \left.\frac{dP_B}{dr}\right]_1 \quad (\text{Eq.(9)}) \end{aligned} \tag{14}$$

In the same way as descrived in Appendix 1, the solution of Eq.(11) is given by

$$P_A = C_1 \frac{e^{m_1' \frac{R}{r}}}{r} + C_2 \frac{e^{-m_1' \frac{R}{r}}}{r} \tag{15}$$

where $m_1' = R\sqrt{\frac{\delta k_{10}}{D_e}}$.

Eq.(15) and the boundary conditions (13) and (14) give the following three relations for three unknowns C_1, C_2 and P_{A1}.

$$P_{AS} = (C_1 e^{m_1'} + C_2 e^{-m_2'}) / R \tag{16}$$

$$P_{A1} = (C_1 e^{m_{11}'} + C_2 e^{-m_{21}'}) / 1 \tag{17}$$

$$\frac{m_{11}^2}{3l} E_{11} P_{A1} = \frac{C_1}{l^2} e^{m_{11}'} (m_{11}' - 1) - \frac{C_2}{l^2} e^{-m_{11}'} (m_{11}' + 1) \tag{18}$$

where subscript ' shows that the rate constant in the modulus is δk_{i0} and subscript 1 shows that the dimension in the modulus is 1.

Combining Eqs.(16), (17) and (18) determines C_1 and C_2. Substituting them into Eq.(15) yields

$$P_A = P_{AS} \frac{R}{r} \frac{(m_{11}^2 E_{11}/3 - m_{11}' + 1) e^{m_{11}'} (1 - \frac{r}{l})}{(m_{11}^2 E_{11}/3 - m_{11}' + 1) e^{-m_{1\Delta}'}} \frac{- (m_{11}^2 E_{11}/3 + m_{11}' + 1) e^{-m_{11}'} (1 - \frac{r}{l})}{- (m_{11}^2 E_{11}/3 + m_{11}' + 1) e^{m_{1\Delta}'}} \tag{19}$$

where subscript Δ shows that the dimension in the modulus is (R - l).

From Eq.(19), the average reaction rate of A inside the catalyst pellet is given by

$$\text{rate of A} = \frac{3}{R} D_e \left.\frac{dP_A}{dr}\right]_{r=R} = k_{10} E_{sbl} P_{AS} \tag{20}$$

where

$$E_{sbl} = \frac{3m_1'}{m_1^2} \left(\frac{(m_{11}^2 E_{11}/3 + 1) \cosh m_{1\Delta}' + m_{11}' \sinh m_{1\Delta}'}{(m_{11}^2 E_{11}/3 + 1) \sinh m_{1\Delta}' + m_{11}' \cosh m_{1\Delta}'} - \frac{1}{m_1'} \right) \tag{21}$$

It is easily known that Eq.(12) has a particular solution $P_B = - \frac{s}{s-1} P_A$. The solution of Eq.(12) is therefore

$$P_B = C_3 \frac{e^{m_2' \frac{r}{R}}}{r} + C_4 \frac{e^{-m_2' \frac{r}{R}}}{r} - \frac{s}{s-1} P_A \tag{22}$$

C_3 and C_4 are determined in the same way as C_1 and C_2, noting the relation of P_{A1} to $\left.\frac{dP_A}{dr}\right]_1$ (Eq.(8)).

As a result, the concentration profile of B is given by

$$P_B = \left(P_{BS} + \frac{s}{s-1} P_{AS} \right) \frac{R}{r} \frac{\left(m_{21}^2 E_{21}/3 - m_{21}' + 1 \right) e^{m_{21}'(1 - \frac{r}{1})}}{\left(m_{21}^2 E_{21}/3 - m_{21}' + 1 \right) e^{-m_2'}}$$

$$\frac{- \left(m_{21}^2 E_{21}/3 + m_{21}' + 1 \right) e^{-m_{21}'(1 - \frac{r}{1})}}{- \left(m_{21}^2 E_{21}/3 + m_{21}' + 1 \right) e^{m_2'}} - \frac{s}{s-1} P_A \tag{23}$$

From Eq.(23), the average formation rate of B inside the catalyst is represented as

$$\text{rate of B} = - \frac{3}{R} D_e \left.\frac{dP_B}{dr}\right]_{r=R}$$

$$= \frac{s - 1/E_{sb1}}{s-1} k_{10} E_{sb1} P_{AS} - k_{20} E_{sb2} P_{BS} \tag{24}$$

where $$E_{sb} = E_{sb1}/E_{sb2} \tag{25}$$

and E_{sb2} is obtained by replacing 1 by 2 in Eq.(21).

From Eqs.(20) and (24), the conversion and the selectivity in a back-mix reactor are derived in much the same way as described in Appendix 1.

$$X = \frac{k_{10} E_{sb1}}{1 + k_{10} E_{sb1}} \tag{26}$$

$$S = \frac{1}{1 + \frac{X}{1-X} \frac{1}{s E_{sb}}} \frac{s - 1/E_{sb}}{s-1} \tag{27}$$

4-2-2 model 2-a

The limits of Eqs.(26) and (27) as δ approaches 0 give the solution for the shell poisoning, model 2-a. The results are

$$X = \frac{k_{10} E_{sa1}}{1 + k_{10} E_{sa1}} \tag{28}$$

$$S = \frac{1}{1 + \frac{X}{1 - X} \frac{1}{s E_{sa}}} \frac{s - 1/E_{sa}}{s - 1} \tag{29}$$

where

$$E_{sai} = \frac{(1/R)^3 E_{i1}}{m_{i1}^2 E_{i1}/3 (1 - 1/R) + 1}, \qquad E_{sa} = E_{sa1}/E_{sa2} \tag{30}$$

4-3 core poisoning

The solution for core poisoning are obtained by exchanging the initial rate constant k_{i0} and the deactivated rate constant δk_{i0} in the solution for shell poisoning 2-b, Eqs.(26) and (27), and substituting $\delta = 0$.

The results are

$$X = \frac{k_{10} E_{c1}}{1 + k_{10} E_{c1}} \tag{31}$$

$$S = \frac{1}{1 + \frac{X}{1 - X} \frac{1}{s E_c}} \frac{s - 1/E_c}{s - 1}, \qquad E_c = E_{c1}/E_{c2} \tag{32}$$

where

$$E_{ci} = \frac{3}{m_i} \left(\frac{\cosh m_{i\Delta} + m_{i1} \sinh m_{i\Delta}}{\sinh m_{i\Delta} + m_{i1} \cosh m_{i\Delta}} - \frac{1}{m_i} \right) \tag{33}$$

$$E_c = E_{c1} / E_{c2} \tag{34}$$

Appendix 5 Shell poisoning ——— micro-macropore model ———

According to the assumption made for this poisoning, the catalyst pellet consists of two parts, one of which is the shell part containing deactivated microparticles of the rate constants δk_{i0} and the other is the core part containing non-deactivated microparticles.

On the analogy of Eqs.(11) and (12) in Appendix 2, where a consecutive reactions system was analyzed on the basis of the micro-macropore model, the conservation equations in the shell part are written as

$$D_M \left(\frac{d^2 P_A}{dr^2} + \frac{2}{r}\frac{dP_A}{dr} \right) = \varepsilon \delta k_{10} \eta_1' P_A \tag{1}$$

$$D_M \left(\frac{d^2 P_B}{dr^2} + \frac{2}{r}\frac{dP_B}{dr^2} \right) = -\varepsilon \frac{s - 1/\eta'}{s - 1} \delta k_{10} \eta_1' P_A + \varepsilon \delta k_{20} \eta_2' P_B \tag{2}$$

where

$$\eta_i' = \frac{3}{\mu_i'} \left(\coth \mu_i' - \frac{1}{\mu_i'} \right), \quad \mu_i' = L \sqrt{\frac{\delta k_{i0}}{D_K}}, \quad \eta' = \frac{\eta_1'}{\eta_2'} \tag{3}$$

The boundary condition at the exterior surface of the shell part is given by

$$\text{at } r = R, \quad P_A = P_{AS} \quad \text{and} \quad P_B = P_{BS} \tag{4}$$

Based upon Eqs.(25) and (26) in Appendix 2, which give the gradients of A and B at the surface of the core part, the other boundary condition at r = 1 is written as

$$\text{at } r = 1, \quad P_A = P_{A1} \quad \text{and} \quad \frac{dP_A}{dr} = \frac{m_{11}^2}{3l} E_{11} P_{A1} \tag{5}$$

$$P_B = P_{B1} \quad \text{and} \quad \frac{dP_B}{dr} = -\frac{m_{11}^2}{3l} \frac{s - 1/\eta E_1}{s - 1} E_{11} P_{A1} + \frac{m_{21}^2}{3l} E_{21} P_{B1} \tag{6}$$

where

$$m_{il} = l \sqrt{\frac{\varepsilon k_{i0} \eta_i}{D_M}}, \quad E_{il} = \frac{3}{m_{il}} \left(\coth m_{il} - \frac{1}{m_{il}} \right), \quad E_1 = \frac{E_{11}}{E_{21}}$$

$$\mu_{il} = L \sqrt{\frac{k_{i0}}{D_K}}, \quad \eta_i = \frac{3}{\mu_i} \left(\coth \mu_i - \frac{1}{\mu_i} \right), \quad \eta = \frac{\eta_1}{\eta_2} \tag{7}$$

Eq.(1) with the boundary conditions (4) and (5) is mathematically equivalent to Eq.(11) with the boundary conditions (13) and (14) in Appendix 2, so that the average rate of A inside the catalyst is given as follows on the analogy of Eq.(20) in the appendix.

$$\text{rate of A} = \frac{3}{R} D_M \frac{dP_A}{dr}\Big]_{r=R} = \varepsilon k_{10} \eta_1 E_{f1} P_{AS} \tag{8}$$

where

$$E_{f1} = \frac{3 m_1'}{m_1^2}\left(\frac{(m_{11}^2 E_{11}/3 + 1) \cosh m_{1\Delta}' + m_{11}' \sinh m_{1\Delta}'}{(m_{11}^2 E_{11}/3 + 1) \sinh m_{1\Delta}' + m_{11}' \cosh m_{1\Delta}'} - \frac{1}{m_1'}\right) \tag{9}$$

where, subscript ' shows that the rate constant in the modulus is $\varepsilon \delta k_{i0} \eta_i'$ and subscript 1 or Δ shows that the dimension in the modulus is 1 or (R - 1).

Because Eq.(2) has a particular solution of

$$P_B = - \frac{\varepsilon \frac{s - 1/\eta'}{s - 1} \delta k_{10} \eta_1'}{\varepsilon \delta k_{10} \eta_1' - \varepsilon \delta k_{20} \eta_2'} P_A = - \frac{s}{s - 1} P_A \tag{10}$$

Eq.(2) is solved with the boundary conditions in much the same way as Eq.(2) in Appendix 2.

On the analogy of Eq.(24) in Appendix 2, the average rate of B inside the catalyst is represented as

$$\text{rate of B} = - \frac{3}{R} D_M \frac{dP_B}{dr}\Big]_{r=R}$$

$$= \frac{s - 1/E_f}{s - 1} \varepsilon k_{10} \eta_1 E_{f1} P_{AS} - \varepsilon k_{20} \eta_2 E_{f2} P_{BS} \tag{11}$$

where E_{f2} is obtained by replacing 1 by 2 in Eq.(9) and

$$E_f = E_{f1} / E_{f2} \tag{12}$$

From Eqs.(8) and (11), the conversion and the selectivity in a backmix reactor are derived in the same way as described in Appendix 1 as

$$X = \frac{\tau \varepsilon k_{10} \eta_1 E_{f1}}{1 + \tau \varepsilon k_{10} \eta_1 E_{f1}} \tag{13}$$

$$S = \frac{1}{1 + \frac{X}{1 - X} \frac{1}{s \eta E_f}} \frac{s - 1/\eta E_f}{s - 1} \tag{14}$$

Appendix 6 Effectiveness factor under the combined gradients of concentration and pressure

The conservation equation in a catalyst pellet, in which a first order reaction $A \longrightarrow B$ takes place with the hydrodynamic flow as given by $u_z = u_{in}$ (constant) and $u_r = u_\theta = 0$, is written in cylindrical co-ordinates as

$$D_e \left(\frac{1}{r} \frac{\partial}{\partial r} \left(r \frac{\partial P_A}{\partial r} \right) + \frac{\partial^2 P_A}{\partial z^2} \right) - u_{in} \frac{\partial P_A}{\partial z} - k_1 P_A = 0 \qquad (1)$$

with boundary conditions

$$\text{at } r = R, \quad P_A = P_{AS} \qquad (2)$$

$$\text{at } z = 0, \quad P_A = P_{AS} \qquad (3)$$

$$\text{at } z = L_p, \quad P_A = P_{AS} \qquad (4)$$

These equations are reduced to dimensionless forms as

$$\frac{\partial^2 a''}{\partial x^2} + \frac{1}{x} \frac{\partial a''}{\partial x} + \omega^2 \frac{\partial^2 a''}{\partial y^2} - PeB\, \omega^2 \frac{\partial a''}{\partial y} - m_1^2 a'' + m_1^2 = 0 \qquad (5)$$

$$\text{at } x = 1, \quad a'' = 0 \qquad (6)$$

$$\text{at } y = 1, \quad a'' = 0 \qquad (7)$$

$$\text{at } y = 0, \quad a'' = 0 \qquad (8)$$

where

$$x = r/R, \quad y = z/L_p, \quad PeB = u_{in} L_p / D_e, \quad m_1 = R\sqrt{\frac{k_1}{D_e}} \quad \text{and } \omega = R/L_p,$$

$$a'' = (P_{AS} - P_A) / P_{AS} \qquad (9)$$

Now, let Bessel transform of an arbitrary function F(x) be defined as

$$\overline{F} = \int_0^1 F(x)\, x\, J_0(j_n x)\, dx \qquad (10)$$

where, $J_0(x)$ represents zero order Bessel fumction and j_n is n'th root of $J_0(x) = 0$.

Noting Eqs.(11) and (12),

$$\int_0^1 \left(\frac{\partial^2 a''}{\partial x^2} + \frac{1}{x} \frac{\partial a''}{\partial x} \right) x\, J_0(j_n x)\, dx = - j_n^2\, \overline{a''} \qquad (11)$$

$$\int_0^1 m_1^2 \, x \, J_0(j_n x) \, dx = \frac{J_1(j_n)}{j_n} m_1^2 \tag{12}$$

the transform of Eq.(5) with respect to x becomes

$$\frac{d^2 \overline{a''}}{dy^2} - PeB \frac{d\overline{a''}}{dy} - \frac{j_n^2 + m_1^2}{\omega^2} \overline{a''} + \frac{J_1(j_n)}{j_n \omega^2} m_1^2 = 0 \tag{13}$$

where $J_1(x)$ represents first order Bessel function.

The solution of Eq.(13) is given by

$$\overline{a''} = C_1 e^{\lambda_1 y} + C_2 e^{\lambda_2 y} + \frac{J_1(j_n) \, m_1^2}{j_n^2 (j_n^2 + m_1^2)} \tag{14}$$

where

$$\lambda_{\substack{1\\2}} = \frac{PeB \pm \sqrt{PeB^2 + 4 (j_n^2 + m_1^2) / \omega^2}}{2} \tag{15}$$

C_1 and C_2 are determined by the boundary conditions with respect to y (7) and (8) and Eq.(14) becomes

$$\overline{a''} = \frac{J_1(j_n) \, m_1^2}{j_n (j_n^2 + m_1^2)} \left(\frac{e^{\lambda_2} - 1}{e^{\lambda_1} - e^{\lambda_2}} e^{\lambda_1 y} - \frac{e^{\lambda_1} - 1}{e^{\lambda_1} - e^{\lambda_2}} e^{\lambda_2 y} + 1 \right) \tag{16}$$

Because the expansion of F(x) by $J_0(j_n x)$ is given by

$$F(x) = \sum_{n=1}^{\infty} A_n J_0(j_n x) \tag{17}$$

$$A_n = \frac{2}{J_1(j_n)^2} \int_0^1 F(x) \, x \, J_0(j_n x) \, dx = \frac{2}{J_1(j_n)^2} \overline{F} \tag{18}$$

, the reverse transform of $\overline{a''}$ is represented as

$$a'' = \sum_{n=1}^{\infty} \frac{2}{J_1(j_n)^2} J_0(j_n x) \, \overline{a''} \tag{19}$$

It is noted that the boundary condition with respect to x is satisfied automatically by the transform.

Substituting Eq.(16) into Eq.(19) yields

$$a'' = \sum_{n=1}^{\infty} \frac{2\, m_1^2\, J_0(j_n x)}{J_1(j_n)\, j_n\, (\, j_n^2 + m_1^2\,)} \left(\frac{e^{\lambda_2} - 1}{e^{\lambda_1} - e^{\lambda_2}}\, e^{\lambda_1 y} - \frac{e^{\lambda_1} - 1}{e^{\lambda_1} - e^{\lambda_2}}\, e^{\lambda_2 y} + 1 \right) \tag{20}$$

According to the definition, effectiveness factor is obtained by

$$E_1 = \frac{\int_0^1\int_0^1 k_1\, (1 - a'')\, x\, dx\, dy}{\int_0^1\int_0^1 k_1\, x\, dx\, dy}$$

$$= 1 - \sum_{n=1}^{\infty} \frac{4\, m_1^2}{j_n^2 (j_n^2 + m_1^2)} \left(1 + \frac{(e^{\lambda_1} - 1)\,(e^{\lambda_2} - 1)}{e^{\lambda_1} - e^{\lambda_2}} \left(\frac{1}{\lambda_1} - \frac{1}{\lambda_2} \right) \right) \tag{21}$$